

Aus der  
Orthopädischen Universitätsklinik mit Poliklinik Tübingen

**Biomechanical assessment of osteoarthritic articular cartilage  
and jaw periosteal cells-based bone constructs**

**Thesis submitted as requirement to fulfill the degree  
„Doctor of Philosophy “(Ph.D)**

**at the  
Faculty of Medicine  
Eberhard Karls University  
Tübingen**

**by  
Danalache Marina**

**2020**

Dean: Professor Dr. B. Pichler

First reviewer: Privatdozent Dr. U. K. Hofmann

Second reviewer: Professor Dr. S. Huber

Date of oral examination: 12.05.2020

To my mom and my husband & to the memory of my dear father

~ *“to him who had given me dreams to look forward to”* ~

“The oak fought the wind and was broken,  
the willow bent when it must and survived.”

Robert Jordan

Adapted from The Oak and the Reeds fable

by Aesop

# Table of Contents

1. Introduction.....	1
1.1. Biomechanical properties of cartilage and their role in osteoarthritis.....	6
1.2. Role of biomechanical properties in bone tissue engineering.....	10
1.3. Aim of the thesis.....	13
2. Results.....	16
2.1. Biomechanical cues of pericellular matrix degradation in osteoarthritic cartilage.....	16
2.2. Biomechanical and biochemical cues for customizing jaw periosteal cells for bone constructs .....	26
3. Discussion.....	43
3.1. Biomechanical cues in early osteoarthritis.....	44
3.2. Biomechanical cues for customizing jaw periosteal cells for bone constructs	48
3.3. Study limitations.....	52
3.4. Conclusions .....	53
4. Summary.....	54
5. Zusammenfassung .....	56
6. Bibliography .....	58
7. Declaration of contribution.....	72
Acknowledgments .....	73

## List of abbreviations and acronyms

---

Abbreviation	Definition
AFM	Atomic force microscopy
BMP2	Bone morphogenic protein 2
BTE	Bone tissue engineering
ECM	Extracellular matrix
EGF	Epidermal growth factor
ELISA	Enzyme-linked Immunosorbent Assay
EM	Elastic modulus
FCS	Fetal calf serum
FWHM	Full-width-half-maximum
GAGs	Glycosaminoglycans
GMP	Good manufacturing practice
hPL	Human plasma lysate
HS	Heparansulfate
IF	Impact factor
ITM	Interterritorial matrix
JPCs	Jaw periosteum derived progenitor cells
MMP	Matrix metalloproteinase enzymes
MSCA-1	Mesenchymal stromal cell antigen-1
MSC	Mesenchymal stem cells
OA	Osteoarthritis
PCM	Pericellular matrix
PDGF	Platelet derived growth factors
sGAGs	Sulfated glycosaminoglycans
TGF	Transforming growth factor
TM	Territorial matrix

---



## 1. Introduction

Tissue performance and its physical properties are closely intertwined processes. They depend on the cells present in the tissue, and on the loading forces to which the respective tissue is exposed. As such, in the context of load bearing tissues, like articular cartilage and bone, cells are capable of generating or resisting mechanical forces that can be many times the weight of these tissues. These tissues and their specific cells therefore need to possess particular biomechanical characteristics with respect to elasticity and rigidity in order to withstand continuous stretch or strain mechanisms, and to maintain their form and function. In this context, analyses of the biomechanical properties of cells have already provided much information about the physiological cellular characteristics, and in many cases information on how to differentiate a healthy cell from a cell in a pathological condition. In fact, micromechanical characteristics have now been proposed as a potential biomarker for allowing differentiation between different physiological and pathological cellular or tissue states (Rianna and Radmacher, 2016). In view of the ongoing demand for cell based and regenerative treatment approaches, biomechanical properties of living cells as well as their response to external stimuli are considered key components which have received much research attention in the past few years (Butler et al., 2009, Guilak et al., 2014b, Tay et al., 2013).

In all complex biological structures, different types of highly specialized cells are embedded in a three-dimensional heterogeneously network termed the extracellular matrix (ECM). The ECM plays a physiological role as an active component of living tissue and is responsible for a variety of functions (Frantz et al., 2010), such as providing support, segregating tissues, and regulating intercellular communication (Gao et al., 2014). Its main components are various types of collagens, fibrous proteins, glycosaminoglycans (GAGs) and proteoglycans. These ECM components link together to form a structurally stable composite, providing the mechanical properties to the tissue, and enabling the communication between tissue and its residing cells (Pizzo et al., 2005). The ECM's biomechanical properties are mainly determined by the relative composition and network structure of its collagens, proteoglycans and elastin (Suki et al., 2011). Interestingly, the cells-as an independent entity-are capable of sensing and responding to mechanical forces of varying magnitude, direction, and frequency (Discher et al., 2005, Cho et al., 2017) through integrin-mediated interactions with the matrix (Plotnikov et al.,

2012). In such, the mechanical features of a matrix influence important cellular processes such as mobility (Lange and Fabry, 2013, Lin et al., 2019), proliferation (Hadjipanayi et al., 2009), differentiation (Smith et al., 2018) and apoptosis (Walker et al., 2018). Moreover, alterations of biomechanical characteristics of the ECM have been associated with severe pathologies such as chronic obstructive pulmonary disease and cancer (Liu et al., 2010, Bidan et al., 2015, Gkretsi and Stylianopoulos, 2018, Broders-Bondon et al., 2018). It is assumed that if a cell cannot sense its mechanical environment, it simply cannot survive (Yusko and Asbury, 2014). The biochemical and biomechanical signature of the ECM as well as cell-microenvironment crosstalk are crucial to understanding the structure-function-effect relationship of healthy as well as pathologic tissues.

To directly measure biomechanical characteristics on a micro- or even nanoscale level, atomic force microscopy (AFM) has emerged as a novel technique. It allows the precise determination of local biomechanical properties of biological components or interfaces, such as ECM-cell interactions. It works at a nanometer resolution, and measurements can be performed without damaging the tested samples (Dufrene and Pelling, 2013). Several studies have shown that AFM is a suitable and reliable technique with a large repertoire of applications. Established applications of its use are for the measurement of mechanical properties, behavior, and function of living cells (Moeendarbary and Harris, 2014), as well as for determining elastic properties of various tissues under normal physiological and pathological conditions (Haase and Pelling, 2015, Dufrière et al., 2017, Marrese et al., 2017, Deng et al., 2018, Kwon et al., 2019). Moreover, AFM can operate in a wide variety of conditions. It can, for example, be performed *in situ*, as well as in a fluid environment, thus allowing for live monitoring in real-time. Additionally, AFM probing can be combined with various microscopy techniques such as fluorescence staining and imaging, to specifically probe a region where the protein/-s of interest are located (Wilusz et al., 2012b, El-Kirat-Chatel and Dufrene, 2012). AFM operates on the principle of surface sensing using an extremely sharp tip (usually 5-10 nm), also known as an AFM probe, that interacts with the sample. The interaction between the AFM probe and the sample then provides information on the sample's biomechanical features.

The setup for AFM consists of the above-mentioned probe tip which is put into contact with the tissue, located at the end of a cantilever. A laser beam is then focused





onto the very end of the cantilever, which it is reflected onto a position-sensitive photodiode. The diode is designed to measure the horizontal and vertical deflection of the laser on the cantilever. An x-y-z piezoelectric scanner allows for the movement of the sample or the cantilever in all three directions (Figure 1)(Gavara, 2017). As the tip scans over the surface, the interactions between the AFM tip and the features on the surface cause displacement or bending of the cantilever. This bending is indicative of the tip-sample interaction force. The up/down and side to side motion of the AFM tip as it scans along the surface is measured by means of a laser beam which is projected on and then reflected off the cantilever. The reflected laser beam is then tracked by the sensitive photo-detector. The deflection sensitivity of these detectors must be calibrated beforehand. The calibration defines a correlation between how many nanometers of motion correspond to a unit of voltage.

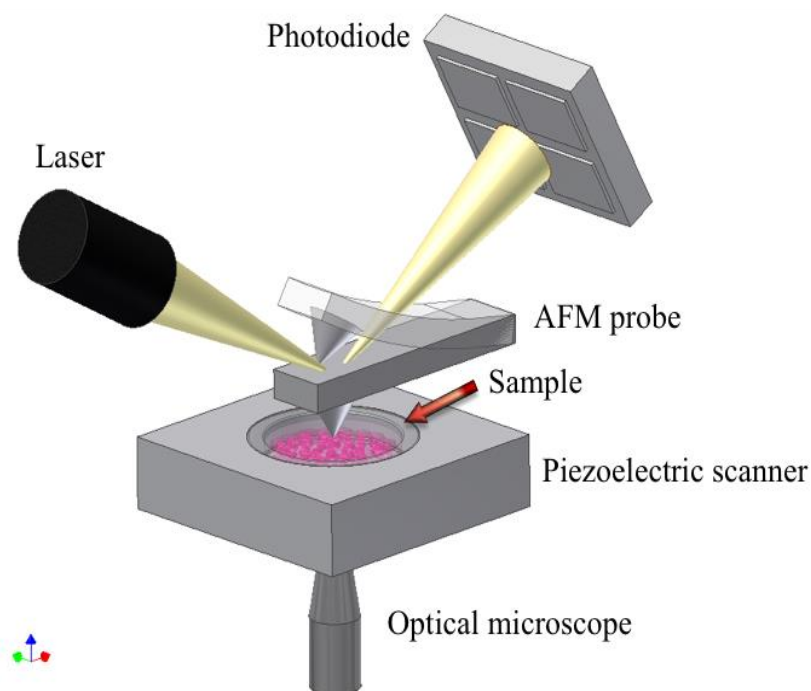


**Figure 1. Schematical representation of the AFM setup.**

*Biological samples can be investigated using an AFM cantilever or probe which is controlled by a piezoelectric scanner. A phase inverted optical microscope attached to the AFM system allows the user to specifically analyze single living cells or specific select areas within the tissue. The laser tracking system for the reflected beam is represented by a photodiode.*

*Abbreviation: AFM- atomic force microscopy*

Depending on the nature of the interaction between the tip and sample surface, the AFM can be operated in different modes, such as the AFM-contact mode (e.g. force-distance curve analysis) or the tapping mode (semi-contact). While in contact mode, the AFM tip is brought into physical contact with the sample, and the cantilever deflection is measured. In tapping mode, the tip is periodically retracted from the sample, and the cantilever height is modulated at the cantilever's resonance frequency. The latter is largely used for imaging biomolecules such as DNA, proteins, and lipids (Viji Babu and Radmacher, 2019). The most basic AFM technique operated in contact mode in terms of quantitative studies of biomechanical characteristics of cells and tissues is represented by a force-distance curve analysis (Figure 2). The applications of these experiments range from nano-mechanical investigation of elastic properties to protein unfolding and investigation of single chemical bonds (Janshoff et al., 2000).

In a force-distance curve, the interaction forces between the AFM probe and sample are measured while the AFM probe is approached to and afterwards retracted from the sample. In doing so, both the approach and the retraction curve offer cues with respect to the viscoelastic properties of the sample, as well as possible adhesion properties between the tip and sample. By fitting the data obtained from the force curve with an appropriate geometric model (e.g. Hertz fit model) of the AFM tip, the sample's Young's modulus can be calculated. The Young's modulus, also known as the elastic modulus (EM), characterizes the resistance of a material/tissue when it is subjected to compression and elongation. This describes the stiffness of the sample. A stiffer material will therefore exhibit a higher elastic modulus and vice versa (Vinckier and Semenza, 1998).

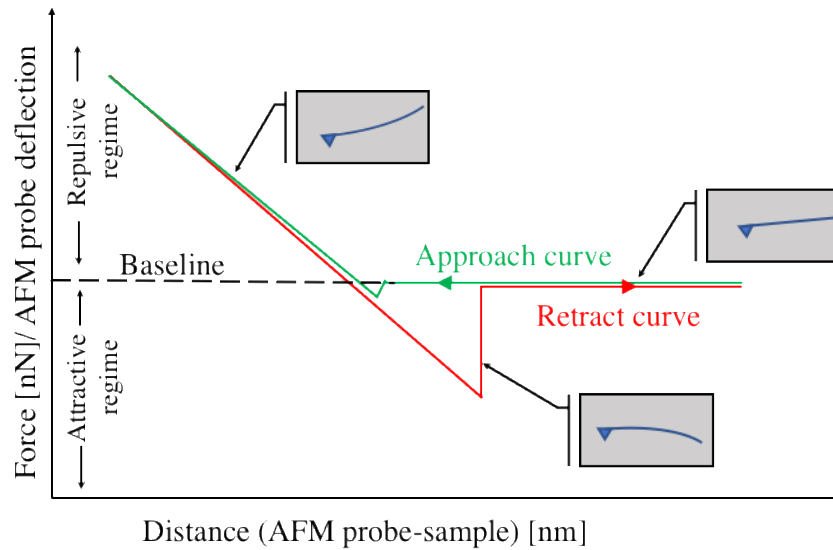


**Figure 2. Schematical representation of a force-distance curve in the AFM contact mode.**

The force curve can be divided into two different segments: 1-(green) refers to motion where the AFM probe approaches the surface, and 2-(red) when the probe retracts from the surface. As the probe initially approaches the surface, the forces are too small to give a measurable deflection of the tip, thus leaving the tip in its undisturbed position. The further the cantilever approaches the sample, the more the force increases. In the retracting regime, the probe and sample are already in contact with one another. Thus, in contrast to the approaching curve where bending forces are solely due to the increasing proximity of the cantilever with the probe, additional adhesion forces are present in the retracting regime while the cantilever is retracted in the z-axis from the sample. As the AFM probe is pulled out of contact with the sample, it first gets “stuck” before it is able to loosen from the adhesion at the interface, which even leads to a short negative deflection of the cantilever. The AFM probe and its subsequent bending up or down and the unperturbed position of the AFM probe are also displayed in blue.

Abbreviation: AFM-atomic force microscopy

The focus of the thesis was to apply a customized AFM approach on load-bearing connective tissue/cells, particularly articular cartilage and bone cells. This was done in order to determine and differentiate between possible structural-functional changes in the biomechanical properties (Young’s moduli) of the encompassing matrix/-es of the targeted tissue/cells. In the first research part, the changes that occur due to alterations in the biochemical signatures of the tissues due to ongoing pathological processes such as osteoarthritis (OA) were investigated. The second research analyses, the changes in the culture settings of the jaw periosteum derived progenitor cells (JPCs), such as media supplementation (human platelet lysate (hPL) versus fetal calf serum (FCS)) were examined.

### ***1.1. Biomechanical properties of cartilage and their role in osteoarthritis***

Osteoarthritis (OA) is a degenerative joint disease that affects large parts of the elderly population. Since there is thus far no defined cut-off threshold for the diagnosis of OA, the condition is difficult to quantify. The incidence of symptomatic knee OA is estimated to be around 1% per year, with a radiographic incidence of about 2% per year (Felson et al., 1995, Oliveria et al., 1995). This results in an overall prevalence of the disease in nearly 50% of adults aged 75 and above (Jordan et al., 2007). OA leads to reduced flexibility and mobility of the joint, and to load-dependent joint pain that can severely disable the patient, which also results in a high socio-economic burden. Risk factors for OA are trauma, systemic inflammatory diseases, bacterial infections, metabolic factors such as obesity, and mechanical factors (Felson, 2009). To date, conservative joint preserving therapies such as pain management, physiotherapy, or local infiltrations cannot restore the original joint architecture. They only serve to alleviate the pain, to help patients cope with the emerging symptoms, and to postpone the disease progression (Huey et al., 2012, Djouad et al., 2009).

Even though OA comprises the capsula and ligaments of the joint, as well as the subchondral bone, the primary tissue destroyed throughout the degenerative process of OA is the articular cartilage. The only cells present within the mature articular cartilage are the chondrocytes, which form specific, unique, and easily distinguishable spatial cellular patterns. These patterns are specific for each joint, as well as the joint's loading mechanism (Rolauffs et al., 2008, Schumacher et al., 2002). In healthy tissue areas, chondrocytes are arranged as single strings in the femoral condyle, and with the onset and progression of degenerative changes during OA, cellular rearrangement occurs: first double strings arise (Rolauffs et al., 2010), followed by clustering of the cells in small and then finally in big clusters (Lotz et al., 2010) (Figure 3).

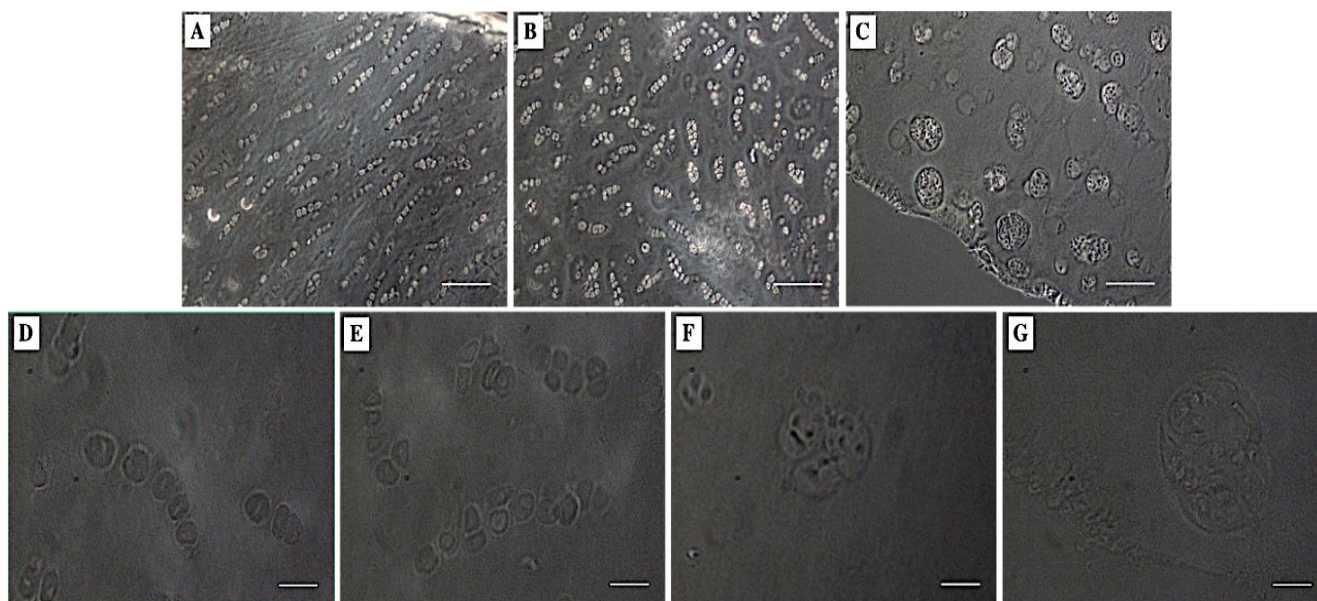


**Figure 3. Light microscopy pictures of chondrocyte rearrangement throughout the course of OA.**

While in healthy cartilage, single strings are present (A/D), OA initiation and progression triggers the occurrence of double strings (B/E), small clusters (F), and ultimately big clusters (C/G).

(A-C) Scale bar (white) measuring 100 $\mu$ m; (D-G) Scale bar (white) of 20 $\mu$ m.

Figure partially adapted from (Danalache et al., 2019).

These remodelling cellular processes have previously been suggested to have potential as an “image-based biomarker” for OA-promoted degenerative processes occurring at a cellular level (Aicher and Rolaufts, 2014). Like in any other connective tissue, cartilage is comprised of a vast and dense ECM. The ECM-arciform collagen fibers not only take their origin but also terminate in the subchondral bone. These fibers possess an enormous tensile strength and keep a large amount of proteoglycans entrapped, which in turn can bind water molecules; in such providing the necessary compressive resilience and elasticity to the tissue.

Within the articular cartilage, there are three different major zones: the superficial, the middle, and the deep zone. Each can be distinguished based on differences in cellular morphology (Kuettner et al., 1991), composition of collagen (Nieminen et al., 2001), content of glycosaminoglycans (Venn and Maroudas, 1977), and water content (Maroudas and Venn, 1977). Within all the layers, a pericellular, a territorial, and an interterritorial matrix (all ramifications of the ECM) are present. The pericellular matrix (PCM) encompasses the chondrocytes and is both biochemically and biomechanically distinct from the ECM.

While the ECM is mainly comprised of collagen type II, the PCM is primarily defined by the presence of collagen type VI (Guilak et al., 2006) and proteoglycans. The PCM, together with the enclosed cell(s), have previously been termed the "chondron"-also known as the metabolic unit of the tissue (Poole, 1997). The PCM is believed to act as a mechano-sensitive cell-matrix interface (Guilak et al., 2006), protecting the chondrocyte (Peters et al., 2011), and modulating its biosynthetic response (Larson et al., 2002). Additionally, the PCM plays a functional role in initiating signal transduction within cartilage under load bearing (Eggli et al., 1985). The territorial matrix (TM) surrounds the PCM, and is composed mostly of fine collagen fibrils, creating a basketlike network around the cells (Muir, 1995, Sophia Fox et al., 2009). It has been suggested that the TM protects the chondrocytes against mechanical stresses, and that it plays a role in the resiliency of articular cartilage (Sophia Fox et al., 2009). In addition to the TM, the interterritorial matrix (ITM) is comprised of randomly oriented bundles of large collagen fibrils that run parallel to the surface of the superficial zone, obliquely in the middle zone, and perpendicular to the joint surface in the deep zone of the tissue (Sophia Fox et al., 2009). The ITM has a high content of proteoglycans, and contributes to the biomechanical properties of the tissue (Mow and Guo, 2002).

OA onset is characterized by a biosynthetic phase, during which the chondrocytes attempt to repair the damaged ECM, followed by a later degradative phase, in which matrix synthesis inhibition and digestion by catabolic enzymes leads to collagen network damage and subsequent matrix fissuring, erosion, and ultimately tissue loss (Sandell and Aigner, 2001, Mankin et al., 1971, Brama et al., 2000, Howell, 1986, Hamerman, 1989). Additionally, it must be borne in mind that articular cartilage is a load bearing tissue. The biomechanical properties are thus of crucial importance for normal functioning of the tissue, especially for the smooth gliding of its surfaces against one another under load. This function is greatly impaired after initial disruption of the tissue architecture, thus leading to increased friction, which in turn propagates tissue destruction in a vicious circle. Intact biomechanical properties of articular cartilage are, naturally, derived from its intact matrixes. OA progression is hence characterized by extensive proteolysis of the type II collagen network and the proteoglycans of the ECM, leading to a loss of mechanical properties (Plaas et al., 2007, Hollander et al., 1995).



Interestingly, OA also triggers early changes in the presence and amount of collagen type VI of the PCM (Felka et al., 2016b). Moreover, proteoglycan distribution within the chondron changes, which is in turn followed by chondrocyte proliferation coupled with expansion and structural alterations of the pericellular microenvironment, and ultimately chondrocyte clustering (Poole et al., 1997). These changes affect the biomechanical signals perceived by the chondrocytes (Guilak et al., 2006), explaining how PCM damage potentially contributes to the ongoing OA-pathology. Recently, OA has even been characterized as being a disease of the PCM (Guilak et al., 2018). The mechanical properties of the cartilage (stiffness, hardness, dynamic Young's modulus, etc.) therefore play an important role in OA initiation and progression. The mechanical properties of the cartilage have been investigated at all length scales (from macro to nano-scale), and all the results obtained notably and consistently illustrated that cartilage properties with respect to tension, compression, and shear forces decline with OA progression (Wilusz et al., 2014).

Several studies have indicated that the stiffness, and implicitly Young's modulus of cartilage is a strong indicator of its material-bearing properties, crucial for joint lubrication and function (Kiviranta et al., 2008, Korhonen et al., 2002). Young's modulus is thus an attribute of cartilage elasticity, indicating its stiffness. A decrease in qualitative stiffness of cartilage in the course of OA was highlighted in various studies by analyzing the mechanical properties of both native and osteoarthritic cartilage in humans or animal models (Kleemann et al., 2005, Desrochers et al., 2010, Vinckier and Semenza, 1998). It must be noted, however, that all of the reported findings until now have been based on macroscopic classification systems for grading the osteoarthritic changes of the cartilage (Wilusz et al., 2012b, McLeod et al., 2013, Kleemann et al., 2005, Kiviranta et al., 2008). As such, cartilage surface parameters were used to grade the tissue, thus, only allowing for the assessment of the micromechanical picture at an average level. The AFM-elasticity measurements guided by more specific OA markers on a cellular level-such as the cellular patterns can, therefore, provide new insights into the actual biomechanical changes occurring during OA. This may refine and improve our current understanding of OA physiopathology.

## ***1.2. Role of biomechanical properties in bone tissue engineering***

In the field of oral and maxillofacial surgery, bone defects in the oral cavity as a result of congenital anomaly, trauma, periodontal disease, chronic infection, or surgical resection following tumor treatment require extensive clinical attention. The current medical practice still faces several significant challenges (Smith et al., 2015), especially when attempting to regenerate the affected tissue and restore its initial function and aesthetics.

Artificial bone tissue constructs represent an essential part of bone tissue engineering (BTE). The basic principle of such artificial constructs is to create a porous scaffold functionalized with a cellular component. The biological functional unit of such constructs is therefore the selected cells, which adhere to and grow on the surface of the implanted scaffold. The goal of the scaffolds is to provide a tissue-like environment, which helps the cells generate the normal biological structural components of their tissue-specific ECM. In both articular cartilage and bone, the ECM provides essential structural support for its cellular constituents, but it also modulates the mechanical properties and the overall performance and efficacy of the tissue. For the design of functional scaffolds for osseous engineered tissues, cell-ECM mechanical properties, structural, and biological characteristics must be taken into consideration. In a native state, the ECM provides the structural support for cell attachment and subsequent tissue development. The main challenge in engineering the constructs is to mimic these ECM properties. To date, the use of engineered scaffolds made of artificial or native materials often fails to allow for the formation of intact cell-cell junctions due to the unnatural cellular surface properties (Kim et al., 2016, Yang and Temenoff, 2009). To overcome this striking limitation, polymeric scaffolds can be replaced by an ECM, which is actually produced by the seeded cells as in native tissue. The final construct could thus closely mimic the ECM architecture of target tissues with respect to both structure and function. An extensive repertoire of scaffold materials ranging from metallic, synthetic, polymeric, bio-polymeric, and smart hydrogel in various forms and compositions have been investigated in the context of bone regeneration. The incorporation of cells and the application of growth factor delivery strategies can significantly influence the regenerative outcome. In terms of cellular components, current strategies include different cell





types, such as osteoblasts, periosteal cells, bone-marrow stromal cells, and stem cell varieties, including mesenchymal stem cells (MSCs). MSCs represent a leading cell type for the majority of regenerative medical purposes due to their self-renewal and their potential for differentiation into different lineages (Fitzsimmons et al., 2018).

When it comes to bone scaffolds, the current state of the art is, however, the use of periosteum progenitor cells (Chang and Knothe Tate, 2012). Particularly in the field of maxillofacial surgery and orthopaedics, a strong emphasis is placed on jaw periosteum derived progenitor cells (JPCs). These JPCs are suitable due to their easy availability and their multipotent capacity at a single cell level (De Bari et al., 2006), coupled with a high proliferation rate (Bruder et al., 1997). Clinically applicable cell-based therapies, particularly tissue constructs intended for maxillofacial reconstruction are focused on the use of patient derived JPCs. Especially in view of the requirements for good manufacturing practice (GMP) to ensure safety and efficacy (Fekete et al., 2012), a detailed characterization of the cells, their expression patterns, and formed matrix compositional signature, coupled with optimized culture conditions for differentiation are essential. In this context, the use of fetal calf serum (FCS) media supplementation is discouraged by regulatory authorities to limit the risk of immune reactions in the transplanted host, and also due to animal welfare concerns. Consequently, substantial efforts have been made in the last 15 years to identify a substitute for FCS supplementation. Recently, human platelets lysate (hPL) has been suggested to be a suitable and effective alternative, outperforming the former FCS supplementation (Tylek et al., 2019). It has been suggested that hPL superiority is due to various growth factors, including platelet-derived growth factor (PDGF), transforming growth factor (TGF), and epidermal growth factor (EGF) (Antoninus et al., 2015), which enhance the proliferation rate of the MSCs while maintaining their multilineage differentiation potential under culture (Hemeda et al., 2014). However, despite aforementioned significant progress in cell-based therapies, critical challenges remain in transitioning the *in vitro* use of JPCs into clinically-applicable approaches. Our present understanding is still limited with respect to the precise biomechanical properties, the biological composition, and the functional performance of the proposed procedures. Specifically, the repair or regeneration processes of tissues are not yet fully understood at a macroenvironment level (scaffold collapse and

on-the-shelf availability) as well as at a microenvironment level (e.g. cell migration, and qualitative ECM formation) (Yuksel et al., 2005).

Although the biomechanical characteristics of the ECM in bone constructs (including mechanobiology and mechanotransduction) have become an active research field, relatively few published studies have investigated the biomechanical properties of JPCs (Horimizu et al., 2013, Att et al., 2009). Especially the analysis of elastic adaptability characteristics, as well as the corresponding biochemical signature (e.g. Raman spectroscopy) of JPCs cultured under hPL media supplementation comparing the results with those obtained with the standard FCS conditions, has not yet been investigated.

Both AFM and Raman spectroscopy are methods used to obtain data about the surface properties of a sample. A combination of these methods could provide crucial correlated morphological and chemical information. While the AFM is based on tip-sample interactions at discrete locations in a sequential manner, in RAMAN spectroscopy, monochromatic light is focused on the sample, and the inelastic scattered light (the Raman effect) is detected. The latter generates a molecular fingerprint of the investigated sample based on the detection of specific wavelength shifts caused by chemical bond vibrations (Kunstar et al., 2013). Raman spectral studies have already been performed for the identification of cell phenotype (Puppels et al., 1990), for assessment of malignancy (Ramos et al., 2015), and for structural analysis of ECM components, such as collagen (Frushour and Koenig, 1975), sulfated glycosaminoglycans (sGAGs), and proteoglycans (Ellis et al., 2009). In mineralized tissue, the technique can detect the vibrations obtained from the collagenous matrix. Even more so, it can give valuable insights with respect to the biochemical structure of the bone, and more importantly the contribution of various matrix proteins on the bone material properties (Bonewald et al., 2003a). Using the combination of Raman microscopy with AFM, the high spatial and topographical resolution obtained with an AFM can be directly linked to the molecular information provided by the Raman spectroscopy. Such an experimental design comprised of AFM coupled with Raman spectroscopy-which may be employed for JPCs investigations, for example is shown in Figure 4.

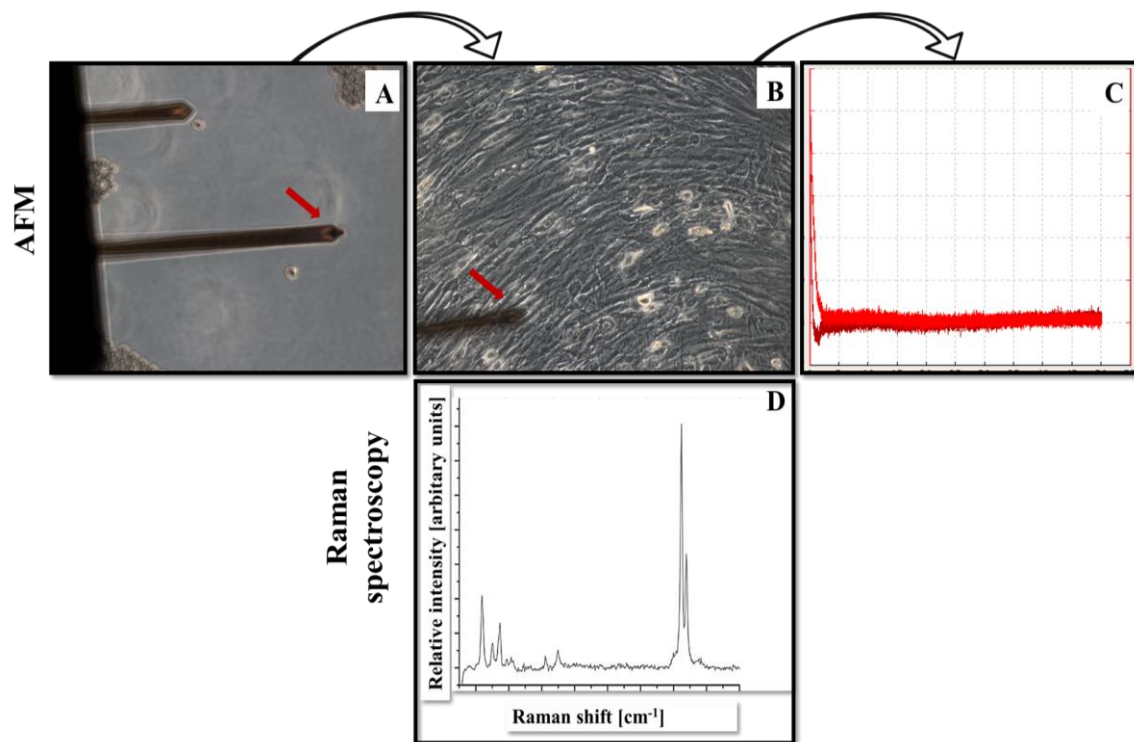


**Figure 4. Experimental setup for biomechanical and biochemical characterization of JPCs**

Biomechanical properties are assessed via AFM-contact mode technique (A/B/C). A polymeric bead (25µm) is attached to an AFM cantilever (A) in order to protect the analyzed cells (B) from contact damage, and to increase the surface area to be measured. By fitting the data generated from the resulting force-distance curve (C), the elastic modulus (EM) can be calculated using the Hertz fit model. Raman spectroscopy can be used for non-invasive sensing of the biochemical composition of the cells and the ECM. It generates a Raman spectrum, which features peaks—each peak corresponds to a specific molecular bond vibration (D).

Abbreviations: AFM—atomic force microscopy, ECM—extracellular matrix, EM—elastic modulus, JPCs—jaw periosteal cells.

It can therefore be summarized that a better biochemical and biomechanical characterization of the JPCs-ECM is still needed to improve the use of these cells for regenerative scaffolds.

### 1.3. Aim of the thesis

The biomechanical characteristics of tissues and of regenerative tissue scaffolds are of crucial importance to their normal in vivo performance. Of note, their biological and mechanobiological characteristics are not just of a passive nature, but they are also critical for regulating cell behavior. Alterations in the mechanical characteristics can occur

as a result of aging, trauma, or disease. These changes directly translate into tissue dysfunction. For this reason, it is crucial to understand the role of the mechanical cues (e.g. elasticity) and their relationship with the structural composition of the tissue. Especially as the role and involvement of the different biomechanical properties in the successful outcome of regenerative processes is not yet fully understood (Guilak et al., 2014a). Manipulating biomechanical features may help to better understand, and in the long run to also produce improved regenerated tissues with high strength and endurance. In this setting, AFM has been emerging as a highly versatile, non-invasive, and interdisciplinary technique that allows for a quantitative and qualitative biomechanical analysis of living cells, tissues, and engineered constructs at a very high resolution. In this study, a customized AFM approach was employed to investigate and quantitatively assess the biomechanical characteristics of:

- (1) pericellular matrix (PCM) degradation in early OA;
- (2) jaw periosteal cells (JPCs)-ECM quality under different media supplementation;

The hypothesis of the first study (1) was that tissue changes in the cellular organizational patterns during OA (strings, double strings, and small respectively big clusters) are associated with structural changes of the PCM and with a loss of elastic properties. Such an association between OA related spatial cellular organization and changes in the local EM accompanied by structural changes of the PCM would also underline the functional role of spatial organization as an image-based biomarker for OA. A better insight into early OA mechanisms, particularly structural and mechanical changes of the PCM, may facilitate our understanding of the patho-mechanism of the disease, and would thus, help the development of better targeted therapies and diagnostic strategies.

The hypothesis of the second study (2) was that hPL substitution leads to a better ECM quality in terms of biochemical composition and biomechanical characteristics in JPCs when compared to FCS. In order to evaluate the suitability of JPCs cultivated under hPL supplementation for *in vitro* culturing and osteogenic differentiation, quantitative and qualitative analysis of the ECM produced by the JPCs under hPL versus FCS supplementation was performed both biochemical (RAMAN spectroscopy) and biomechanical (AFM-elasticity measurements).



As the focus of this study was placed on bone tissue constructs, the ECM formed by JPCs should mimic a “bone-like” structure and show similar biochemical and biomechanical functions.

The research projects presented in this thesis have already been published and will be presented in the following order:

1. **Danalache, M.**, Kleinert, R., Schneider, J., Erler, A.L., Schwitalle, M., Riestter, R., Traub, F., Hofmann, U.K., 2019. Changes in stiffness and biochemical composition of the pericellular matrix as a function of spatial chondrocyte organisation in osteoarthritic cartilage. *Osteoarthritis and cartilage* 27, 823-832. 2018 impact factor (IF): 4.9.
2. **Danalache, M.**, Kliesch, S.M., Munz, M., Naros, A., Reinert, S., Alexander, D., 2019a. Quality Analysis of Minerals Formed by Jaw Periosteal Cells under Different Culture Conditions. *International journal of molecular sciences* 20. 2018 IF: 4.2.



## 2. Results

### 2.1. Biomechanical cues of pericellular matrix degradation in osteoarthritic cartilage

Osteoarthritis and Cartilage 27 (2019) 823–832

## Osteoarthritis and Cartilage



### Changes in stiffness and biochemical composition of the pericellular matrix as a function of spatial chondrocyte organisation in osteoarthritic cartilage



M. Danalache †, R. Kleinert †, J. Schneider †, A.L. Erler †‡, M. Schwitalle §, R. Riester †, F. Traub † ||, U.K. Hofmann † ||\*

† Laboratory of Cell Biology, Department of Orthopaedic Surgery, University Hospital of Tübingen, Waldhörnlestraße 22, D-72072 Tübingen, Germany

‡ Medical Faculty of the University of Tübingen, D-72076 Tübingen, Germany

§ Wingofer Medicum, Röntgenstraße 38, D-72108 Rottenburg am Neckar, Germany

|| Department of Orthopaedic Surgery, University Hospital of Tübingen, Hoppe-Seyler-Strasse 3, D-72076 Tübingen, Germany

#### ARTICLE INFO

##### Article history:

Received 17 June 2018

Accepted 20 January 2019

##### Keywords:

Osteoarthritis

Cellular organisation

Articular cartilage

Pericellular matrix

Atomic force microscopy

Stiffness

#### SUMMARY

**Objective:** During osteoarthritis (OA), chondrocytes seem to change their spatial arrangement from single to double strings, small and big clusters. Since the pericellular matrix (PCM) appears to degrade alongside this reorganisation, it has been suggested that spatial patterns act as an image-based biomarker for OA. The aim of this study was to establish the functional relevance of spatial organisation in articular cartilage.

**Method:** Cartilage samples were selected according to their predominant spatial cellular pattern. Young's modulus of their PCM was measured by atomic force microscopy (AFM) (~500 measurements/pattern). The distribution of two major PCM components (collagen type VI and perlecan) was analysed by immunohistochemistry (8 patients) and protein content quantified by enzyme-linked immunosorbent assay (ELISA) (58 patients).

**Results:** PCM stiffness significantly decreased with the development from single to double strings ( $p = 0.030$ ), from double strings to small clusters ( $p = 0.015$ ), and from small clusters to big clusters ( $p < 0.001$ ). At the same time, the initially compact collagen type VI and perlecan staining progressively weakened and was less focalised. The earliest point with a significant reduction in protein content as shown by ELISA was the transition from single strings to small clusters for collagen type VI ( $p = 0.016$ ) and from double strings to small clusters for perlecan ( $p = 0.008$ ), with the lowest amounts for both proteins seen in big clusters.

**Conclusions:** This study demonstrates the functional relevance of spatial chondrocyte organisation as an image-based biomarker. At the transition from single to double strings PCM stiffness decreases, followed by protein degradation from double strings to small clusters.

© 2019 Osteoarthritis Research Society International. Published by Elsevier Ltd. All rights reserved.

#### Introduction

Articular cartilage is a specialised anisotropic connective tissue<sup>1</sup> composed of three layers: superficial, middle, and deep. Each of

these layers is characterised by unique structural, functional, and biomechanical properties. Within the cartilage, chondrocytes form specific spatial patterns that are characteristic of each joint<sup>2,3</sup> and that appear to depend on joint-specific loading mechanisms<sup>4</sup>. The

**Abbreviations:** AFM, atomic force microscope; BC, big clusters; DS, double strings; DMEM, Dulbecco's modified Eagle's medium; ECM, extracellular matrix; ELISA, enzyme-linked immunosorbent assay; FDR, false discovery rate; OA, osteoarthritis; PBS, phosphate-buffered saline; PCM, pericellular matrix; SC, small clusters; SS, single strings.

\* Address correspondence and reprint requests to: Laboratory of Cell Biology, Department of Orthopaedic Surgery, University Hospital of Tübingen, Waldhörnlestraße 22, D-72072 Tübingen, Germany.

**E-mail addresses:** danalachemarina@yahoo.com (M. Danalache), robinkleinert@web.de (R. Kleinert), 95janineschneider@gmail.com (J. Schneider), anna-lisa-erler@web.de (A.L. Erler), m.schwitalle@winghofer-medicum.de (M. Schwitalle), rosa.riester@med.uni-tuebingen.de (R. Riester), frank.traub@med.uni-tuebingen.de (F. Traub), ulf.hofmann@med.uni-tuebingen.de (U.K. Hofmann).

<https://doi.org/10.1016/j.joca.2019.01.008>

1063-4584/© 2019 Osteoarthritis Research Society International. Published by Elsevier Ltd. All rights reserved.



predominant physiological cellular pattern found in the femoral condyle is that of single strings<sup>5</sup>. With osteoarthritis (OA) initiation and progression, spatial chondrocyte organisation changes: rearrangement can be observed from single strings to double strings<sup>6</sup>, followed by small clusters, and finally big clusters<sup>7</sup>. In end-stage tissue degeneration, huge chondrocyte clusters are enclosed in densely packed tissue that is not well characterised<sup>8,9</sup>. This reorganisation of cellular spatial patterns has been suggested to act as an image-based biomarker for OA events occurring at a cellular level<sup>4</sup>.

Characteristic for articular cartilage is the presence of a distinct and unique structure termed the pericellular matrix (PCM). The PCM has been primarily defined as the presence of collagen type VI<sup>10,11</sup>. It encompasses the chondrocytes, thus forming the structural, functional, and metabolic unit of articular cartilage termed the “chondron”<sup>12</sup>. Other key components of the PCM are the heparin-sulphate proteoglycan perlecan<sup>13</sup>, aggrecan monomers<sup>14</sup> and aggregates<sup>15</sup>, laminin<sup>16</sup>, fibronectin<sup>17</sup>, hyaluronan<sup>18</sup>, biglycan<sup>19</sup>, and collagen type IX<sup>20</sup>. The PCM acts as a mechano-sensitive cell matrix interface, protects the chondrocytes from apoptosis, and modulates biosynthetic response<sup>21–23</sup>. In contrast to the extracellular matrix (ECM), the PCM contains higher concentrations of proteoglycans<sup>24</sup>, because, for example, the ECM proteoglycans biglycan and decorin bind near the N-terminal region of the collagen type VI triple helix<sup>25</sup>. The mesh-like capsule of the PCM defines its mechanical properties<sup>26</sup>, which also determines the stiffness of the cartilage. Interestingly, the compressive mechanical properties also seem to depend on the position of the chondron within the cartilage<sup>27</sup>.

OA onset is associated with collagen fibril denaturation<sup>28,29</sup> accompanied by a loss of small and large proteoglycans<sup>30</sup>. Local changes in perlecan expression and content have also been reported during OA development<sup>31</sup>. The loss of these molecules is correlated with the presence and elevated activity of various matrix metalloproteinases<sup>32,33</sup>. As a result, despite the fact that the expression of collagen is upregulated<sup>34</sup>, the net amount of, for example, collagen type II in the ECM decreases<sup>35,36</sup>. Similar changes during OA have also been described specifically for collagen type VI: in the lower middle and upper deep zones of the articular cartilage, its expression and presence seems to increase; in the upper middle zone, it appears to be lost; and in the superficial zone, it shows heterogeneous expression<sup>7,37</sup>.

Our aim in the present study was to evaluate the biomechanical degenerative changes of the PCM from human articular cartilage explants through determination of Young's moduli (stiffness) by using the spatial organisation of chondrocytes as an image-based biomarker. To evaluate the biomechanical properties of articular cartilage, we used atomic force microscopy (AFM), which is a powerful technique that allows direct quantification of the biomechanical tissue properties *in situ* at a microscale with minimal risk of interfering with its natural physiological state<sup>38</sup>. We also analysed the associated changes in PCM composition by examining two of its main components: collagen type VI and perlecan. We hypothesised (I) that the more pathological the spatial chondrocyte arrangement, the lower the stiffness of the cellular microenvironment and (II) that the presence of collagen type VI and perlecan would decrease with increasing tissue destruction.

## Materials and methods

### Cartilage samples

Tissue was obtained from patients undergoing total knee arthroplasty in the Department of Orthopaedic Surgery of the University Hospital of Tuebingen, Germany, and the Winghofer-

clinic, Rottenburg a.N., Germany, for end-stage OA of the knee. Full departmental, institutional, and local ethical committee approval were obtained before commencement of the study (project number 674/2016B02). Written informed consent was received from all patients before participation.

### Tissue sample preparation for AFM testing

After surgery resection, the tissue was temporarily stored in serum-free Dulbecco's modified Eagle's medium (DMEM; Gibco, Life Technologies, Darmstadt, Germany) with 2 % (v/v) penicillin-streptomycin and 1.2 % (v/v) amphotericin B. Full-thickness articular cartilage samples were then collected and embedded in water-soluble embedding medium (Tissue-Tek O.C.T. Compound, Sakura Finetek, Alphen aan den Rijn, Netherlands). Sectioning of the topmost layer of articular cartilage (representing the first 300 µm) was performed with a Leica cryotome type CM3050S (Leica Biosystems, Wetzlar, Germany) with 35 µm thickness ( $n = 4$  cuts per patient). Cartilage slices were rinsed with phosphate-buffered saline (PBS) to remove the water-soluble embedding medium, glued (biocompatible sample glue, JPK Instruments AG, Berlin, Germany) onto tissue culture dishes (TPP Techno Plastic Products AG, Trasadingen, Switzerland), and covered with Leibovitz's L-15 medium w/o L-glutamine (Merck KGaA, Darmstadt, Germany) until AFM measurements. Processing of the cartilage samples and the AFM measurements was done immediately after tissue resection to reduce artefacts from swelling of the tissue.

### Biomechanical characterisation of the PCM via AFM

Elastic moduli of the PCM were assessed by using an AFM system (CellHesion 200, JPK Instruments, Berlin, Germany) integrated into an inverted phase contrast microscope (AxioObserver D1, Carl Zeiss Microscopy, Jena, Germany), which allowed simultaneous visualisation of the cartilage samples. This allowed us to measure specific cellular spatial patterns. Calibration of the cantilever was done on the retracted curve, and the spring constant was determined by using the thermal noise method incorporated into the device software (JPK Instruments, Berlin, Germany). Measurements were performed in force spectroscopy mode by recording single force–distance curves at the position of interest without laterally scanning the sample. For microscale indentation, a polymeric microsphere (25 µm in diameter, Polysciences, Inc., Warrington, PA, USA) was attached to an AFM cantilever (tip C,  $k = 7.4$  N/m, All-In-One-AI-TI, Budget Sensors, Sofia, Bulgaria). Indentation curves were sampled at 2 kHz, with a force trigger of ~300 nN and a velocity of 5 µm/s. To evaluate elastic properties of the PCM as a function of the cellular spatial organisation, we applied indentations over the chosen region of interest identified by microscopic examination (9 measurement repetitions/measurement site; two distinct cellular patterns/histologic cut) (Fig. 1). In case a pattern was not present on a histologic cut, this measurement was left out. Young's modulus was calculated from the force–distance curves by using the Hertz-fit model of the data processing software (JPK Instruments, Berlin, Germany). Young's modulus is the ratio of uniaxial force per unit surface in pascal divided by the adimensional proportional deformation of the examined tissue.

### PCM immunostaining

Following AFM measurements, cartilage samples were fixed with 4 % (w/v) paraformaldehyde in PBS for 30 min at room temperature, and then processed and labelled for collagen type VI and perlecan. Enzymatic pretreatment of samples was done as

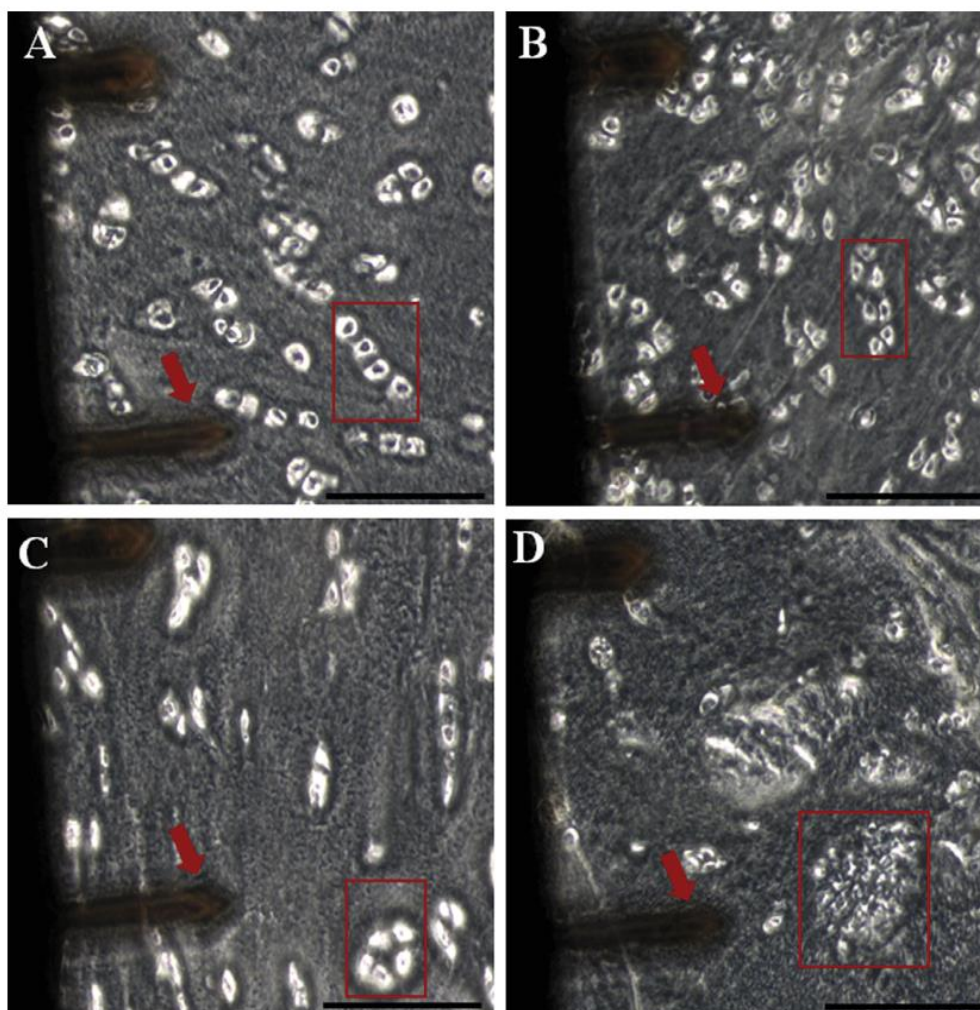


**Fig. 1.** Light microscopy pictures indicating regions of interest, atomic force microscopy (AFM) pictures showing the distinct cellular spatial patterns of strings (A), double strings (B), small clusters (C), and big clusters (D) (red box). Red arrow showing the cantilever that was used. Scale bar (black) represents 150  $\mu\text{m}$ .

previously described<sup>39,40</sup> with some modifications. Briefly, histological sections were pretreated with 0.1 % (w/v) hyaluronidase (Sigma–Aldrich, Taufkirchen, Germany) for perlecan staining and 0.2 % (w/v) collagenase type XI (Sigma–Aldrich, Taufkirchen, Germany) for collagen type VI staining in PBS at 37°C for 1 h, followed by three washing steps with PBS. Sections were incubated with a mix of 5 % (w/v) bovine serum albumin and 0.3 % (v/v) Triton X-100 in PBS as a blocking agent for 30 min, followed by incubation with collagen type VI (rabbit anti-collagen VI, ab-182744, Abcam, Cambridge, UK) and perlecan (mouse anti-perlecan, sc-377219, Santa Cruz Biotechnology Inc., Dallas, TX, USA) primary monoclonal antibodies at a dilution of 1:100 in 2.5 % (w/v) bovine serum albumin-PBS overnight at 4°C in a humidity chamber. Afterwards, sections were incubated with secondary antibodies (Alexa Fluor 555 goat anti-rabbit IgG, a-21429, Thermo Scientific, Waltham, MA, USA, and Alexa Fluor 594 goat anti-mouse IgG, ab-150116, Abcam, Cambridge, UK) for 2 h with a dilution of 1:100 at room temperature in the dark. Nuclear staining was performed with 1 % (v/v) DAPI in PBS for 5 min prior to imaging. Fluorescence-stained tissue sections were visualised with a Carl Zeiss Observer Z1 fluorescence microscope (Carl Zeiss Microscopy, Jena, Germany).

#### Tissue preparation for biochemical quantification of the PCM

Thin pieces of articular cartilage were cut with a scalpel blade no. 21 from the surface of the femoral condyle. A self-made cutting device was used to generate 300  $\mu\text{m}$  discs of tissue representing the top-most layer of articular cartilage. Fresh-cut pieces of articular cartilage from each patient were stained with 4 $\mu\text{M}$  Calcein AM fluorescence dye (Cayman Chemical, Ann Arbor, Michigan, USA) in serum-free DMEM (Gibco, Life Technologies, Darmstadt, Germany) with 2 % (v/v) penicillin-streptomycin and 1.2 % (v/v) amphotericin B for 30 min at 37°C. Calcein-stained samples were visually classified and sorted according to their predominant cellular spatial patterns<sup>41</sup> by using a fluorescence microscope (Leica DM IMBRE, Germany). Discs were then assigned to each of the four individual cellular spatial pattern groups. The discs were then snap-frozen in liquid nitrogen and stored at  $-80^{\circ}\text{C}$  until further analysis.

#### Assessment of PCM components by enzyme-linked immunosorbent assay (ELISA)

Frozen cartilage explants from each group were crushed with a pestle and mortar under liquid nitrogen and placed on ice for





15 min in homogenisation buffer (25 mM Tris–HCl pH 7.5, 100 mM NaCl, 1 % (v/v) IGEPAL CA-630) supplemented with proteinase inhibitors. A soluble fraction was obtained by centrifugation at 15,000g for 15 min at 4°C. For normalisation of the amount of tissue, aliquots were first analysed for total protein concentration by Bradford protein assay (Bio-Rad Laboratories, Richmond, CA, USA). A total of 15 µg of protein for each individual cellular pattern was subjected to sandwich ELISA for collagen type VI (MyBiosource Inc., San Diego, CA, USA) and 10 µg of protein for perlecan (BIOZOL Diagnostica Vertrieb GmbH, Eching, Germany) following the manufacturer's protocol. Absorbance was recorded at 450 nm by using an EL 800 reader (BioTek Instruments GmbH, Bad Friedrichshall, Germany). Protein content was calculated from the absorbance according to the prior established protein specific standard absorption curve. Three independent measurements of the ELISA assays were performed for each spatial pattern.

### Statistical analysis

Normality of the data was assessed by histograms. For further analyses, the median of the nine AFM measurements per measurement site was used. Extreme values were screened and filtered by the 2-standard deviation (SD) method. Depending on normality, values are presented as median (minimum–maximum) and graphically displayed as boxplots, or as mean (SD) and graphically displayed as bar diagrams. Even though our AFM results were not normally distributed, the mean, SD, and standard error of the mean of the AFM data are additionally displayed (Table II) to allow a direct comparison of our results with those reported in the literature.

To further analyse the results, the same approach and assumptions were employed as described previously by Wilusz et al.<sup>42</sup>: Briefly, each median of the nine AFM measurements per measurement site was treated as an independent value within each group of cellular spatial pattern. This assumption could be made as cartilage biomechanical properties display “greater variations spatially than among individuals”<sup>42</sup>. The biomechanical properties of the articular cartilage are prone to significant spatial variations

across the joint<sup>43</sup>, also varying with depth from the articular surface<sup>44</sup> and they are influenced by loading changes occurring during joint motion<sup>45</sup>. Since measured regions were chosen over the entire length of each sample and were not adjacent to one another, it is extremely unlikely that the measured regions within the same joint would have experienced the same biomechanical environment *in situ* or been influenced by each other.

Comparison between experimental results was therefore performed with the Kruskal–Wallis test by using the Mann–Whitney *U* test for *post hoc* analysis, or by one-way analysis of variance and *t*-test for independent samples as a *post hoc* test, as appropriate. Alpha adjustment on the basis of a significance level of 0.05 was performed for each calculation by using the Benjamini–Hochberg procedure. Statistical analysis was performed with SPSS Statistics 22 (IBM Corp., Armonk, NY, USA).

### Results

Articular cartilage samples from eight patients were subjected to elasticity measurements of the pericellular region via AFM. Thus, a total of 2070 measurements were done (single strings: 513, double strings: 504, small clusters: 531, big clusters: 522). After exclusion of extreme values, the median for 56 single strings, 52 double strings, 55 small clusters, and 55 big clusters were included in the final analysis. The measured PCM elastic moduli results are shown in Fig. 2 and Table I. Stiffness of the patterns significantly decreased along the entire scale of patterns from single strings to double strings ( $p = 0.030$ ), from double strings to small clusters ( $p = 0.015$ ), and from small clusters to big clusters ( $p < 0.001$ ). Absolute values were thereby reduced by 84 % with a median of 38 kPa for single strings to a median of 6 kPa for big clusters.

In the immunofluorescence analysis, healthy tissue areas represented by single strings exhibited a PCM composed of densely compact, intact, and well-defined collagen type VI [Fig. 3(A)] and perlecan [Fig. 3(E)]. With initiation and progression of tissue degeneration represented by the cellular pattern shift from single strings (Fig. 3(A/E)) to double strings (Fig. 3(B/F)) to small clusters (Fig. 3(C/G)) and eventually to big clusters (Fig. 3(D/H)), a change in staining localisation and integrity of collagen type VI was observed and, to a lesser extent, of perlecan: the PCM contour around the chondrocytes softened, especially for collagen type VI immunolabelling. Moreover, PCM staining of collagen type VI no longer exhibited a precise localisation restricted to the pericellular region of the chondrocytes; rather, it was scattered between the cells. By comparison, in advanced tissue degeneration represented by chondrocyte clustering (small and big clusters), perlecan was still present and localised in the PCM.

Tissue samples from 58 patients ( $n = 25$  for collagen type VI assays and  $n = 33$  for perlecan assays) were included in the ELISA analysis. Since not all patients presented all spatial patterns, 46–52 cartilage discs per pattern for collagen type VI and perlecan were used. Complementary to immunolabelling, quantitative ELISA analyses showed that the more pathological the cellular pattern, the more collagen type VI (Fig. 4(A)) and perlecan (Fig. 4(B)) decreased. The earliest point in the sequence of events where a significant reduction could be observed was the transition from single strings to small clusters for collagen type VI ( $p = 0.016$ ) and for perlecan ( $p = 0.008$ ) (Table III and Table IV). For both collagen type VI and perlecan, the lowest amounts were measured in big clusters.

### Discussion

The aim of this study was to evaluate whether stiffness of the PCM decreases as a function of OA initiation and progression by using the spatial arrangement of chondrocytes as an image-based

**Table I**  
Comparison of elasticity measurements (Young's modulus) as a function of cellular spatial organisation

Comparison	<i>P</i> -value	FDR-adjusted alpha values
All Groups	<0.001*	<0.001
SS–DS	0.030*	0.030
SS–SC	<0.001*	<0.001
SS–BC	<0.001*	<0.001
DS–SC	0.013*	0.015
DS–BC	<0.001*	<0.001
SC–BC	<0.001*	<0.001

\*Kruskal–Wallis test, \*Mann–Whitney *U* test. Abbreviations: SS – single strings; DS – double strings; SC – small clusters; BC – big clusters; FDR – false discovery rate.

**Table II**  
Stiffness measurements by atomic force microscopy (AFM)

Descriptive statistics	Cellular organisational pattern			
	SS	DS	SC	BC
Median	37.611	25.330	13.714	5.643
Minimum	5.447	2.581	0.500	0.332
Maximum	174.315	122.213	58.066	24.487
Mean	49.479	33.828	18.983	7.615
Standard deviation	40.376	29.159	14.161	5.849
Standard error	5.395	4.043	1.909	0.788

Values displayed in kPa. Abbreviations: SS – single strings; DS – double strings; SC – small clusters; BC – big clusters.

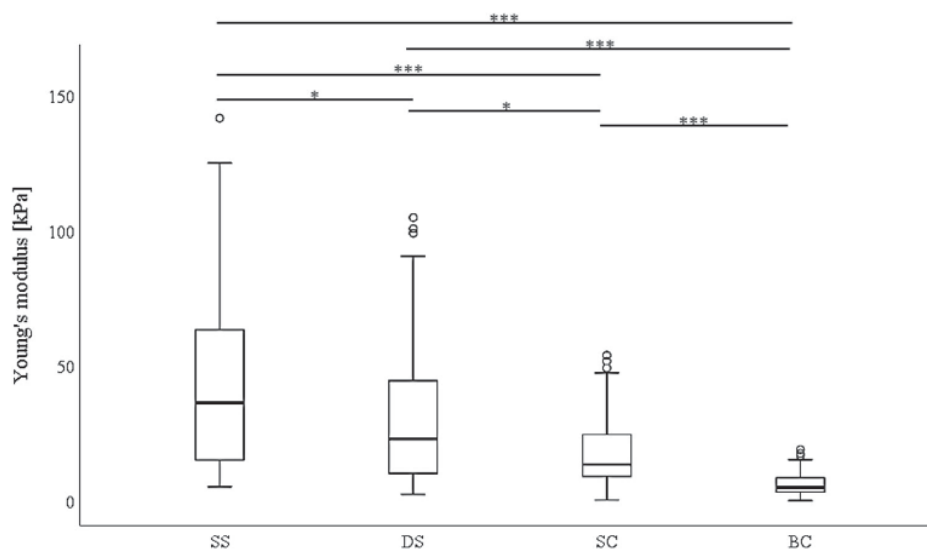


**Fig. 2.** Comparison of quantified Young's modulus of the pericellular matrix (PCM) as a function of cellular organisation. Boxplots of the stiffness measured by AFM of the different chondrocyte patterns. A continuous reduction of stiffness in the PCM during the rearrangement from the SS to the BC pattern can be observed. \* $p < 0.05$ ; \*\*\* $p < 0.001$  (for exact  $P$ -values, see Table 1). Abbreviations: SS – single strings; DS – double strings; SC – small clusters; BC – big clusters.

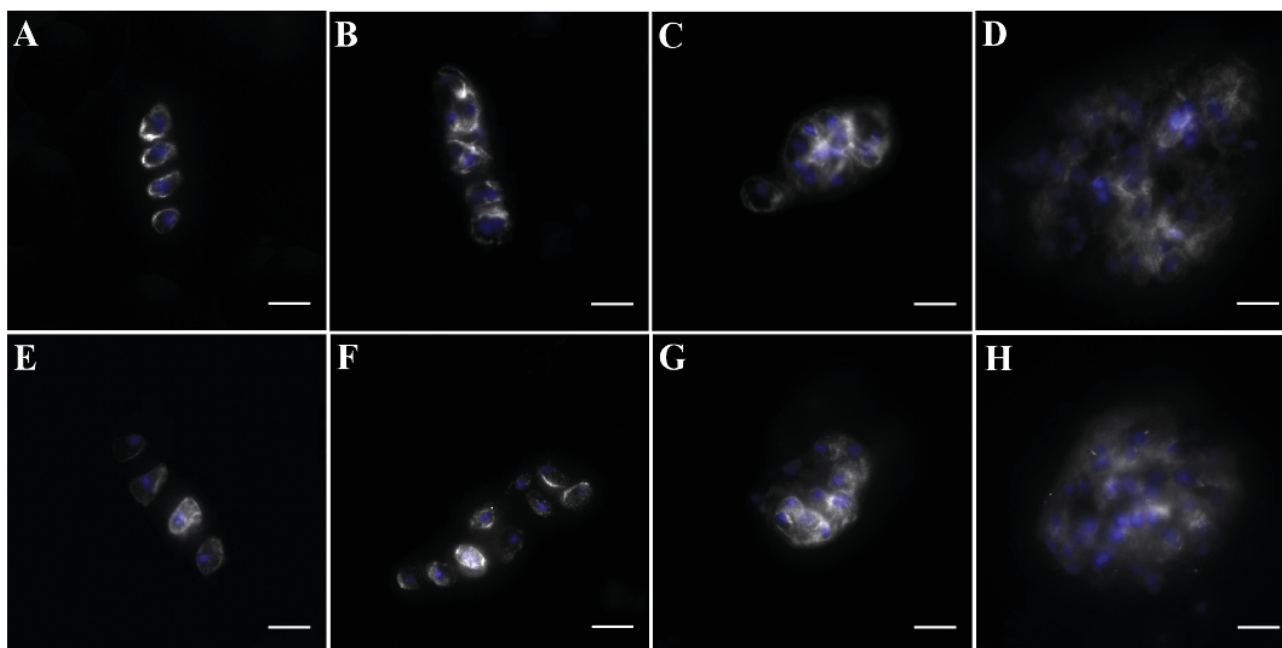


**Fig. 3.** PCM immunolabelling for collagen type VI and perlecan for the different cellular spatial patterns. Immunolabelled PCM with Alexa Fluor 555 anti-collagen type VI antibody (A–D) and Alexa Fluor 594 anti-perlecan antibody (A/E – single strings, B/F – double strings, C/G – small clusters, D/H – big clusters). While a decrease in collagen type VI from single strings to big clusters can be observed (A–D), the intensity of the decrease for perlecan is much less pronounced (E–H). 20-fold magnification, scale bar represents 20  $\mu$ m.

biomarker. We found that the more pathological the spatial arrangement of the chondrocytes, the lower the stiffness of the single chondron (hypothesis 1). This translates into a total difference in the mean of Young's modulus of 30 kPa (~60 %) between single strings and small clusters, and of 41 kPa between single strings and big clusters (~80 %). The results of our stiffness measurements of supposedly healthy cartilage (i.e., single strings) are comparable to data from previous publications for native healthy articular cartilage<sup>46,47</sup>. The same applies to small clusters when we compared them with the values obtained by Wilusz et al. (2013),

where the PCM from early OA cartilage was measured<sup>42</sup>. A comparable 30–40 % decrease in the PCM moduli was also reported when we measured chondrons extracted by micropipette aspiration of OA cartilage and of macroscopically intact tissue<sup>8,48</sup>. Interestingly, the earliest statistically significant decrease observed in our AFM data was at the first possible time point: the transition from single to double strings ( $p = 0.030$ , Table 1). Since double strings are a feature most commonly observed in macroscopically intact cartilage<sup>6</sup>, this underlines the biomechanical relevance of spatial organisation as a functional biomarker.

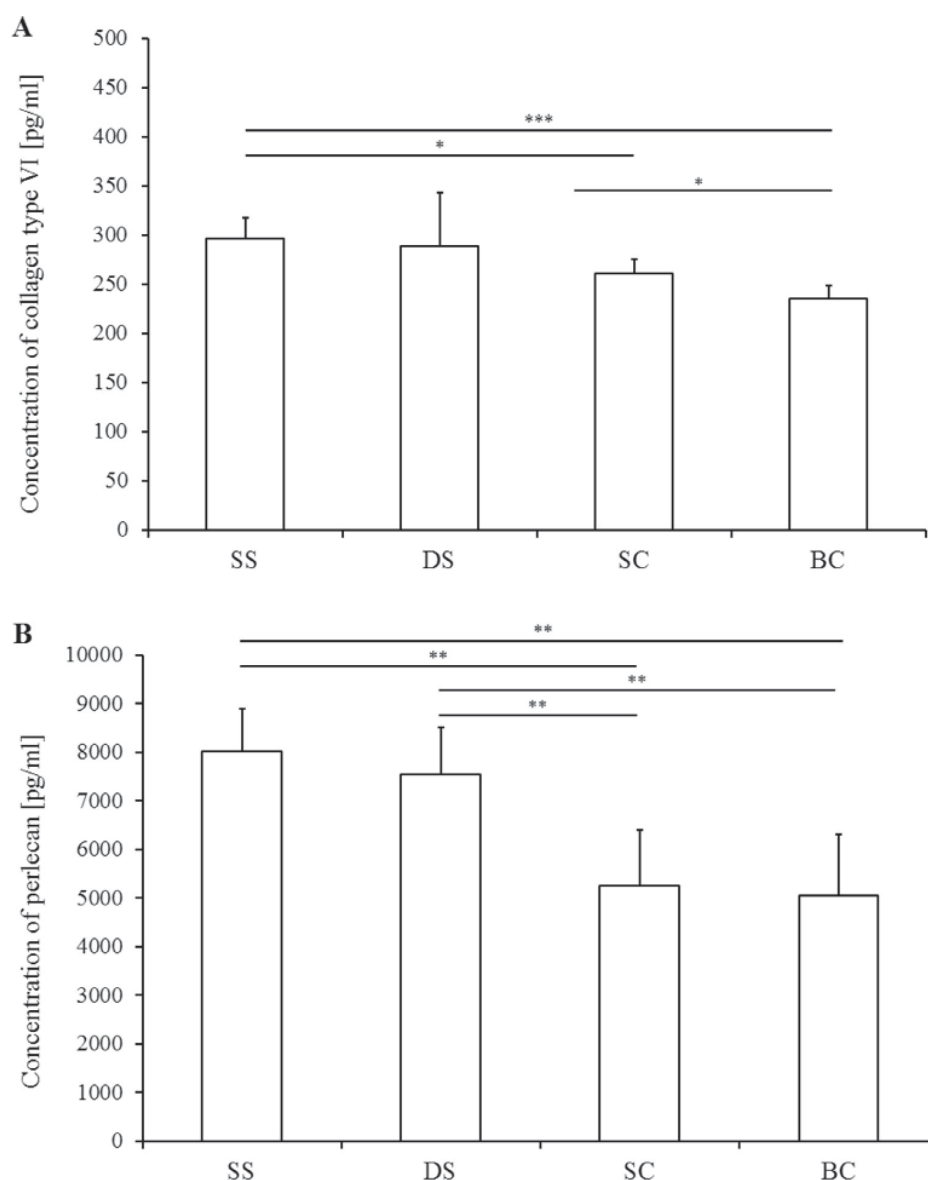


**Fig. 4.** Biochemical analysis of the PCM by quantification of collagen type VI and perlecan as a function of cellular pattern organisation. ELISAs performed with homogenised cartilage to quantify changes in content of collagen type VI (**A**) and perlecan (**B**) according to the predominant spatial cellular pattern. From single strings to big clusters, a decrease in collagen type VI and a significantly lower amount of perlecan can be observed in small clusters and big clusters compared with that in single strings and double strings. \* $p < 0.05$ ; \*\* $p < 0.01$ ; \*\*\* $p < 0.001$ . Abbreviations: SS – single strings; DS – double strings; SC – small clusters; BC – big clusters.

**Table III**

Comparison of ELISA assays for collagen type VI as a function of cellular spatial organisation

Comparison	P-value	FDR-adjusted alpha values
All Groups	0.010*	0.017
SS–DS	0.739°	0.739
SS–SC	0.007°	0.016
SS–BC	<0.001°	<0.001
DS–SC	0.267°	0.311
DS–BC	0.042°	0.058
SC–BC	0.004°	0.014

\*ANOVA, °t-test for independent samples. Abbreviations: SS – single strings; DS – double strings; SC – small clusters; BC – big clusters; FDR – false discovery rate.

**Table IV**

Comparison of ELISA assays for perlecan as a function of cellular spatial organisation

Comparison	P-value	FDR-adjusted alpha values
All Groups	0.002*	0.004
SS–DS	0.393°	0.458
SS–SC	0.001°	0.003
SS–BC	<0.001°	0.003
DS–SC	0.006°	0.008
DS–BC	0.003°	0.005
SC–BC	0.790°	0.790

\*ANOVA, °t-test for independent samples. Abbreviations: SS – single strings; DS – double strings; SC – small clusters; BC – big clusters; FDR – false discovery rate.

We also analysed the changes in PCM composition accompanying spatial rearrangement by examining two of its main components: collagen type VI and perlecan. As previously described, collagen type VI<sup>10,49</sup> and perlecan<sup>50</sup> were present at high levels in single strings representing healthy cartilage. As hypothesised (hypothesis II), ELISA analyses showed that the protein content decreased in conjunction with the spatial physiopathological model. In this case, the earliest point in the sequence of events with a significant protein content reduction was at the transition from single strings to small clusters for collagen type VI ( $p = 0.016$ ) and from double strings to small clusters for perlecan ( $p = 0.008$ ) (Tables III and IV). In the immunohistological analyses, the PCM contour around the chondrocytes also softened with increasingly pathological spatial organisation. In particular, in small and large clusters, collagen type VI and perlecan staining was no longer clearly restricted to the pericellular region, but also showed a diffuse blur between adjacent cells. The reasons for this observation remain, so far, speculative. The observed nonhomogeneous distribution of collagen type VI is most likely the consequence of nonhomogeneous degradation of collagen type VI occurring in OA<sup>37</sup>. The loss of perlecan from the PCM could be due to an inflammatory change in  $\beta 1$  integrin, as it is suggested to mediate interactions between the cell surface and perlecan<sup>51–53</sup>.

Several publications have linked the PCM to biomechanical functions in tensional and load-bearing connective tissue<sup>27,46,47,54–56</sup>, indicating that the PCM acts as transducer of mechanical and physicochemical signals<sup>21,57</sup> and that it is susceptible to OA triggered degenerative changes<sup>58</sup>. It has also been reported that collagen type VI<sup>59,60</sup> is reduced and perlecan is altered in OA<sup>31</sup>. We are the first, however, to describe these changes as a function of cellular spatial rearrangement. The decrease in PCM stiffness that is observed simultaneously with the reduction in collagen type VI and perlecan suggests that these two phenomena are linked to each other. This idea is supported by the observation that knockdown collagen type VI mice also exhibit lower PCM elastic moduli, and, at the same time, show increased chondrocyte swelling<sup>57</sup>. With respect to the role of perlecan, Xu *et al.* (2016) showed in a murine model of Schwartz-Jampel syndrome that perlecan knockdown alters matrix organisation and causes a reduction in stiffness<sup>61</sup>. In 2012, Wilusz *et al.* reported that isolated enzymatic depletion of perlecan increases PCM elastic moduli, pointing out the possible involvement of perlecan in biomechanical properties<sup>62</sup>. To explain this unexpected finding, they used the analogy of a spring system in series with a stiffer and a softer spring, where “the effective spring constant of the system is lower than the spring constant of either component<sup>62</sup>”. In our study, a decrease in perlecan led to a reduction in stiffness. Yet at the same time, we also observed a decrease in collagen type VI, which – continuing with Wilusz’s analogy – would also lower the second spring stiffness. From the present data, the question remains open to discussion whether a spring system in series would in fact illustrate the observed phenomenon, or whether instead the perlecan and collagen type VI are somehow functionally intertwined, the isolated depletion of perlecan leading to an increase in stiffness of the collagen type VI fibres. It will also be interesting to investigate how the PCM is connected microbiomechanically with the ECM and if disruption of the PCM correlates also with changes in ECM elasticity during degeneration.

Of note, the AFM data show significant reductions in stiffness between all of the spatial chondrocyte patterns. The decrease in protein quantity is first measured at the change from double strings to small clusters. While the elasticity of the PCM is thus already clearly affected from the earliest rearrangement on, this is not immediately translated into a reduction in protein content. One simple explanatory approach to this phenomenon could be that at

the transition from single to double strings, the number of cells within a defined cartilage area increases. While the total protein content for key PCM components remains at a similar level, this means that the amount of protein available per PCM per cell would be reduced, leading to an early reduction in PCM mechanical moduli. Alternatively, at the transition from single to double strings, collagen type VI and perlecan might be fragmented without being degraded. Söder *et al.* (2002) suggested that two types of collagen type VI destruction occur in osteoarthritic cartilage: induced molecular degradation resulting in the diffusion of collagen type VI fragments into the adjacent interterritorial matrix, and transformation of collagen type VI filaments to banded structures that no longer provide the flexible mechanical interface to the ECM-collagen type II<sup>63</sup>.

Since spatial chondrocyte organisation indeed has functional relevance, the impact of this image-based biomarker is strongly enhanced. Our data affirm that first degenerative changes are already measurable functionally at the transition from single to double strings, where macroscopically the cartilage still appears intact. This implies that such a biomarker could be used for diagnosis of early stages of OA. If researchers use regenerative therapies to pursue the goal of recreating physiological cartilage architecture, this model can also serve as a landmark parameter, with single strings being the target organisational form in the cellular reorganisation process.

### Study limitations

Values from AFM measurements show a relevant individual range between patterns as well as in repeated measurements. This phenomenon can be counteracted by choosing a large sample size as we did in our study. One possible explanation for the variation in values for the same patterns may be the regional variation in biomechanical properties of the PCM<sup>47</sup>. Experimental parameters used for mechanical testing, such as indentation velocity and depth, indenter shape and size, and accurate representation of tip geometry in model fitting<sup>64</sup> may impact absolute values of the measured mechanical properties<sup>65,66</sup>. They should not, however, affect the results within one study and their relation to each other.

### Conclusion

This study demonstrates the functional relevance of using spatial chondrocyte organisation as an image-based biomarker. At the transition from single to double strings, PCM stiffness is beginning to decrease, where macroscopically the cartilage still appears intact. This is followed by a reduction in collagen type VI and perlecan content, suggesting that the degeneration of these components and functional disruption of the PCM are closely intertwined events in OA physiopathology.

### Authors' contribution

MD designed the study, performed the experiments, did the statistical analyses, and wrote the manuscript; RK helped interpret the data and to write the manuscript; JS performed the experiments and helped with the statistical analyses; ALE helped with the immunohistochemistry and the statistical analyses; MS provided the cartilage samples, helped interpret the data, and critically revised the manuscript; RR helped perform the experiments; FT helped design the study and write the manuscript; and UKH designed and supervised the study, helped with the statistical analyses, and wrote the manuscript. All authors read and approved the final manuscript.



### Conflict of interest

All authors declare that they have no conflict of interest.

### Role of the funding source

No funding was received for the study.

### Acknowledgements

We thank the orthopaedic surgeons from the Department of Orthopaedic Surgery of the University Hospital of Tuebingen and from Winghamer-Clinic/Rottenburg for providing the tissue samples. We thank Barbara Every, ELS, of BioMedical Editor, for English language editing.

### References

- Heinegard D, Oldberg A. Structure and biology of cartilage and bone matrix noncollagenous macromolecules. *FASEB J* 1989;3: 2042–51.
- Rolauffs B, Williams JM, Grodzinsky AJ, Kuettner KE, Cole AA. Distinct horizontal patterns in the spatial organization of superficial zone chondrocytes of human joints. *J Struct Biol* 2008;162:335–44.
- Schumacher BL, Su JL, Lindley KM, Kuettner KE, Cole AA. Horizontally oriented clusters of multiple chondrons in the superficial zone of ankle, but not knee articular cartilage. *Anat Rec* 2002;266:241–8.
- Rolauffs B, Rothdiener M, Bahrs C, Badke A, Weise K, Kuettner KE, et al. Onset of preclinical osteoarthritis: the angular spatial organization permits early diagnosis. *Arthritis Rheum* 2011;63:1637–47.
- Aicher WK, Rolauffs B. The spatial organisation of joint surface chondrocytes: review of its potential roles in tissue functioning, disease and early, preclinical diagnosis of osteoarthritis. *Ann Rheum Dis* 2014;73:645–53.
- Rolauffs B, Williams JM, Aurich M, Grodzinsky AJ, Kuettner KE, Cole AA. Proliferative remodeling of the spatial organization of human superficial chondrocytes distant from focal early osteoarthritis. *Arthritis Rheum* 2010;62:489–98.
- Felka T, Rothdiener M, Bast S, Uynuk-Ool T, Zouhair S, Ochs BG, et al. Loss of spatial organization and destruction of the pericellular matrix in early osteoarthritis in vivo and in a novel in vitro methodology. *Osteoarthritis Cartilage* 2016;24: 1200–9.
- Alexopoulos LG, Haider MA, Vail TP, Guilak F. Alterations in the mechanical properties of the human chondrocyte pericellular matrix with osteoarthritis. *J Biomech Eng* 2003;125:323–33.
- Hellio Le Graverand MP, Sciore P, Eggerer J, Rattner JP, Vignon E, Barclay L, et al. Formation and phenotype of cell clusters in osteoarthritic meniscus. *Arthritis Rheum* 2001;44: 1808–18.
- Poole CA, Ayad S, Gilbert RT. Chondrons from articular cartilage. V. Immunohistochemical evaluation of type VI collagen organisation in isolated chondrons by light, confocal and electron microscopy. *J Cell Sci* 1992;103(Pt 4):1101–10.
- Youn I, Choi JB, Cao L, Setton LA, Guilak F. Zonal variations in the three-dimensional morphology of the chondron measured in situ using confocal microscopy. *Osteoarthritis Cartilage* 2006;14:889–97.
- Poole CA. Articular cartilage chondrons: form, function and failure. *J Anat* 1997;191(Pt 1):1–13.
- Melrose J, Hayes AJ, Whitelock JM, Little CB, Perlecan, the “jack of all trades” proteoglycan of cartilaginous weight-bearing connective tissues. *Bioessays* 2008;30:457–69.
- Knudson W, Ishizuka S, Terabe K, Askew EB, Knudson CB. The pericellular hyaluronan of articular chondrocytes. *Matrix Biol* 2018, <https://doi.org/10.1016/j.matbio.2018.02.005>. in press.
- Poole AR, Pidoux I, Reiner A, Rosenberg L. An immunoelectron microscope study of the organization of proteoglycan monomer, link protein, and collagen in the matrix of articular cartilage. *J Cell Biol* 1982;93:921–37.
- Durr J, Lammi P, Goodman SL, Aigner T, von der Mark K. Identification and immunolocalization of laminin in cartilage. *Exp Cell Res* 1996;222:225–33.
- Chang J, Nakajima H, Poole CA. Structural colocalisation of type VI collagen and fibronectin in agarose cultured chondrocytes and isolated chondrons extracted from adult canine tibial cartilage. *J Anat* 1997;190(Pt 4):523–32.
- Poole CA, Glant TT, Schofield JR. Chondrons from articular cartilage. (IV). Immunolocalization of proteoglycan epitopes in isolated canine tibial chondrons. *J Histochem Cytochem* 1991;39:1175–87.
- Kavanagh E, Ashhurst DE. Development and aging of the articular cartilage of the rabbit knee joint: distribution of biglycan, decorin, and matrilin-1. *J Histochem Cytochem* 1999;47:1603–16.
- Poole CA, Gilbert RT, Herbage D, Hartmann DJ. Immunolocalization of type IX collagen in normal and spontaneously osteoarthritic canine tibial cartilage and isolated chondrons. *Osteoarthritis Cartilage* 1997;5:191–204.
- Guilak F, Alexopoulos LG, Upton ML, Youn I, Choi JB, Cao L, et al. The pericellular matrix as a transducer of biomechanical and biochemical signals in articular cartilage. *Ann N Y Acad Sci* 2006;1068:498–512.
- Peters HC, Otto TJ, Enders JT, Jin W, Moed BR, Zhang Z. The protective role of the pericellular matrix in chondrocyte apoptosis. *Tissue Eng* 2011;17:2017–24.
- Larson CM, Kelley SS, Blackwood AD, Banes AJ, Lee GM. Retention of the native chondrocyte pericellular matrix results in significantly improved matrix production. *Matrix Biol* 2002;21:349–59.
- Poole CA, Flint MH, Beaumont BW. Morphological and functional interrelationships of articular cartilage matrices. *J Anat* 1984;138(Pt 1):113–38.
- Wiberg C, Hedbom E, Khairullina A, Lamande SR, Oldberg A, Timpl R, et al. Biglycan and decorin bind close to the n-terminal region of the collagen VI triple helix. *J Biol Chem* 2001;276:18947–52.
- Poole CA, Flint MH, Beaumont BW. Chondrons in cartilage: ultrastructural analysis of the pericellular microenvironment in adult human articular cartilages. *J Orthop Res* 1987;5: 509–22.
- Choi JB, Youn I, Cao L, Leddy HA, Gilchrist CL, Setton LA, et al. Zonal changes in the three-dimensional morphology of the chondron under compression: the relationship among cellular, pericellular, and extracellular deformation in articular cartilage. *J Biomech* 2007;40:2596–603.
- Hollander AP, Pidoux I, Reiner A, Rorabeck C, Bourne R, Poole AR. Damage to type II collagen in aging and osteoarthritis starts at the articular surface, originates around chondrocytes, and extends into the cartilage with progressive degeneration. *J Clin Invest* 1995;96:2859–69.
- Poole AR. An introduction to the pathophysiology of osteoarthritis. *Front Biosci* 1999;4:D662–70.
- Poole AR, Rosenberg LC, Reiner A, Ionescu M, Bogoch E, Roughley PJ. Contents and distributions of the proteoglycans decorin and biglycan in normal and osteoarthritic human articular cartilage. *J Orthop Res* 1996;14: 681–9.



31. Tesche F, Miosge N. Perlecan in late stages of osteoarthritis of the human knee joint. *Osteoarthritis Cartilage* 2004;12: 852–62.
32. Chubinskaya S, Kuettner KE, Cole AA. Expression of matrix metalloproteinases in normal and damaged articular cartilage from human knee and ankle joints. *Lab Invest* 1999;79: 1669–77.
33. Woessner Jr JF, Gunja-Smith Z. Role of metalloproteinases in human osteoarthritis. *J Rheumatol Suppl* 1991;27:99–101.
34. Hollander AP, Heathfield TF, Webber C, Iwata Y, Bourne R, Rorabeck C, et al. Increased damage to type II collagen in osteoarthritic articular cartilage detected by a new immun assay. *J Clin Invest* 1994;93:1722–32.
35. Hollander AP, Heathfield TF, Webber C, Iwata Y, Bourne R, Rorabeck C, et al. Increased damage to type II collagen in osteoarthritic articular cartilage detected by a new immun assay. *J Clin Invest* 1994;93:1722–32.
36. Stoop R, Buma P, van der Kraan PM, Hollander AP, Billinghurst RC, Meijers TH, et al. Type II collagen degradation in articular cartilage fibrillation after anterior cruciate ligament transection in rats. *Osteoarthritis Cartilage* 2001;9: 308–15.
37. Hambach L, Neureiter D, Zeiler G, Kirchner T, Aigner T. Severe disturbance of the distribution and expression of type VI collagen chains in osteoarthritic articular cartilage. *Arthritis Rheum* 1998;41:986–96.
38. Radmacher M, Tillmann RW, Fritz M, Gaub HE. From molecules to cells: imaging soft samples with the atomic force microscope. *Science* 1992;257:1900–5.
39. Roberts S, Ayad S, Menage PJ. Immunolocalisation of type VI collagen in the intervertebral disc. *Ann Rheum Dis* 1991;50: 787–91.
40. Ahrens MJ, Dudley AT. Chemical pretreatment of growth plate cartilage increases immunofluorescence sensitivity. *J Histochem Cytochem* 2011;59:408–18.
41. Rolaffs B, Williams JM, Grodzinsky AJ, Kuettner KE, Cole AA. Distinct horizontal patterns in the spatial organization of superficial zone chondrocytes of human joints. *J Struct Biol* 2008;162:335–44.
42. Wilusz RE, Zauscher S, Guilak F. Micromechanical mapping of early osteoarthritic changes in the pericellular matrix of human articular cartilage. *Osteoarthritis and Cartilage/OARS. Osteoarthritis Res Soc* 2013;21:1895–903, <https://doi.org/10.1016/j.joca.2013.1008.1026>.
43. Athanasiou KA, Rosenwasser MP, Buckwalter JA, Malinin TI, Mow VC. Interspecies comparisons of in situ intrinsic mechanical properties of distal femoral cartilage. *J Orthop Res* 1991;9:330–40.
44. Schinagl RM, Gurskis D, Chen AC, Sah RL. Depth-dependent confined compression modulus of full-thickness bovine articular cartilage. *J Orthop Res* 1997;15:499–506.
45. Coleman JL, Widmyer MR, Leddy HA, Utturkar GM, Spritzer CE, Moorman 3rd CT, et al. Diurnal variations in articular cartilage thickness and strain in the human knee. *J Biomech* 2013;46: 541–7.
46. Darling EM, Wilusz RE, Bolognesi MP, Zauscher S, Guilak F. Spatial mapping of the biomechanical properties of the pericellular matrix of articular cartilage measured in situ via atomic force microscopy. *Biophys J* 2010;98:2848–56.
47. Wilusz RE, DeFrate LE, Guilak F. Immunofluorescence-guided atomic force microscopy to measure the micromechanical properties of the pericellular matrix of porcine articular cartilage. *J R Soc Interface* 2012;9:2997–3007.
48. Alexopoulos LG, Williams GM, Upton ML, Setton LA, Guilak F. Osteoarthritic changes in the biphasic mechanical properties of the chondrocyte pericellular matrix in articular cartilage. *J Biomech* 2005;38:509–17.
49. Horikawa O, Nakajima H, Kikuchi T, Ichimura S, Yamada H, Fujikawa K, et al. Distribution of type VI collagen in chondrocyte microenvironment: study of chondrons isolated from human normal and degenerative articular cartilage and cultured chondrocytes. *J Orthop Sci* 2004;9:29–36.
50. Melrose J, Roughley P, Knox S, Smith S, Lord M, Whitelock J. The structure, location, and function of perlecan, a prominent pericellular proteoglycan of fetal, postnatal, and mature hyaline cartilages. *J Biol Chem* 2006;281:36905–14.
51. Endothelial cells interact with the core protein of basement membrane perlecan through beta 1 and beta 3 integrins: an adhesion modulated by glycosaminoglycan. *J Cell Biol* 1992;119:945–59.
52. Brown JC, Sasaki T, Göhring W, Yamada Y, Timpl R. The C-terminal domain V of perlecan promotes p1 integrin-mediated cell adhesion, binds heparin, nidogen and fibulin-2 and can be modified by glycosaminoglycans. *Eur J Biochem* 1997;250: 39–46.
53. Gomes R, Kirn-Safran C, Farach-Carson MC, Carson DD. Perlecan: an important component of the cartilage pericellular matrix. *J Musculoskelet Neuronal Interact* 2002;2:511–6.
54. Prein C, Lagugne-Labarthe F, Beier F. Investigation of articular cartilage structural and biomechanical properties by atomic-force microscopy. *Osteoarthritis Cartilage* 2018;26:S400.
55. McLeod MA, Wilusz RE, Guilak F. Depth-Dependent anisotropy of the micromechanical properties of the extracellular and pericellular matrices of articular cartilage evaluated via atomic force microscopy. *J Biomech* 2013;46:586–92.
56. Cao L, Guilak F, Setton LA. Three-dimensional finite element modeling of pericellular matrix and cell mechanics in the nucleus pulposus of the intervertebral disk based on in situ morphology. *Biomechanics Model Mechanobiol* 2011;10: 1–10.
57. Zelenski NA, Leddy HA, Sanchez-Adams J, Zhang J, Bonaldo P, Liedtke W, et al. Type VI collagen regulates pericellular matrix properties, chondrocyte swelling, and mechanotransduction in mouse articular cartilage. *Arthritis Rheum* 2015;67:1286–94.
58. Guilak F, Nims RJ, Dicks A, Wu CL, Meulenbelt I. Osteoarthritis as a disease of the cartilage pericellular matrix. *Matrix Biol* 2018;71–72:40–50.
59. Ronziere MC, Ricard-Blum S, Tiollier J, Hartmann DJ, Garrone R, Herbage D. Comparative analysis of collagens solubilized from human foetal, and normal and osteoarthritic adult articular cartilage, with emphasis on type VI collagen. *Biochim Biophys Acta* 1990;1038:222–30.
60. McDevitt CA, Pahl JA, Ayad S, Miller RR, Uratsuji M, Andrish JT. Experimental osteoarthritic articular cartilage is enriched in guanidine soluble type VI collagen. *Biochem Biophys Res Commun* 1988;157:250–5.
61. Xu X, Li Z, Leng Y, Neu CP, Calve S. Knockdown of the pericellular matrix molecule perlecan lowers in situ cell and matrix stiffness in developing cartilage. *Dev Biol* 2016;418: 242–7.
62. Wilusz RE, DeFrate LE, Guilak F. A biomechanical role for perlecan in the pericellular matrix of articular cartilage. *Matrix Biol* 2012;31:320–7.
63. Soder S, Hambach L, Lissner R, Kirchner T, Aigner T. Ultrastructural localization of type VI collagen in normal adult and osteoarthritic human articular cartilage. *Osteoarthritis Cartilage* 2002;10:464–70.
64. Costa KD, Yin FC. Analysis of indentation: implications for measuring mechanical properties with atomic force microscopy. *J Biomech Eng* 1999;121:462–71.



832

*M. Danalache et al. / Osteoarthritis and Cartilage 27 (2019) 823–832*

65. Stolz M, Raiteri R, Daniels AU, VanLandingham MR, Baschong W, Aebi U. Dynamic elastic modulus of porcine articular cartilage determined at two different levels of tissue organization by indentation-type atomic force microscopy. *Biophys J* 2004;86:3269–83.
66. Park S, Costa KD, Ateshian GA, Hong KS. Mechanical properties of bovine articular cartilage under microscale indentation loading from atomic force microscopy. *Proc Inst Mech Eng H* 2009;223:339–47.

## 2.2. Biomechanical and biochemical cues for customizing jaw periosteal cells for bone constructs




International Journal of  
*Molecular Sciences*



Article

# Quality Analysis of Minerals Formed by Jaw Periosteal Cells under Different Culture Conditions

Marina Danalache <sup>1</sup>, Sophie-Maria Kliesch <sup>2</sup>, Marita Munz <sup>3</sup>, Andreas Naros <sup>3</sup> , Siegmar Reinert <sup>3</sup> and Dorothea Alexander <sup>3,\*</sup>

<sup>1</sup> Department of Orthopedic Surgery, University Hospital, 72076 Tübingen, Germany

<sup>2</sup> Quality Analysis GmbH, 72622 Nürtingen, Germany

<sup>3</sup> Department of Oral and Maxillofacial Surgery, University Hospital, 72076 Tübingen, Germany

\* Correspondence: dorothea.alexander@med.uni-tuebingen.de; Tel.: +49-7071-2982418; Fax: +49-7071-294365

Received: 25 June 2019; Accepted: 22 August 2019; Published: 27 August 2019



**Abstract:** Previously, we detected a higher degree of mineralization in fetal calf serum (FCS) compared to serum-free cultured jaw periosteum derived osteoprogenitor cells (JPCs). By Raman spectroscopy, we detected an earlier formation of mineralized extracellular matrix (ECM) of higher quality under serum-free media conditions. However, mineralization potential remained too low. In the present study, we aimed to investigate the biochemical composition and subsequent biomechanical properties of the JPC-formed ECM and minerals under human platelet lysate (hPL) and FCS supplementation. JPCs were isolated ( $n = 4$  donors) and expanded under FCS conditions and used in passage five for osteogenic induction under both, FCS and hPL media supplementation. Raman spectroscopy and Alizarin Red/von Kossa staining were employed for biochemical composition analyses and for visualization and quantification of mineralization. Osteocalcin gene expression was analyzed by quantitative PCR. Biomechanical properties were assessed by using atomic force microscopy (AFM). Raman spectroscopic measurements showed significantly higher ( $p < 0.001$ ) phosphate to protein ratios and in the tendency, lower carbonate to phosphate ratios in osteogenically induced JPCs under hPL in comparison to FCS culturing. Furthermore, higher crystal sizes were detected under hPL culturing of the cells. With respect to the ECM, significantly higher ratios of the precursor protein proline to hydroxyproline were detected in hPL-cultured JPC monolayers ( $p < 0.001$ ). Additionally, significantly higher levels ( $p < 0.001$ ) of collagen cross-linking were calculated, indicating a higher degree of collagen maturation in hPL-cultured JPCs. By atomic force microscopy, a significant increase in ECM stiffness ( $p < 0.001$ ) of FCS cultured JPC monolayers was observed. The reverse effect was measured for the JPC formed precipitates/minerals. Under hPL supplementation, JPCs formed minerals of significantly higher stiffness ( $p < 0.001$ ) when compared to the FCS setting. This study demonstrates that hPL culturing of JPCs leads to the formation of an anorganic material of superior quality in terms of biochemical composition and mechanical properties.

**Keywords:** bone mineral formation; fetal calf serum; human platelet lysate; osteoprogenitor jaw periosteal cells; mechanical properties; atomic force microscopy; Raman spectroscopy

### 1. Introduction

Bone tissue engineering (BTE) has been continuously developing as a multidisciplinary field involving innovative biomaterials, mesenchymal stromal/stem cells and activating factors with the overall aim to restore and regenerate bone defects. Jaw periosteum derived progenitor cells (JPCs) are emerging as promising candidates in the field of maxillofacial reconstruction [1,2] due to their relatively easy availability, multipotency capacity at singular cellular level [3] and high proliferation rates [4].



To realize cell-based clinical applications using JPCs, a detailed characterization of the cells, their expression patterns and formed extracellular matrix, coupled with optimized culture and defined differentiation conditions are key factors to ensure the success of BTE constructs. Since fetal calf serum (FCS) supplementation of cell cultures is no longer up-to-date, especially when *in vitro* cultivated mesenchymal stem cells (MSC) are intended to be used for therapeutic purposes, human platelet lysate (hPL) has been taken into consideration as a suitable and promising alternative to FCS [5,6]. Additionally, the transmission of animal components and potential immune responses should be avoided. For hPL manufacturing, platelets have to be lysed for growth factor release from the contained alpha granules [6,7]. Moreover, several studies have shown that media supplemented with hPL actually shortened MSC expansion time while maintaining the cells phenotype and differentiation capacities [8–10]. Despite the aforementioned advantages, it must be taken into consideration that hPL has similar limitations as the use of FCS: There is no precise characterization of its entire composition, it is seldom distributed commercially, whereby the number of supplier companies is increasing and hPL might facilitate the transmission of human diseases [11]. In order to minimize the contamination risks, it has been recommended to store hPL for three months (quarantine time) and reanalyze afterwards for possible serum conversions [12]. The variations in composition can be addressed by using a large number of donors (20–120) [13].

In a scientific era in which static and two-dimensional culture conditions become obsolete and three-dimensional cell culture/bioreactors/3D-printing/microfluidic organ-on-a-chip systems are emerging, the demand of optical imaging approaches for live-monitoring of these systems, increases continuously [14]. Suitable optical technologies should be tested and improved in order to assure quality assessment of formed cell aggregates/tissue engineered constructs/small organs. In our opinion, Raman spectroscopy and atomic force microscopy (AFM) should be combined in order to monitor biochemical composition and stiffness and therefore the maturity of resulting bone-like extracellular matrix (ECM) formed by JPCs *in vitro*.

Raman spectroscopy has been emerging as a powerful tool in elucidating the biological compositions and signatures with a wide spectrum of applications, ranging from various pathological conditions [15–18] to tissues and cells [19,20]. Raman spectral studies have already been performed on structural analysis of various extracellular matrix (ECM) components [21–24].

Moreover, this technology has been successfully shown to provide a nondestructive readout of collagen-containing ECM in a medium-throughput culture system [25]. Additionally, we previously showed by Raman spectroscopy that the biochemical composition of crystals formed extracellularly differs under cultivation of JPCs without and with fetal calf serum (FCS).

The ECM not only provides structural support or anchoring of cellular components, but it also initiates and modulates the biomechanical signals required for the regulation of cellular behavior, such as differentiation, proliferation and migration [26–28]. The mechanical features of the JPC niche and implicitly its surrounding microenvironment are of particular relevance, especially in the field of bone constructs, as they should uphold and withstand continuous stretch/strain mechanisms. Atomic force microscopy (AFM) is a powerful tool that enables the investigation of local mechanical properties with a nanoscale resolution. This technology has been suggested to be a suitable and reliable technique with a large repertoire of applications [29]. Moreover, mechanical testing can be performed *in situ* under liquid physiological conditions, making it an appropriate approach to investigate local micromechanical properties, such as those of the ECM [30]. LeBlon et al. indicated that percentages of positively stained cells for osteogenic markers (osteopontin, osteocalcin) negatively correlated with increasing cell elastic modulus as detected by the Pearson correlation coefficient [31]. Therefore, an increasing elastic modulus led to decreased osteogenic differentiation. In accordance to these findings, it has been demonstrated that human MSCs undergoing osteogenesis develop a decreased cytoskeleton elasticity, which was attributed to the reorganization/arrangement of the actin network during differentiation [32].

In a previous study, we performed phenotypic and functional characterization of JPCs under FCS and hPL supplementation and detected significantly higher proliferation and metabolic activities as well as higher mineralization potential of JPCs under hPL conditions [33]. In the present study, we extend this knowledge and examine biochemical composition and mechanical properties of the formed matrix during *in vitro* osteogenesis under FCS and hPL medium supplementation using the high precision techniques of Raman spectroscopy and atomic force microscopy.

## 2. Results and Discussion

### 2.1. Analysis of JPC Mineralization under hPL and FCS Supplementation

In terms of JPCs mineralization degree/ECM appearance, representative microscopic images in Figure 1 show a different consistency of hPL-supplemented (right) and osteogenically induced JPC monolayers compared to the FCS-supplemented (left) counterparts derived from two donors (#1, #2). JPCs formed an ECM of gel-like viscosity and consistency and appeared to be thicker under hPL compared to FCS supplementation.

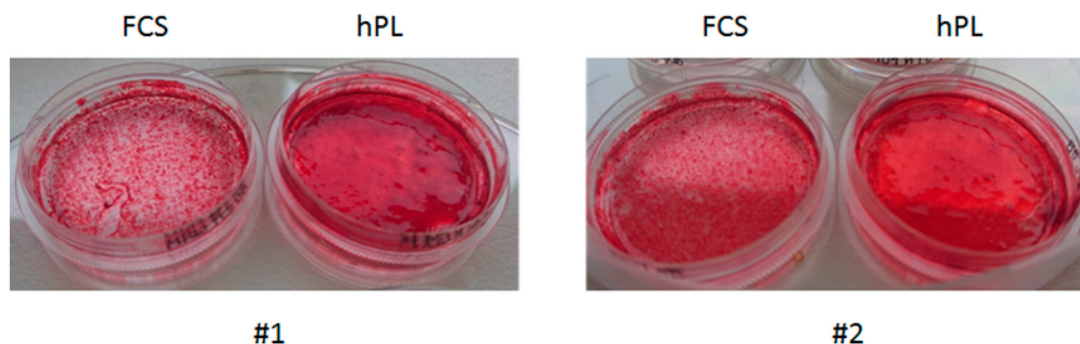


**Figure 1.** Different consistency and macroscopic appearance of osteogenically induced JPC monolayers following FCS and hPL medium supplementation (Alizarin Red staining). Representative images of cell monolayers from two donors (#1, #2) cultured in AFM petri dishes (plastic bottom) under both supplementations. Abbreviations: FCS—fetal calf serum, hPL—human platelet lysate.

When JPCs were cultured in AFM and Raman glass dishes, respectively, FCS-cultured JPCs mineralized much better in AFM dishes compared to Raman ones, where cell mineralization occurred to a later time point (Figure 2A). In contrast, hPL-supplemented JPCs strongly mineralized in both culture plates. Interestingly, in two of the three tested patient cells (Figure 2—#2 and #3), Raman dishes seemed to further support cell mineralization of hPL-supplemented JPCs, as also confirmed by the subsequent quantification of the Alizarin staining (Figure 2B). The differences in calcium concentration detected in Raman and AFM dishes were highly significant for both FCS- and hPL-cultured JPCs. Under hPL supplementation, cell mineralization was shown to be significantly higher in cells derived from Figure 2 #1 and #2. Cells derived from patient Figure 2 #3 showed a significantly higher osteogenic potential under FCS supplementation particularly in AFM dishes (as shown in Figure 2B) in contrast to Raman dishes. Under hPL supplementation exactly the opposite was the case and JPCs in Raman dishes showed a significantly higher mineralization potential.

JPCs cultured in Raman glass dishes were additionally stained by von Kossa after 35 days of osteogenic induction, as shown in Figure 3.

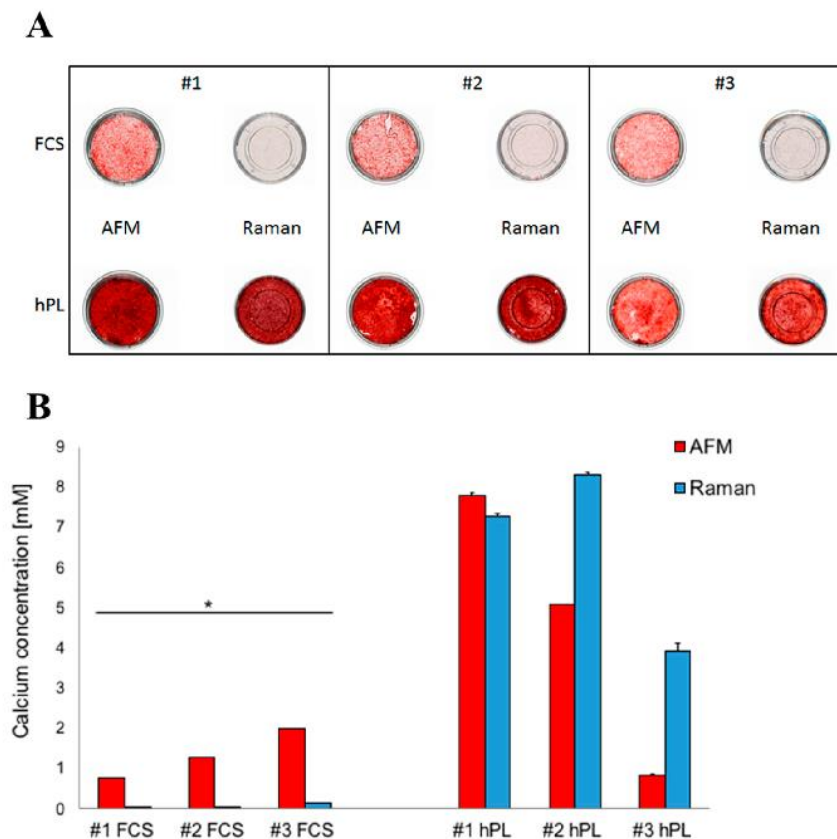


**Figure 2.** Detection of JPCs mineralization (Alizarin Red staining) in AFM and Raman petri dishes under FCS and hPL supplementation. Macroscopic images: JPC mineralization from three donors (#1, #2, #3) cultured in AFM (plastic bottom) and Raman (glass bottom) petri dishes was observed after osteogenic induction for 25 days under both medium supplementations (A). Quantification of JPC mineralization degrees in cell monolayers from the three donors (B). Calcium levels detected in cell monolayers cultured in AFM dishes are represented by red columns and those in Raman petri dishes by blue columns. Abbreviations: AFM—atomic force microscopy, FCS—fetal calf serum, hPL—human platelet lysate, \*  $p < 0.05$ .

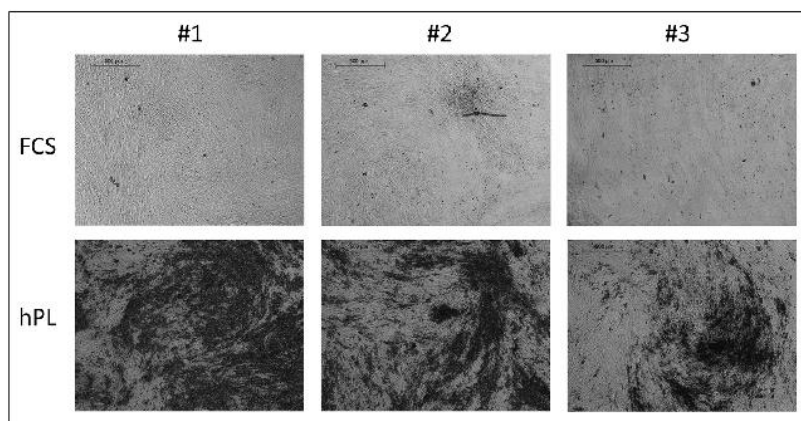


**Figure 3.** Detection of JPCs mineralization by von Kossa staining in Raman dishes under FCS and hPL supplementation. Microscopic images showing JPC mineralization from three donors (#1, #2, #3) cultured in Raman (glass bottom) dishes were observed after osteogenic induction for 25 days under both medium supplementations. Abbreviations: FCS—fetal calf serum, hPL—human platelet lysate.

### 2.2. Detection of Osteocalcin Gene Expression Levels in JPCs Cultured under FCS and hPL Supplementation

JPCs from four donors were cultured under normal (Co) and osteogenic (Ob) culture conditions for five and 10 days under FCS and hPL supplementation. Osteocalcin transcript levels were shown to be highly upregulated (4.2-fold) in osteogenically-induced JPCs only in hPL-supplemented JPCs at day 10. However, due to high variations between the donor cells, differences did not reach significance (Figure 4).

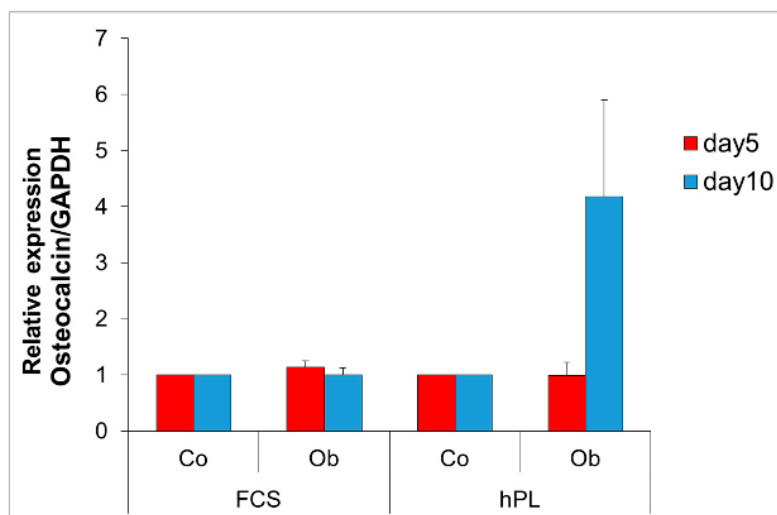


**Figure 4.** Relative gene expression levels of human osteocalcin transcript levels by quantitative PCR. JPCs from four donors were cultured in 75 cm<sup>2</sup> culture flasks under normal (Co) and osteogenic (Ob) conditions for five and 10 days under both medium supplementations, following RNA isolation for osteocalcin gene quantification. Gene expression in untreated JPCs were set as 1 and induction indices in relation to untreated controls were calculated. Abbreviations: FCS—fetal calf serum, hPL—human platelet lysate.

### 2.3. Characterization of hPL- and FCS-Cultured JPC-Formed Extracellular Matrix ECM by Raman Spectroscopy

Mean Raman spectra containing information about the biochemical composition of JPC-formed ECM (derived from four (#1–#4) donors) under osteogenic conditions and different supplementation (FCS versus hPL) are illustrated in Figure 5.

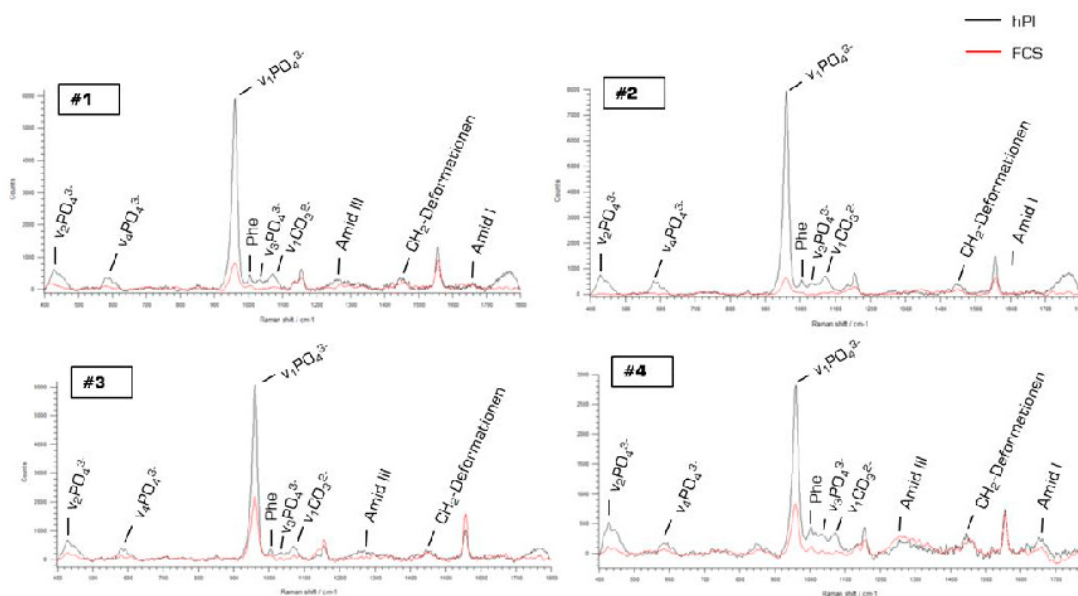


**Figure 5.** Mean Raman spectra from hPL- and FCS-supplemented JPCs. Mean Raman spectra from four donors (#1, #2, #3, #4) generated from JPCs growing in Raman glass dishes under hPL (black spectra) and FCS (red spectra) supplementation. Abbreviations: FCS—fetal calf serum, hPL—human platelet lysate.

As illustrated in Figure 5, apart from the main hydroxyapatite peak at  $960\text{ cm}^{-1}$ , the three other phosphate peaks were shown to be higher under hPL, compared to FCS, supplementation. Further differences were detected in other peaks such as phenylalanine at  $1004\text{ cm}^{-1}$ , carbonate at  $1070\text{ cm}^{-1}$ , amid III at  $1244\text{ cm}^{-1}$  and amid I at  $1660\text{ cm}^{-1}$ . From these Raman spectra and considering the mentioned peaks, different phosphate to protein ratios (HA to phenylalanine, HA to amid III, HA to amid I) were calculated by considering the respective wave numbers (as shown in Figure 6). Furthermore, the carbonate content (carbonate to phosphate) and the crystal size (reflected by the HA crystallinity: reverse of the full width of half maximum of the HA peak) were assessed in order to be able to evaluate the replacement of phosphate by carbonate and mineralization degree by comparing crystal sizes. Collagen matrix maturity was assessed by the calculation of proline to hydroxyproline with proline being the precursor of hydroxyproline which in turn is responsible for collagen fibril stability. Illustrated columns in Figure 6 depict means of 126–162 measurements per donor cells with four donors in total. We detected significantly higher HA to phenylalanine, HA to amid I and HA to III ratios (Figure 6A–C) in hPL-supplemented JPC monolayers indicating higher HA deposition in comparison to FCS-cultured JPCs. Furthermore, significantly lower carbonate content (Figure 6D) was calculated for the ECM from this group. JPCs cultured under hPL supplementation formed significantly larger crystals, as reflected in the diagram in Figure 6E by the means of FWHM values. Significant differences between the FCS- and hPL-group with calculated *p*-values are listed in Table 1.

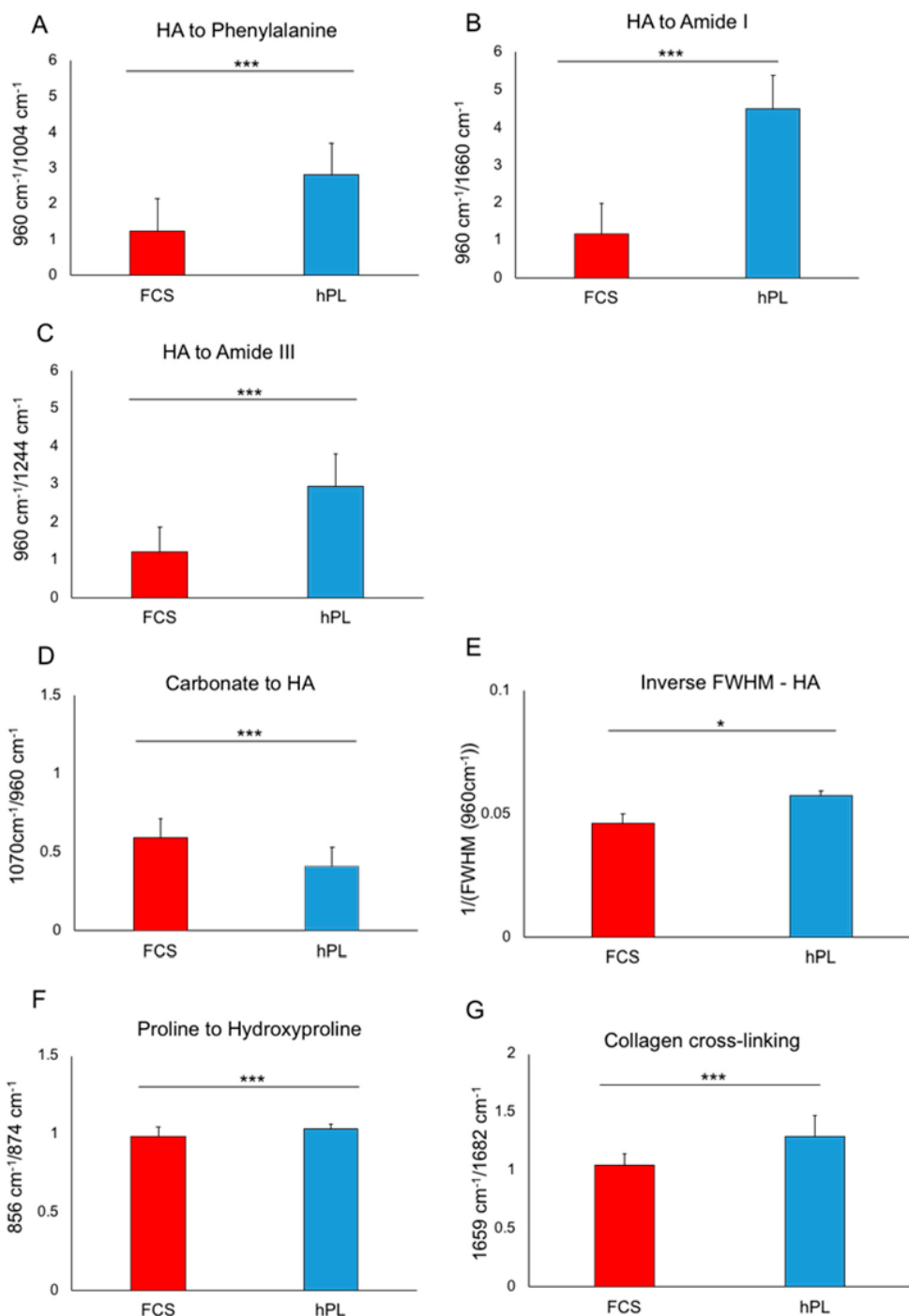


**Figure 6.** Ratios calculated from mean Raman spectra reflecting the biochemical composition of osteogenically-induced (OB) JPCs (four donors) under hPL and FCS supplementation. Phosphate to protein ratios (A) HA to phenylalanine; (B) HA to amid I; (C) HA to amid III; (D) carbonate content; (E) crystal size; (F) proline to hydroxyproline; (G) collagen cross-linking. Means (126–162 measurements per donor)  $\pm$  standard deviations are depicted. \*  $p < 0.05$ ; \*\*\*  $p < 0.001$ . Abbreviations: FCS—fetal calf serum, hPL—human platelet lysate.



**Table 1.** Calculation of significant differences of Raman ratios in FCS/hPL groups.

Ratios	<i>p</i> -Values
	FCS/hPL
HA to Phenylalamine	<0.001
HA to Amide I	<0.001
HA to Amide III	<0.001
Carbonate to HA	<0.001
Inverse FWHN–HA	0.029
Proline to hydroxyproline	<0.001
Collagen cross-linking	<0.001

Mann–Whitney U test with calculated *p*-values. Abbreviations: FCS—fetal calf serum, hPL—human platelet lysate, HA—hydroxyapatite.

#### 2.4. Characterization of Mechanical Properties of hPL- and FCS-Cultured JPC-Formed ECM by Atomic Force Microscopy (AFM)

Osteogenically induced JPCs under FCS and hPL medium supplementation from four donors were subjected to AFM elasticity measurements of the ECM. Therefore, a total of 1122 measurements were performed. After exclusion of extreme values, a total of 330 measurements for the control group (FCS—169 and hPL—161), 339 for the osteogenic induced group (FCS—171 and hPL—168) and 417 measurements for the group of precipitates (FCS—211 and hPL—206) were included in the final analysis. The measured JPCs elastic moduli results are shown in Figure 7 and Table 3.

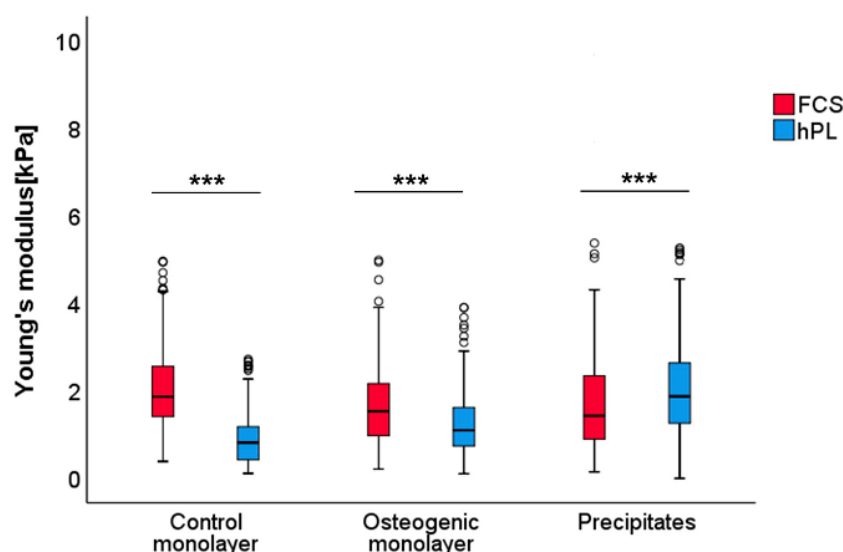


**Figure 7.** Analysis of Young's modulus of JPC monolayers cultured under FCS and hPL supplementation. Boxplots (medians, minimum, maximum) of the stiffness (kPa) measured by atomic force microscopy for each analyzed group are depicted. In both, control (untreated) and osteogenic monolayers of FCS cultured monolayers analyzed ECM revealed higher stiffness when compared to hPL groups. The reversed effect was observed for the group of precipitates. \*\*\*  $p < 0.001$  (for exact *p*-values, see Table 3). Abbreviations: FCS—fetal calf serum, hPL—human platelet lysate.

Stiffness of the ECM significantly increased under FCS culturing conditions when compared to hPL culturing settings for both the untreated controls ( $p < 0.001$ ) and the osteogenic induced ( $p < 0.001$ ) monolayers. In contrast, for the JPC-formed precipitates under hPL supplementation, a significant increase in stiffness ( $p < 0.001$ ) was detected compared to the FCS group. Absolute values were thereby reduced by 57% under hPL culture conditions (median of 1.8 kPa for the FCS to 0.8 kPa for the hPL group) in control monolayers and by 28% (median of 1.5 kPa for the FCS to 1.1 kPa for the hPL group)

in osteogenic monolayers. As mentioned before, the reverse observation was made for the group of precipitates where a 24% increase of Young's modulus was detected under hPL culture conditions (median of 1.4 kPa for the FCS to 1.9 kPa for the hPL group). Descriptive statistics and *p*-values for significant differences between the FCS- and hPL-group are listed in Tables 2 and 3.

**Table 2.** Calculation of significant differences of Young's moduli detected in untreated (control) and osteogenic monolayers and of calcium phosphate precipitates in FCS/hPL groups.

Groups	<i>p</i> -Values
	FCS/hPL
Control monolayer	<0.001
Osteogenic monolayer	<0.001
Precipitates	<0.001

Mann–Whitney U test with calculated *p*-values. Abbreviations: FCS—fetal calf serum, hPL—human platelet lysate.

**Table 3.** Descriptive statistics of Young's moduli in untreated (control) and osteogenic monolayers and of calcium phosphate precipitates in FCS/hPL groups. Medians with minimum and maximum, means, standard deviations and standard errors of mean are depicted.

Descriptive Statistics	Control Monolayer		Control Monolayer		Precipitates	
	FCS	hPL	FCS	hPL	FCS	hPL
Median	1.868	0.820	1.538	1.102	1.433	1.875
Minimum	0.390	0.116	0.214	0.109	0.151	0.003
Maximum	4.966	2.728	4.992	3.913	362.826	88.979
Mean	2.081	0.961	1.663	1.297	10.385	5.114
Standard deviation	0.994	0.671	0.907	0.774	44.799	12.688
Standard error	0.076	0.052	0.693	0.597	0.884	3.084

### 3. Discussion

Since the pioneering work of Nakahara and co-authors in the early 1990s, who explored the suitability of JPCs for bone tissue constructs applications [34], several studies have shown that they are comparable to, if not superior to bone marrow MSCs with respect to their bone healing and regeneration capacity [35,36]. For tissue engineering applications of jaw periosteal cells [1], a well-defined and clinical oriented approach has to be defined in terms of cell harvesting, serum-free culturing conditions and subsequent characterization has to be established. In the present study, we cultivated JPCs in hPL- and FCS-supplemented media in order to investigate the biochemical and biomechanical effects of different types of media on the JPC-formed ECM.

JPCs expanded under hPL supplementation grew significantly faster than the FCS-supplemented ones, as we published previously [33]. This might be indicative of upregulated S, G<sub>2</sub>/M phases as previously shown by Xia Et al. [37]. Additionally, we demonstrated in the same publication significantly higher mineralization degrees of JPCs expanded under hPL compared to FCS supplementation [33]. Even though the exact mechanism that triggers JPCs fast expansion and differentiation by hPL supplementation is not fully understood, it might be attributed to elevated concentrations of growth and differentiation factors contained in hPL. While the content of growth factors varies with hPL preparation, several studies emphasized EGF, bFGF, HGF, PDGF-AB, TGF-β1 and VEGF as being secreted by platelets [37–39]. Additionally, while a combination of the factors PDGF, bFGF and TGF-β1 was described as being “sufficient” to expand MSCs in a serum-free culture setting [40], the combination of PDGF, bFGF and IGF-1 has been shown to induce osteogenic differentiation of MSCs [41–43]. In order to improve in vitro JPC mineralization by optimization of cell culture conditions and for the simultaneous establishment of clinical-grade protocols, we tested in a further former study a serum-free medium for JPC cultivation and osteogenic differentiation. Analyses of the resulting phenotype and functional differences in comparison to FCS-supplemented cultures revealed higher



proliferation activities and a selection of osteoprogenitor cells (MSCA-1 positive cells) under serum-free cultivation [44]. Raman analysis of the extracellular matrix showed a more mature mineralization and a higher quality of minerals formed under serum-free culture conditions [45]. Despite these advantages, mineralization degree remained too low, probably based partly on insufficient matrix component secretion such as type I collagen. In order to move a step further, we tested clinical-grade platelet lysate for JPC supplementation and detected, as already mentioned, significantly higher proliferation rates and mineralization potential of JPCs even without the addition of dexamethasone [33]. In the present study, we analyzed the biochemical composition and mechanical properties of the extracellular matrix synthesized under hPL supplementation in order to get a deeper understanding of JPC osteogenesis and in order to move forward to clinical applications. By Raman analyses, we detected higher phosphate to protein ratios indicating higher phosphate deposition under hPL supplementation. Under these conditions, carbonate content was found to be lower and crystal size to be significantly higher, thus reflecting a higher quality of formed crystals containing lesser carbonate and a stronger mineralization potential. Concerning the maturation process of collagen, a higher release of the precursor amino acid proline was detected while amounts of the mature hydroxyproline were proportionally lower under hPL, compared to FCS supplementation. Since hydroxyproline is responsible for collagen fibril stability, these findings could indicate a softer consistency of the collagen matrix, as already observed and illustrated in Figure 2 (gel-like appearance). However, collagen cross-linking seems to be significantly higher under hPL conditions, thus potentially conferring a higher tensile strength of the collagen matrix. Moreover, similar observations have been made by Gupta and co-authors. They showed in an *in vivo* setting after implantation of MSC-seeded calcium phosphate carriers in nude mice, a more mature mineralized tissue when MSCs were pre-expanded under hPL supplementation. FCS-expanded cells exhibited after implantation in nude mice the formation of a rather fibrous tissue [46].

It is known that MSCs differentiation characteristics and phenotypic manifestation are strongly regulated by ECM stiffness and density [47]. The arising question in our study was whether biochemical signals induced by hPL and FCS media supplementation could be transferred into physical mechanical properties reflecting mineralization capability of the JPCs. As indicated by our AFM data, the JPC-ECM exhibited a significant stiffness increase ( $p < 0.001$ ) for control and osteogenically-induced monolayers under FCS when compared to hPL supplementation. In contrast, in terms of JPC-formed precipitates under hPL conditions, a significant stiffness increase ( $p < 0.001$ ) was detected compared to FCS culturing settings. As shown by Roberts and co-authors, even though the FCS supplementation of periosteal cells has a positive effect on the osteocalcin and alkaline phosphatase (APL) expression in the early stages of osteogenic differentiation, further osteoinductive agents are required for the terminal differentiation into mature osteoblasts, such as: trans-retinoic acid, dexamethasone and bone morphogenic protein 2 (BMP2) [48]. Platelet lysate contains a potpourri of factors platelets are composed of, and therefore superior to xenogenic serum [49].

A relatively large variation in the Young's moduli of JPC-formed EMC was detected, even within the same subgroups. This may reflect partially the heterogeneity of the cells. Furthermore, since a polymeric bead of  $\sim 25 \mu\text{m}$  was used for AFM indentation of ECM regions present in close vicinity of the cells, local structural variations such as the presence of stress fibers and distribution of various cytoskeleton elements (i.e., actin filaments, microtubules and intermediate filaments) might contribute to the increase in overall stiffness variability. This phenomenon was already described two decades ago [50].

## 4. Material and Methods

### 4.1. Cell Isolation and Culture of Jaw Periosteal Cells (JPCs)

JPCs derived from 4 donors were included in this study in accordance with the local ethical committee (approval number 618/2017BO2; date (15.12.2017 and 26.03.2019) and after obtaining written informed consent for the participants. The jaw periosteal tissue was cut in small pieces with a scalpel and



enzymatically digested with type XI collagenase (1500 U/ml, Sigma-Aldrich, Steinheim, Germany) for 90 min. Enzymatically isolated cells were expanded in DMEM/F12 + 10% fetal calf serum (FCS) for up to 4 passages until used in passage 5–6 for osteogenic differentiation experiments. Detailed phenotypic and functional characterization of arisen JPCs under FCS and hPL supplementation was published previously by our group [33]. These cells represent the population of JPCs targeted and analyzed in the present study. For Raman measurements, glass bottom dishes (Cellview cell culture dishes from Greiner Bio-One GmbH, Germany) were used for JPC culturing and measuring. For AFM analyses, JPCs were cultured and measured in tissue culture dishes (TPP, Trasadingen, Switzerland). In the following, the terms Raman and AFM dishes will be used in order to distinguish between both culture plates. Comparison of the biochemical composition and mechanical properties of cell-formed extracellular matrix followed under DMEM/F-12 (Invitrogen-BioSource Europe, Nivelles, Belgium) culturing containing 10% FCS (Sigma-Aldrich, Steinheim, Germany) or 10% platelet lysate, both containing 1% amphotericin B and penicillin/streptomycin (Biochrom, Berlin, Germany). The used hPL was provided by the Centre for Clinical Transfusion Medicine in Tübingen, it did not contain heparin and was referred to as a research lysate based on the absent quarantine period. DMEM-cultured cells were passaged using trypsin-versene EDTA (1x, Lonza, Basel, Switzerland) and medium change was performed three times per week.

Osteogenic conditions were performed for all experiments by the addition of dexamethasone (4  $\mu$ M),  $\beta$ -glycerophosphate (10 mM) and L-ascorbic acid 2-phosphate (100  $\mu$ M) for at least 20 days. Due to the fact that especially FCS-supplemented JPCs mineralized in AFM dishes much more quickly than in Raman dishes, we chose different time points for the respective Raman and AFM measurements.

#### 4.2. Quantification of Cell Mineralization by Alizarin Dye Staining

hPL- and FCS-supplemented JPCs from 3 donors were induced osteogenically in Raman and AFM dishes ( $n = 3$  per culture condition, untreated and osteogenic) for at least 20 days and cell monolayers were fixed with 4% formalin for 20 min. After two wash steps with PBS, 1 mL of a 40 mM Alizarin dye solution with a pH of 4.2 was added to the monolayers for 20 min while shaking. Unbound dye was washed 4 times with distilled water for 15 min. Alizarin dye was dissolved out from the monolayers by the addition of 10% acetic acid solution, for 20 min while shaking. Cell layers were detached by scraping and pipetted into 1.5 mL tubes for heating at 85 °C for 10 min while vigorously mixing. After cooling the samples on ice for 5 min and centrifugation at 20,000  $g$  for 20 min, supernatants were neutralized by the addition of 10% ammonium hydroxide. The standard curve for the calculation of calcium concentrations in the samples was plotted as a function of a serially diluted (1:2 dilution) Alizarin Red stock solution (40 mM) to standard concentrations between 2 mM and 0.031 mM. Photometrical measurements were performed at a wavelength of 405 nm using the ELx800 photometer (BioTek Instruments GmbH, Bad Friedrichshall, Germany). Additionally, JPCs grown within Raman dishes were also stained by von Kossa. Therefore, cell monolayers were cold-fixed with 100% ethanol for 15 min and washed with distilled water three times before incubation with 5% silver nitrate for 1 hour at room temperature. After washing, sodium carbonate (0.05 g/mL) in a 9% formalin containing solution was added for 2 min and finally sodium thiosulfate (0.05 g/mL) was added for an additional 2 min of incubation. After three wash steps, images were taken in the water solution.

#### 4.3. Raman Spectroscopy Measurements of hPL- and FCS-Supplemented JPC Monolayers

An inVia Qontor Raman microscope (Renishaw GmbH, Pliezhausen, Germany) was employed for all measurements by Sophie-Maria Kliesch at the company Quality Analysis (Nürtingen, Germany). Raman spectra were excited by a 785 nm laser beam through a 40 $\times$  water-immersion objective (Leica Microsystems GmbH, Wetzlar, Germany). The system was calibrated based on the silicon peak at 520  $\text{cm}^{-1}$  prior to all measurements. The laser output power was set on 150 mW (due to scattering losses, only 50% of the laser power reaches the sample) for spectra acquisition. Raman spectra were collected from either JPCs cultured with serum or human platelet lysate containing media (DMEM/F12),



after visible and robust cell mineralization for 20–30 days of osteogenic induction. JPCs from 4 donors were cultured for Raman measurements in uncoated glass bottom cell culture dishes (Greiner Bio-One GmbH, Frickenhausen, Germany), in the following referred to as Raman dishes. The total acquisition time per spectrum was 3 seconds within a mapping measurement with 126–162 single spectra. A background spectrum from the glass dish containing the cell culture medium was taken for each set of data. All acquired Raman spectra were background-subtracted using the specific background spectrum and then baseline corrected (arithmetic operation) using WiRE (Renishaw GmbH, Pliezhausen, Germany). A smoothing algorithm (Savitzky–Golay, second polynomial order, 7 data points) was employed on all spectra.

Raman spectra were investigated to compare the biochemical composition of JPC-formed extracellular matrix under FCS and hPL supplementation. For this purpose, the following spectral ratios were calculated from the Raman spectra: hydroxyapatite (HA) to phenylalanine ( $960/1004\text{ cm}^{-1}$ ), HA to amide I ( $960/1660\text{ cm}^{-1}$ ), HA to amide III ( $960/1244\text{ cm}^{-1}$ ) and carbonate to HA ( $1070/960\text{ cm}^{-1}$ ). For the calculation of HA crystallinity (crystal size), the inverse of the full-width half maximum (FWHM) was taken into consideration for the spectral range from  $900\text{--}1000\text{ cm}^{-1}$  using WiRE software. The apatite peak was fitted using a standard Gaussian curve. Based on the fitted curve the inverse of FWHM ( $1/\text{FWHM}$ ) was calculated for the HA peak at  $960\text{ cm}^{-1}$ .

#### *4.4. Biomechanical Characterization of hPL- and FCS-Supplemented JPC Monolayers by Atomic Force Microscopy (AFM)*

Elastic moduli of JPCs were assessed ( $n = 4$  donors) using an AFM system (CellHesion 200, JPK Instruments, Berlin, Germany) mounted on to an inverted light microscope (AxioObserver D1, Carl Zeiss Microscopy, Jena, Germany), which allowed simultaneous visualization of the cells. This modular approach allowed us to position and measure specific regions of interest within the dishes. Calibration of the cantilever was done on a clean surface of a petri dish; it was performed on the retracted curve and the spring constant was determined by using the thermal noise method incorporated into the device software (JPK Instruments, Berlin, Germany). Measurements were performed in force spectroscopy mode by recording single force–distance curves at the position of interest without laterally scanning the sample. For microscale indentation, a polymeric microsphere ( $25\text{ }\mu\text{m}$  in diameter, Polysciences, Inc., Warrington, PA, USA) was glued (M-Bond 610 Adhesive, Micro-Measurements, Raleigh, NC, USA) to an AFM cantilever (tip A,  $k = 0.2\text{ N/m}$ , All-In-One-AI-TI, Budget Sensors, Sofia, Bulgaria). Indentation curves were sampled at  $2\text{ kHz}$ , with a force trigger of  $\sim 10\text{ nN}$  and a velocity of  $5\text{ }\mu\text{m/sec}$ . To evaluate elastic properties of the JPC-formed ECM under FCS and hPL culturing conditions, we applied indentations over the chosen region of interest identified by microscopic examination ( $\sim 50$  different positions/culture condition) (Figure 8). The Young's modulus is the ratio of uniaxial force per unit surface in pascal divided by the adimensional proportional deformation of the examined sample and was calculated from the force–distance curves by using the Hertz fit model incorporated in the data processing software (JPK Instruments, Berlin, Germany).

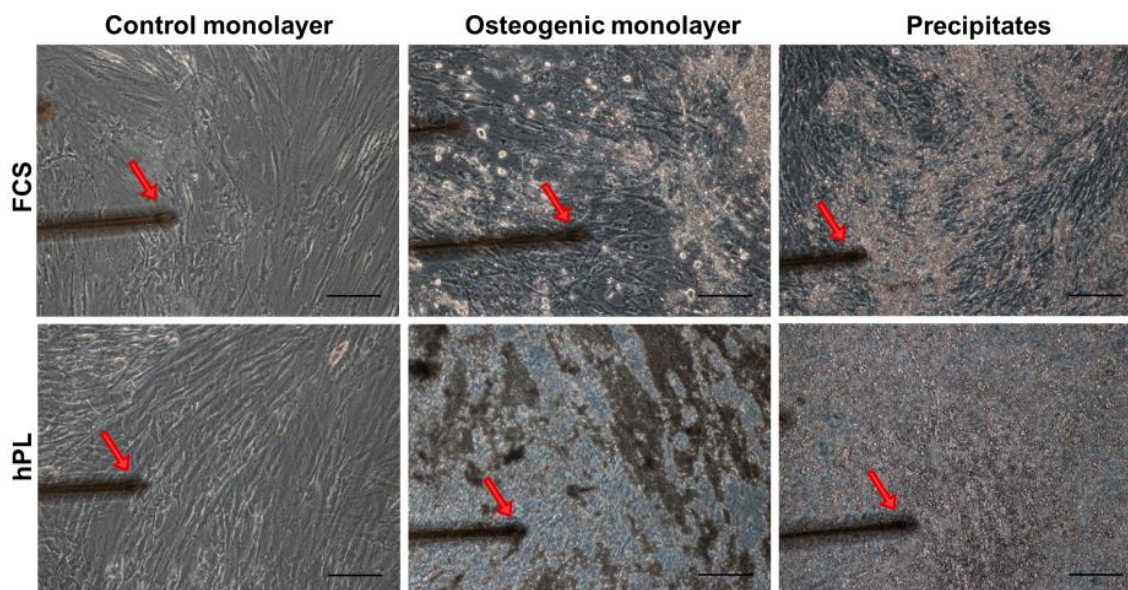


**Figure 8.** Representative microscopic images indicating the regions of interest subjected to elasticity measurements. Microscopic pictures of AFM measured JPCs—control monolayers (left pictures), osteogenic induced JPCs (middle) and calcium phosphate precipitates (right pictures) formed under hPL and FCS culturing conditions, respectively. Red arrows depict the position of the cantilever for elasticity measurements of non-mineralized regions in untreated (left) and osteogenic monolayers (middle, without precipitates) and of calcium phosphate precipitates. Images were acquired with the inverted AxioObserver D1 light microscope attached to the AFM system at a 10× magnification. Scale bar (black) represents 30  $\mu\text{m}$ . Abbreviations: AFM—atomic force microscopy, JPCs—jaw periosteum derived progenitor cells, FCS—fetal calf serum, hPL—human platelet lysate.

#### 4.5. Osteocalcin Gene Expression by Quantitative PCR

Untreated and osteogenically induced JPCs under FCS and hPL supplementation from 4 donors were cultured for 5 and 10 days before RNA isolation followed using the RNeasy Mini kit following manufacturer's instructions. RNA concentration was determined using fluorescent staining (RNA HS Assay kit from ThermoFisher Scientific, Waltham, MA, USA) and measurement with a Qubit 3.0 fluorometer (Life Technologies/ThermoFisher Scientific, Waltham, MA, USA). 100 ng RNA was used for cDNA synthesis with the SuperScript™ Vilo™ Master Mix (Invitrogen/ThermoFisher Scientific, Waltham, MA, USA). For PCR reactions, commercially available primer kits from Search-LC (Heidelberg, Germany) and the DNA Master SybrGreen I kit (Roche, Basel, Switzerland) were used. PCR amplifications were performed with the LightCycler System (Roche, Mannheim, Germany) following a touchdown PCR protocol (annealing temperature between 68 and 58 °C). Osteocalcin transcript levels were normalized to those of the house keeping gene glyceraldehyde 3-phosphate dehydrogenase (GAPDH). Ratios of osteocalcin/GAPDH in untreated JPCs were set as 1 and induction indices of osteogenically induced samples were calculated.

#### 4.6. Statistical Analysis

Normality of the data was assessed by means of Shapiro–Wilks tests and histograms. Based on normality, for both the Raman and AFM data sets, the non-parametric Mann–Whitney U test was used to determine whether the differences between the groups were significant or not. Raman values are displayed as means  $\pm$  standard deviations ( $p$ -values are listed in Table 1), while AFM values are presented as median (minimum–maximum,  $p$ -values in Table 2) and graphically displayed as boxplots. Additionally, for the AFM results, means, standard deviations, and standard errors of the mean are additionally listed in Table 3. In terms of calcium quantification (Alizarin Red staining) data are shown



as means  $\pm$  standard deviations and a two-tailed Student's *t*-test was used to determine statistically significant differences between the groups. Statistical analysis was performed using the SPSS Statistics 22 (IBM Corp., Armonk, NY, USA) software. A *p*-value  $< 0.05$  was considered significant.

## 5. Conclusions

In summary, nanoindentation combined with the Raman technology represent an exciting tool for the biochemical and mechanical examination of bone-like matrix formed by osteogenically-induced JPCs. By using these technologies, we detected higher degrees of mineralization in hPL compared to FCS supplemented monolayers, based on higher phosphate to matrix ratios and increased size and stiffness of calcium phosphate precipitates. Therefore, hPL supplementation not only accelerates JPCs proliferation activities as already demonstrated in our previous study [33], but also leads to the formation of anorganic material of superior quality in terms of biochemical composition and mechanical properties.

**Author Contributions:** Conceptualization, D.A.; methodology, M.M, M.D. and S.-M.K.; software, M.D., M.M. and S.-M.K.; validation, M.D., M.M. and S.-M.K.; formal analysis, S.-M.K.; investigation, A.N.; resources, S.R.; data curation, M.D., M.M., S.-M.K.; writing—original draft preparation, M.D. and D.A.; writing—review and editing, A.N., S.R. and D.A.; visualization, M.D and D.A.; supervision, D.A.; project administration, D.A.; funding acquisition, D.A.

**Funding:** This work was partly supported by the Deutsche Forschungsgemeinschaft (AL1486/6-1AV133/7-1) and partly by AiF (KF2662003SB4).

**Conflicts of Interest:** The authors declare no conflict of interest.

## References

- Alexander, D.; Hoffmann, J.; Munz, A.; Friedrich, B.; Geis-Gerstorfer, J.; Reinert, S. Analysis of OPLA scaffolds for bone engineering constructs using human jaw periosteal cells. *J. Mater. Sci. Mater. Med.* **2008**, *19*, 965–974. [[CrossRef](#)]
- Ferretti, C.; Mattioli-Belmonte, M. Periosteum derived stem cells for regenerative medicine proposals: Boosting current knowledge. *World J. Stem Cells* **2014**, *6*, 266–277. [[CrossRef](#)] [[PubMed](#)]
- De Bari, C.; Dell'Accio, F.; Vanlauwe, J.; Eyckmans, J.; Khan, I.M.; Archer, C.W.; Jones, E.A.; McGonagle, D.; Mitsiadis, T.A.; Pitzalis, C.; et al. Mesenchymal multipotency of adult human periosteal cells demonstrated by single-cell lineage analysis. *Arthritis Rheum.* **2006**, *54*, 1209–1221. [[CrossRef](#)] [[PubMed](#)]
- Bruder, S.P.; Jaiswal, N.; Haynesworth, S.E. Growth kinetics, self-renewal, and the osteogenic potential of purified human mesenchymal stem cells during extensive subcultivation and following cryopreservation. *J. Cell Biochem.* **1997**, *64*, 278–294. [[CrossRef](#)]
- Tylek, T.; Schilling, T.; Schlegelmilch, K.; Ries, M.; Rudert, M.; Jakob, F.; Groll, J. Platelet lysate outperforms FCS and human serum for co-culture of primary human macrophages and hMSCs. *Sci. Rep.* **2019**, *9*, 3533. [[CrossRef](#)] [[PubMed](#)]
- Altaie, A.; Owston, H.; Jones, E. Use of platelet lysate for bone regeneration—Are we ready for clinical translation? *World J. Stem Cells* **2016**, *8*, 47–55. [[CrossRef](#)] [[PubMed](#)]
- Shih, D.T.; Burnouf, T. Preparation, quality criteria, and properties of human blood platelet lysate supplements for ex vivo stem cell expansion. *New Biotechnol.* **2015**, *32*, 199–211. [[CrossRef](#)]
- Ben Azouna, N.; Jenhani, F.; Regaya, Z.; Berraais, L.; Ben Othman, T.; Ducrocq, E.; Domenech, J. Phenotypical and functional characteristics of mesenchymal stem cells from bone marrow: Comparison of culture using different media supplemented with human platelet lysate or fetal bovine serum. *Stem Cell Res. Ther.* **2012**, *3*, 6. [[CrossRef](#)]
- Pérez-Illarbe, M.; Díez-Campelo, M.; Aranda, P.; Tabera, S.; Lopez, T.; del Cañizo, C.; Merino, J.; Moreno, C.; Andreu, E.J.; Prósper, F.; et al. Comparison of ex vivo expansion culture conditions of mesenchymal stem cells for human cell therapy. *Transfusion* **2009**, *49*, 1901–1910. [[CrossRef](#)]

10. Riordan, N.H.; Madrigal, M.; Reneau, J.; de Cupeiro, K.; Jiménez, N.; Ruiz, S.; Sanchez, N.; Ichim, T.E.; Silva, F.; Patel, A.N. Scalable efficient expansion of mesenchymal stem cells in xeno free media using commercially available reagents. *J. Transl. Med.* **2015**, *13*, 232. [[CrossRef](#)]
11. Hemeda, H.; Giebel, B.; Wagner, W. Evaluation of human platelet lysate versus fetal bovine serum for culture of mesenchymal stromal cells. *Cytotherapy* **2014**, *16*, 170–180. [[CrossRef](#)]
12. Fekete, N.; Gadelorge, M.; Fürst, D.; Maurer, C.; Dausend, J.; Fleury-Cappellesso, S.; Mailänder, V.; Lotfi, R.; Ignatius, A.; Sensebé, L.; et al. Platelet lysate from whole blood-derived pooled platelet concentrates and apheresis-derived platelet concentrates for the isolation and expansion of human bone marrow mesenchymal stromal cells: Production process, content and identification of active components. *Cytotherapy* **2012**, *14*, 540–554. [[PubMed](#)]
13. Strunk, D.; Lozano, M.; Marks, D.C.; Loh, Y.S.; Gstraunthaler, G.; Schennach, H.; Rohde, E.; Laner-Plamberger, S.; Öller, M.; Nystedt, J.; et al. International Forum on GMP-grade human platelet lysate for cell propagation. *Vox Sang.* **2018**, *113*, e1–e25. [[CrossRef](#)] [[PubMed](#)]
14. Arandian, A.; Bagheri, Z.; Ehtesabi, H.; Najafi Nobar, S.; Aminoroaya, N.; Samimi, A.; Latifi, H. Optical Imaging Approaches to Monitor Static and Dynamic Cell-on-Chip Platforms: A Tutorial Review. *Small* **2019**, *15*, e1900737. [[CrossRef](#)] [[PubMed](#)]
15. Daniel, A.; Prakasarao, A.; Ganesan, S. Near-infrared Raman spectroscopy for estimating biochemical changes associated with different pathological conditions of cervix. *Spectrochim. Acta A Mol. Biomol. Spectrosc.* **2018**, *190*, 409–416. [[CrossRef](#)]
16. Pandey, R.; Paidi, S.K.; Kang, J.W.; Spegazzini, N.; Dasari, R.R.; Valdez, T.A.; Barman, I. Discerning the differential molecular pathology of proliferative middle ear lesions using Raman spectroscopy. *Sci. Rep.* **2015**, *5*, 13305. [[CrossRef](#)]
17. Pavlou, E.; Zhang, X.; Wang, J.; Kourkoumelis, N. Raman spectroscopy for the assessment of osteoarthritis. *Ann. Jt.* **2018**, *3*, 83. [[CrossRef](#)]
18. Cui, S.; Zhang, S.; Yue, S. Raman Spectroscopy and Imaging for Cancer Diagnosis. *J. Healthc. Eng.* **2018**, *2018*, 11. [[CrossRef](#)]
19. Brauchle, E.; Schenke-Layland, K. Raman spectroscopy in biomedicine—Non-invasive in vitro analysis of cells and extracellular matrix components in tissues. *Biotechnol. J.* **2013**, *8*, 288–297. [[CrossRef](#)]
20. Boyd, A.R.; Burke, G.A.; Meenan, B.J. Monitoring cellular behaviour using Raman spectroscopy for tissue engineering and regenerative medicine applications. *J. Mater. Sci. Mater. Med.* **2010**, *21*, 2317–2324. [[CrossRef](#)]
21. Frushour, B.G.; Koenig, J.L. Raman scattering of collagen, gelatin, and elastin. *Biopolymers* **1975**, *14*, 379–391. [[CrossRef](#)]
22. Ellis, R.; Green, E.; Winlove, C.P. Structural Analysis of Glycosaminoglycans and Proteoglycans by Means of Raman Microspectrometry. *Connect. Tissue Res.* **2009**, *50*, 29–36. [[CrossRef](#)]
23. Votteler, M.; Carvajal Berrio, D.A.; Pudlas, M.; Walles, H.; Stock, U.A.; Schenke-Layland, K. Raman spectroscopy for the non-contact and non-destructive monitoring of collagen damage within tissues. *J. Biophotonics* **2012**, *5*, 47–56. [[CrossRef](#)]
24. Pudlas, M.; Brauchle, E.; Klein, T.J.; Hutmacher, D.W.; Schenke-Layland, K. Non-invasive identification of proteoglycans and chondrocyte differentiation state by Raman microspectroscopy. *J. Biophotonics* **2013**, *6*, 205–211. [[CrossRef](#)]
25. Kunstar, A.; Otto, C.; Karperien, M.; Blitterswijk, C.; van Apeldoorn, A. Raman Microspectroscopy: A Noninvasive Analysis Tool for Monitoring of Collagen-Containing Extracellular Matrix Formation in a Medium-Throughput Culture System. *Tissue Eng. Part C Methods* **2011**, *17*, 737–744. [[CrossRef](#)]
26. Macrí-Pellizzeri, L.; Pelacho, B.; Sancho, A.; Iglesias-García, O.; Simón-Yarza, A.M.; Soriano-Navarro, M.; González-Granero, S.; García-Verdugo, J.M.; De-Juan-Pardo, E.M.; Prosper, F. Substrate stiffness and composition specifically direct differentiation of induced pluripotent stem cells. *Tissue Eng. Part A* **2015**, *21*, 1633–1641. [[CrossRef](#)]
27. Yeh, Y.T.; Hur, S.S.; Chang, J.; Wang, K.C.; Chiu, J.J.; Li, Y.S.; Chien, S. Matrix stiffness regulates endothelial cell proliferation through septin 9. *PLoS ONE* **2012**, *7*, e46889. [[CrossRef](#)]
28. Ng, M.R.; Besser, A.; Danuser, G.; Brugge, J.S. Substrate stiffness regulates cadherin-dependent collective migration through myosin-II contractility. *J. Cell Biol.* **2012**, *199*, 545–563. [[CrossRef](#)]



29. Dufre ne, Y.F.; Ando, T.; Garcia, R.; Alsteens, D.; Martinez-Martin, D.; Engel, A.; Gerber, C.; M ller, D.J. Imaging modes of atomic force microscopy for application in molecular and cell biology. *Nat. Nanotechnol.* **2017**, *12*, 295. [[CrossRef](#)]
30. Jorba, I.; Uriarte, J.J.; Campillo, N.; Farr , R.; Navajas, D. Probing Micromechanical Properties of the Extracellular Matrix of Soft Tissues by Atomic Force Microscopy. *J. Cell Physiol.* **2017**, *232*, 19–26. [[CrossRef](#)]
31. LeBlon, C.E.; Casey, M.E.; Fodor, C.R.; Zhang, T.; Zhang, X.; Jedlicka, S.S. Correlation between in vitro expansion-related cell stiffening and differentiation potential of human mesenchymal stem cells. *Differentiation* **2015**, *90*, 1–15. [[CrossRef](#)]
32. Titushkin, I.; Cho, M. Modulation of cellular mechanics during osteogenic differentiation of human mesenchymal stem cells. *Biophys. J.* **2007**, *93*, 3693–3702. [[CrossRef](#)]
33. Wanner, Y.; Umrath, F.; Waidmann, M.; Reinert, S.; Alexander, D. Platelet Lysate: The Better Choice for Jaw Periosteal Cell Mineralization. *Stem Cells Int.* **2017**, *2017*, 8303959. [[CrossRef](#)]
34. Nakahara, H.; Bruder, S.; Goldberg, V.M.; Caplan, A.I. In Vivo Osteochondrogenic Potential of Cultured Cells Derived from the Periosteum. *Clin. Orthop. Relat. Res.* **1990**, *259*, 223–232. [[CrossRef](#)]
35. Evans, S.F.; Chang, H.; Knothe Tate, M.L. Elucidating multiscale periosteal mechanobiology: A key to unlocking the smart properties and regenerative capacity of the periosteum? *Tissue Eng. Part B Rev.* **2013**, *19*, 147–159. [[CrossRef](#)]
36. Agata, H.; Asahina, I.; Yamazaki, Y.; Uchida, M.; Shinohara, Y.; Honda, M.J.; Kagami, H.; Ueda, M. Effective bone engineering with periosteum-derived cells. *J. Dent. Res.* **2007**, *86*, 79–83. [[CrossRef](#)]
37. Xia, W.; Li, H.; Wang, Z.; Xu, R.; Fu, Y.; Zhang, X.; Ye, X.; Huang, Y.; Xiang, A.P.; Yu, W. Human platelet lysate supports ex vivo expansion and enhances osteogenic differentiation of human bone marrow-derived mesenchymal stem cells. *Cell Biol. Int.* **2011**, *35*, 639–643. [[CrossRef](#)]
38. Christgau, M.; Moder, D.; Hiller, K.A.; Dada, A.; Schmitz, G.; Schmalz, G. Growth factors and cytokines in autologous platelet concentrate and their correlation to periodontal regeneration outcomes. *J. Clin. Periodontol.* **2006**, *33*, 837–845. [[CrossRef](#)]
39. Doucet, C.; Ernou, I.; Zhang, Y.; Llense, J.R.; Begot, L.; Holy, X.; Lataillade, J.J. Platelet lysates promote mesenchymal stem cell expansion: A safety substitute for animal serum in cell-based therapy applications. *J. Cell Physiol.* **2005**, *205*, 228–236. [[CrossRef](#)]
40. Ng, F.; Boucher, S.; Koh, S.; Sastry, K.S.; Chase, L.; Lakshmiopathy, U.; Choong, C.; Yang, Z.; Vemuri, M.C.; Rao, M.S.; et al. PDGF, TGF-beta, and FGF signaling is important for differentiation and growth of mesenchymal stem cells (MSCs): Transcriptional profiling can identify markers and signaling pathways important in differentiation of MSCs into adipogenic, chondrogenic, and osteogenic lineages. *Blood* **2008**, *112*, 295–307.
41. Kumar, A.; Salimath, B.P.; Stark, G.B.; Finkenzeller, G. Platelet-derived growth factor receptor signaling is not involved in osteogenic differentiation of human mesenchymal stem cells. *Tissue Eng. Part A* **2010**, *16*, 983–993. [[CrossRef](#)]
42. Ito, T.; Sawada, R.; Fujiwara, Y.; Tsuchiya, T. FGF-2 increases osteogenic and chondrogenic differentiation potentials of human mesenchymal stem cells by inactivation of TGF-beta signaling. *Cytotechnology* **2008**, *56*, 1–7. [[CrossRef](#)]
43. Giustina, A.; Mazziotti, G.; Canalis, E. Growth hormone, insulin-like growth factors, and the skeleton. *Endocr. Rev.* **2008**, *29*, 535–559. [[CrossRef](#)]
44. Alexander, D.; Rieger, M.; Klein, C.; Ardjomandi, N.; Reinert, S. Selection of osteoprogenitors from the jaw periosteum by a specific animal-free culture medium. *PLoS ONE* **2013**, *8*, e81674. [[CrossRef](#)]
45. Brauchle, E.; Carvajal Berrio, D.; Rieger, M.; Schenke-Layland, K.; Reinert, S.; Alexander, D. Raman Spectroscopic Analyses of Jaw Periosteal Cell Mineralization. *Stem Cells Int.* **2017**, 1651376. [[CrossRef](#)]
46. Gupta, P.; Hall, G.N.; Geris, L.; Luyten, F.P.; Papantoniou, I. Human Platelet Lysate Improves Bone Forming Potential of Human Progenitor Cells Expanded in Microcarrier-Based Dynamic Culture. *Stem Cells Transl. Med.* **2019**, *8*, 810–821. [[CrossRef](#)]
47. Li, B.; Moshfegh, C.; Lin, Z.; Albuschies, J.; Vogel, V. Mesenchymal Stem Cells Exploit Extracellular Matrix as Mechanotransducer. *Sci. Rep.* **2013**, *3*, 2425. [[CrossRef](#)]
48. Roberts, S.J.; Chen, Y.; Moesen, M.; Schrooten, J.; Luyten, F.P. Enhancement of osteogenic gene expression for the differentiation of human periosteal derived cells. *Stem Cell Res.* **2011**, *7*, 137–144. [[CrossRef](#)]

49. Bieback, K. Platelet lysate as replacement for fetal bovine serum in mesenchymal stromal cell cultures. *Transfus. Med. Hemother.* **2013**, *40*, 326–335. [[CrossRef](#)]
50. Hofmann, U.G.; Rotsch, C.; Parak, W.J.; Radmacher, M. Investigating the cytoskeleton of chicken cardiocytes with the atomic force microscope. *J. Struct. Biol.* **1997**, *119*, 84–91. [[CrossRef](#)]



© 2019 by the authors. Licensee MDPI, Basel, Switzerland. This article is an open access article distributed under the terms and conditions of the Creative Commons Attribution (CC BY) license (<http://creativecommons.org/licenses/by/4.0/>).





### 3. Discussion

Cells are capable of adjusting their shape and function by altering their mechanical properties through structural rearrangements in their biochemical composition at a nanometer scale. The mechanical properties of a tissue are the sum of the comprised cells and the vast matrix (i.e. ECM). There is a continuous interaction between the cellular components and the surrounding ECM. On one side, these interactions actively dictate the physiological remodeling of the tissue, thus its regeneration-and on the other side, the catabolic degeneration of the tissue. Insights into the interaction between the cellular components and the ECM, and into actual ECM functional biomechanical transduction might hold a key for both the development of high-quality engineered tissues, and clinical tools for early diagnostics.

In its physiological state, but even more in pathological conditions, the ECM is constantly subjected to either enzymatic or non-enzymatic remodeling processes, and its molecular components are subjected to a myriad of post-translational modifications (Frantz et al., 2010). It is these ongoing ECM remodeling characteristics that dictate the biochemical and mechanical properties of each organ, such as its tensile and compressive strength and elasticity. So far, the ECM and its biomechanical properties have been the root of useful pieces of information with respect to the presence of specific protein biomarkers in a tissue e.g.: de novo collagen and proteoglycan synthesis. Moreover, the non-invasive determination of biomechanical attributes can be used as a biomarker capable differentiating between the physiological and pathological state (Rianna and Radmacher, 2016, Janmey and Miller, 2011). Correlating the biomechanical properties of tissue with its function is an emerging area of research with a potential impact on diagnostics and therapeutics, as well as on prognostics of pathological conditions. A common parameter evaluated with the aim of differentiating between normal and diseased tissue is tissue elasticity (respectively stiffness), which is generally expressed as the EM. Malignant tumors, for example, are characteristically much stiffer than the normal surroundings. The reason for this increase in stiffness lies in the excess ECM deposition and the resulting increased rigidity (Cox and Erler, 2011). Measuring forces at micro- or even nanoscale levels is a critical approach for defining our understanding of cell-matrix interactions, and for understanding how the ECM regulates cellular function and how it contributes to the biomechanical functions of the tissue.

Among the available techniques for measuring the mechanical properties of biological tissues, AFM has emerged as a non-invasive and highly versatile technique. It is capable of quantifying and spatially mapping tissue and cellular mechanics, and physical properties, at a nanometer resolution. Information obtained from the AFM includes surface morphology, frictional force on the nanoscale, hardness of surfaces, stiffness and elasticity, load distribution, magnetization, yield stress, and elastic-plastic deformation dynamics (Polini and Yang, 2017). In particular, the AFM-elasticity determination technique, sometimes referred to as force-distance analysis, is used to measure the EM of a sample at distinct and user-defined points as the probe indentations are done across a specified region.

In the present thesis, the biomechanical elasticity of load bearing tissue and cells (cartilage and bone derived cells) were quantitatively assessed by means of AFM. The results obtained from the two analyses are further discussed individually and in detail.

### ***3.1. Biomechanical cues in early osteoarthritis***

OA is a set of complex and difficult-to-identify processes leading to progressive and irreversible degeneration of articular cartilage. It has been suggested that OA triggers cellular remodelling processes which have been previously suggested to act as an image-based biomarker for early OA promoted degenerative processes occurring at a cellular level (Aicher and Rolauuffs, 2014). The chondrocytes are fully surrounded by the PCM. This microenvironment is believed to play a critical role in the transduction of ECM compression into local physicochemical signals for the cell (Wilusz et al., 2014). Any direct interactions between cell surface receptors such as integrins and the tissue matrix are thus likely to occur first at the level of the PCM. In fact, evidence suggests that the PCM acts as a transducer for both biomechanical as well as biochemical signals for the cells it surrounds (Guilak et al., 2006, Chen et al., 2013, Vincent et al., 2007). The PCM has been primarily defined by the presence of collagen type VI (Poole et al., 1992) and perlecan, a large heparansulfate (HS) proteoglycan (Melrose et al., 2005). It is known that during OA, changes in the collagen type VI synthesis of the PCM and proteoglycan distribution within the chondron are followed by chondrocyte proliferation, expansion of the pericellular microenvironment, structural disruption, and chondrocyte clustering (Poole, 1997, Poole et al., 1996).



Changes in the PCM thus herald the upcoming degenerative processes and are associated with a significant loss of mechanical properties. Several technical challenges arise when aiming to investigate and quantify the biochemical properties of the PCM, such as the micrometer scale of the PCM (Youn et al., 2006), embedment of the PCM into the ECM of the cartilage, and the low cell density of articular cartilage (Stockwell, 1971). Recent reports have, however, indicated that AFM-based microindentation allows for direct quantification of PCM properties *in situ* with minimal disruption of the native matrix integration between the PCM and ECM (Darling et al., 2010, Wilusz et al., 2013, McLeod et al., 2013).

In this research study, the aim to evaluate whether the elasticity-EM (as measured via AFM) of the PCM decreases as a function of OA onset and progression. OA tissue categorization was done by employing the spatial arrangement of chondrocytes as an image-based biomarker. EM was assessed by means of AFM on tissue selected according to the locally predominant spatial chondrocyte pattern. Additionally, the pattern related changes of two major PCM components (collagen type VI and perlecan) were analyzed by ELISA (Enzyme-linked Immunosorbent Assay). The results obtained indicate that there is a significant and stepwise EM decrease alongside each of the cellular pattern rearrangements. The Young's modulus of the PCM of healthy cartilage (single strings) was about ~50 kPa (range 6-174 kPa). These results are comparable with those obtained from isolated chondrons by micropipette aspiration technique (~40-70 kPa) and *in situ* AFM measurements of the PCM from native human cartilage (range: 27-205 kPa) (Darling et al., 2010, Wilusz et al., 2013). Similar observations were made when comparing the measured results of small clusters (early OA) with those obtained from macroscopically assigned early OA samples measured by Wilusz et al. (Wilusz et al., 2013). Overall, our study shows that a decrease of approximately 40% was observed between healthy tissue and osteoarthritic cartilage, results which are again in line with those of measured chondrons extracted by the micropipette aspiration technique (Alexopoulos et al., 2005, Alexopoulos et al., 2003). Additionally, various computational models have also indicated similar values for EM reduction in OA, emphasizing that the PCM in cartilage is approximately 1 order of magnitude less stiff than that of the ECM. Also, while the hydraulic permeability of the PCM is 1-2 orders of magnitude lower than that of the ECM, it seems to double with OA (Alexopoulos et al., 2003, Alexopoulos et al., 2005).

It needs to be pointed out, however, that cartilage slices subjected to AFM indentations in the present study were obtained in the horizontal plane with respect to the cartilage surface. In still intact cartilage areas where mostly strings are present, the main collagen fiber orientation is also horizontal. Thus, these fibers remained largely intact within the histologic sections. This was not the case in areas with already macroscopic cartilage damage. When obtaining tissue from these areas, the section was rather preferably obtained from the middle or deep zone of the cartilage. Especially in the deep zone of the cartilage, the collagen arcades are in their ascending/descending orientation (Mow and Guo, 2002), and thus they were cut perpendicularly when sectioning. Since it is in these areas with advanced local tissue degeneration where more pathologic cellular patterns are observed, such as small and big clusters, it is possible that the measured values bear a negative bias and appear worse than they would truly be without sectioning. At the same time, it is known that osteoarthritis is a disease affecting the whole joint (Loeser et al., 2012), with the inflammatory processes also changing cartilage areas that still appear macroscopically intact (own data not shown). It can thus be assumed that in still intact and healthy cartilage, the values for the single strings would have still been higher than the ones measured in the present study.

In terms of the structural composition of the PCM with OA onset and progression, two of its main components (collagen type VI and perlecan) became progressively structurally impaired. This structural impairment was coupled with a reduction in the total protein content of these components as measured by ELISA. The progressive impairment of the PCM, particularly collagen type VI, with increasingly pathological spatial organization had been described previously (Felka et al., 2016a). Changes in the perlecan expression in OA have also been documented before (Tesche and Miosge, 2004), pinpointing its possible involvement in the pathogenesis of the disease. Both proteins have been suggested to dictate the overall biomechanical properties of the PCM (Wilusz et al., 2012b, Wilusz et al., 2012a). Collagen type VI, which was initially well defined pericellularly in strings and in double strings, showed a much more dispersed and unorganized signal in big clusters, where its intracellular signal was completely lost. In terms of perlecan staining, in strings it had a signal extra- and intracellularly, followed by the same diffuse signal loss with cellular rearrangement. It could also be noted that in advanced degenerative cartilage (as represented by big clusters), both components were destroyed. As OA is characterized by an upregulation of protein pro-



duction of proteolytic enzymes (e.g. matrix metalloproteinase enzymes (MMPs)) (Martel-Pelletier et al., 1994), the loss of structural proteins (collagen type VI and perlecan) might represent the synergetic result of the catabolic activity of these enzymes. Another possible cause for inconsistent PCM destruction of observed cell clusters could be the consequence of nonhomogeneous matrix degradation, as already suggested by Söder et al (Soder et al., 2002). In terms of collagen type VI, no relevant changes in protein content and distribution could be observed between strings and double strings. Clear and significant differences were visible, however, between small and big clusters, as well as at the transition site from double strings to small clusters; this is the earliest time point where relevant OA-triggered changes take place in the PCM. It could also be noted that the earliest functional impairment with respect to the EM of the PCM was detected at the transition from strings to double strings. Importantly, this is still at a stage where the cartilage appears macroscopically to be intact. The EM decrease was observed simultaneously with the alteration and destruction of the PCM. This suggests that the two phenomena are linked to one another.

Up until now, most studies investigating the OA-related degeneration of cartilage biochemically and/or biomechanically have based their grading of the severity of the disease on macroscopic assessment grading systems such as the International Cartilage Repair Society (ICRS) system (Kleemann et al., 2005), or the Collins grading system (Wilusz et al., 2013). These grading systems have, however, limited utility, reproducibility, and validity, particularly for early OA stages (Pritzker et al., 2006). To the knowledge of the author, this is the first study to describe PCM structural and EM changes based on tissue categorization by spatial arrangement of chondrocytes. The fact that the EM decreases alongside the cellular rearrangement does not prove any causality. In a recently accepted manuscript from the author, the observed changes of the PCM could also be observed in the ECM (Danalache et al., 2019). This leads to the speculation that the cellular rearrangement is not solely and strictly involved in the PCM changes and its microbiomechanical characteristics, rather that the processes of cellular rearrangement and tissue destruction either go hand in hand, or tissue destruction is a prerequisite for cellular rearrangement. Interestingly, changes in spatial organization are not just correlated with the biomechanical features in the pericellular region, but also with those of the ECM. It is indeed true that the decrease in EM of the PCM and ECM goes simultaneously, unidirectionally, and at a comparable speed, suggesting that the

underlying mechanisms are of the same nature (Danalache et al., 2019). This finding is further supported by previous theoretical models of cell-matrix interactions in cartilage, which suggest that the ratio of the two matrixes (ECM and PCM) with respect to their mechanical properties may significantly influence the mechanical environment of the chondrocyte (Alexopoulos et al., 2003, Guilak and Mow, 2000).

Overall, the present data shows that the first OA-PCM related degenerative changes are already measurable at the cellular transition from single to double strings, where cartilage still appears macroscopically “intact”. This further strengthens the idea that the cellular spatial patterns play a measurable and functional role throughout the course of the disease, instead of just being the passive result of OA-related remodeling and rearrangement processes. As such there is potential to use an optical based biomarker in the clinical setting for diagnosis of early stages of OA.

### ***3.2. Biomechanical cues for customizing jaw periosteal cells for bone constructs***

The justification for the ongoing research efforts in BTE is founded on the fact that bone autografting is still the golden standard in treating bone defects, despite the invasiveness and traumatic nature of the procedure. In this respect, the ongoing demand for personalized therapeutic approaches has enhanced the scientific interest and research focus towards cell-based therapies and cell-enriched constructs for regenerative purposes. In terms of a cell source, human jaw periosteum tissue contains osteoprogenitor cells (JPCs) that have potential for tissue engineering applications in oral and maxillofacial surgery. However, in order to bring such cell-based approaches into the clinical setting, defined animal free culture conditions coupled with a precise characterization of the cells and their formed ECM are a must. Hitherto, the benchmark in terms of media supplementation for *in vitro* settings has been FCS. hPL has however been recently suggested to be a suitable and “clinically acceptable” alternative.

In a former study, Wanner et al. 2017 showed that JPCs (to be precise: mesenchymal stromal cell antigen-1 (MSCA-1<sup>+</sup>) cells) cultivated under hPL supplementation were characterized by a higher proliferation and mineralization potential than JPCs cultivated under FCS settings (Wanner et al., 2017). In the present study, the aim was to further quantitatively analyze the biochemical composition as well as the biomechanical properties (particularly elasticity) of the ECM formed by JPCs under both hPL and FCS



supplementation. RAMAN spectroscopy was used to investigate the biochemical composition and the biomechanical elasticity were assessed by AFM. In the present study, we observed higher proliferation rates of JPCs expanded under hPL conditions, results which are in accordance with the ones previously obtained by Wanner et al (Wanner et al., 2017). hPL is obtained via freeze-thaw cycles of platelets and subsequent centrifugal separation of the debris from all the bioactive platelet factors (Schallmoser and Strunk, 2013). These platelets include various growth factors, such as PDGF, TGF- $\beta$ 1, VEGF, EGF, attachment factors, and enzymes (Antoninus et al., 2015). It is conceivable that such a potpourri of growth factors might indeed actually be the reason for the JPCs fast expansion and differentiation.

The structural composition of the ECM determines the biomechanical properties. These properties depend on the abundance of collagen and other proteins (non-mineralized components), as well as on matrix mineralized components (phosphates). Human bone minerals are constituted of a poorly crystallized apatite, comprised mainly of calcium-deficient apatite, hydrogen phosphate, calcium-carbonate, and other ions. The hydroxyapatite crystal structure exhibits a “hydrated layer”, where reactive ions form the non-apatitic domains, which surround the stable apatite domains of the bone crystals (Farlay et al., 2010). With bone maturation, the size and number of crystals increase. Bone mineral maturity is expressed as the ratio of apatitic and non-apatitic domains. The mineral crystallinity depends on both the size and amount, as well as on the symmetry of the apatite crystalline domains and their size/strain (Farlay et al., 2010). Even tough staining approaches such as Alizarin Red S and von Kossa are commonly used (Bonewald et al., 2003b, Gregory et al., 2004), when analyzing the mineralization degree and bone quality formation, they fail to assess the quality of the mineralized species. In this respect, RAMAN spectroscopy has already been successfully used to identify changes in bone composition in metabolic bone diseases such as osteoporosis and osteogenesis imperfecta (Roschger et al., 2008).

The RAMAN spectra results of the present study showed a higher phosphate to protein ratio in the hPL group, indicative of higher phosphate ECM deposition. Moreover, the carbonate to phosphate ratio was higher in FCS containing culture conditions. Similar observations were made by Brauchle et al. in a study where *in vitro* formation of bone-specific matrixes by JPCSs was analyzed under serum free and FCS containing media culture conditions (Brauchle et al., 2017). The authors of that study actually indi-

cated that a higher carbonate to phosphate ratio combined with a low mineral to matrix ratio might be indicative of poor bone quality (Brauchle et al., 2017). An inverse proportionality relationship was observed in the case of carbonate and crystal content; while carbonates exhibited a significant decrease in content, the crystal content increased. This is indicative of a higher quality of the formed crystals. A lower carbonate content coupled with a higher mineralization potential is usually the result of higher-quality bone. Also, in the here presented study, hPL conditions led to overall lower carbonate levels than those obtained under FCS settings. As already suggested by Young et al., FCS contains active components such as complement components 3 and 4A, fetuin-A, and apolipoproteins A1 and B100, which are capable of accelerating crystallization of free phosphates (Young et al., 2009). The mineral crystallinity can also be estimated from the RAMAN spectra by using the width of the primary phosphate band, which is mathematically described as the reciprocal of the full-width-half-maximum (FWHM) (Freeman et al., 2001). According to the RAMAN data presented here, the mineral crystallinity was significantly higher under hPL settings when compared to the one under FCS supplementation. A lower mineral crystallinity, as observed under FCS settings, might translate into altered bone mechanics by the occurrence of micro-strains within and around the crystal lattice. In fact, in human cortical bone, Yerramshetty and Akkus reported that the tissue-level strength and stiffness both increase with increasing crystallinity while ductility decreases (Yerramshetty and Akkus, 2008). In terms of collagen maturity and quality, the RAMAN data shows that collagen cross-linking was significantly higher under hPL than under FCS conditions; hPL supplementation might thus induce a higher tensile strength of the matrix collagen. In support of this hypothesis, the proline to hydroxyproline (amino acids precursors) ratio was also significantly higher in hPL-JPCs than in FCS ones; hPL enriched media therefore seems to support mineralization via maturation of collagens in JPCs.

The next question to address was whether or not the aforementioned observed biochemical composition ECM variations under FCS and hPL supplementation actually translate into physical mechanical properties which reflect the JPCs' mineralization capability. Until now, ample evidence suggested that biomechanical properties of the ECM, particularly its stiffness, are capable of regulating and dictating MSC differentiation characteristics (Lv et al., 2017). Even more so, according to a 2018 study by Sun et al., the stiffness of the ECM actually seems to regulate MSC osteogenic differentiation





through mechanotransduction events mediated by integrin  $\alpha 5$  (Sun et al., 2018). The AFM results of our study indicated an EM increase of the ECM for the control as well as the osteogenically induced JPCs under FCS settings as compared to the hPL setting. The opposite effect was noted for the JPCs formed precipitates, where a significant EM decrease was observed under FCS supplementation. Similar observations were made for tissue engineered cartilage, where hPL media enrichment led to a significantly higher EM (~ 45% increase), and a tissue with implicitly greater compressive mechanical properties overall as when compared to FCS conditions (Petrera et al., 2013). The matrix remodeling capacities of tissues cultured in hPL might therefore be higher than those of tissues cultured in FCS.

In a study conducted by van Geemen where the formation and mechanical properties of heart valve engineered constructs was analyzed, MMP levels were shown to be higher in the hPL group than in standard FCS culturing (van Geemen et al., 2011). MMPs are key players in both inflammatory and remodeling phases of wound healing. Their presence and upregulation might be indicative of an active remodeling process, similar to that occurring in wound healing and formation of scar tissue. As suggested by van Geerme, during wound healing, the presence of the scar, which can be recognized by a disorganized collagen network and high remodeling properties, might result in an initially weaker tissue (van Geemen et al., 2011). It is therefore conceivable that with time, tissue cultured in hPL could undergo a remodeling process which might ultimately lead to stronger and more organized tissue. This is in accordance with the AFM data from the present study on JPCs-ECM, as lower EM were observed in early stages (control and osteogenic monolayers), followed by a significant increase in the JPCs formed precipitates. In addition, even though FCS enhances early osteogenic differentiation, the presence of osteo-inductive agents such as all trans-retinoic acid, bone morphogenic protein 2 (BMP2), and dexamethasone are required for the expression of transcription factors governing osteogenesis and hence differentiation towards a mature osteoblast cell population (Roberts et al., 2011). Plasma platelets are known to be a rich source of growth factors (Weibrich et al., 2002), and are therefore more efficient in terms of cell differentiation capability and proliferation rates (Doucet et al., 2005) than using exogenous recombinant growth factors and standard serum enriched media. The superiority of hPL supplementation is thus further supported.

Biomechanical characteristics are attributed also, to the orientation of the collagen fibrils, as well as to differences in collagen content and its spatial distribution (Silva et al., 2006). As observed in the here presented results and in accordance with previous studies, changes in medium supplementation determine changes in the collagen expression (Brauchle et al., 2017). As already suggested by Brauchle et al., structural changes in the orientation of collagen fibers might affect crystallization of phosphate along the collagen fiber, ultimately controlling the mineralization process (Brauchle et al., 2017). To the knowledge of the author, the here presented study is the first to investigate and quantify cell mineralization quality, both biochemically and biomechanically, under standard FCS and hPL settings.

All in all, the study illustrates that JPCs cultured under hPL supplementation form an ECM of superior quality in terms of biochemical composition and elasticity.

### ***3.3. Study limitations***

It has to be borne in mind that AFM analysis is generally restricted to analysis of the outer surface of cell membranes. As AFM is not capable of scanning the inside of a cell membrane, this implicitly means that it is not able to directly investigate intracellular structures. One solution for overcoming this limitation is suggested by Usukura et al., who employed a so called "unroofing" method consisting of the breakage of cellular membrane and the removal of cytoplasmic-soluble components (Usukura et al., 2016). The focus of the both of studies presented here, however, was to investigate average matrix-EM changes rather than probing specific cellular/intracellular components. Also, values obtained from AFM measurements from both studies indicate consistent and individual ranges between groups; this might be explained by local variations in the biomechanical properties of the PCM and ECM. Due to the limited availability of human tissue samples, the trade-off of using such a procedure is the mixing of statistically dependent and independent data, which formally is not indicated. Even though the obtained p-values thus need to be interpreted with the necessary caution, the measured tendency should still not be affected. Experimental AFM parameters used for mechanical testing, such as indentation velocity and depth, indenter shape and size, microsphere size (25  $\mu\text{m}$ ), and accuracy of tip geometry in model fitting (Costa and Yin, 1999) might also impact the absolute values of the measured mechanical properties (Stolz et al.,



2004, Park et al., 2009). These parameters should, however, not affect the results presented in both of the studies.

### ***3.4. Conclusions***

It remains a persistent challenge to understand how complex molecules biosynthesized by cells assemble and function within the context of living cells, tissues, and organs. Cellular functioning is governed by a multitude of processes. Quantifying cell and tissue dynamics, particularly biomechanical features at multiple scales, is essential for comprehensive studies of cellular function, as well as for unveiling the structure-function relationship. Tissue and cell stiffness as measured by AFM is a widely used parameter for fine cellular biomechanics, and it has been used to differentiate between healthy and diseased states, as well as to assess structural changes. In both studies in the present thesis, AFM was successfully used to assess the changes in elasticity, and to investigate whether structural changes translate into physical mechanical properties.

In the first study, it was concluded that OA related changes occurring in the structural composition of PCM and EM are associated with changes in cellular organization as a biomarker for local tissue destruction. Early OA cellular changes represented by transition from single to double strings are characterized by a significant PCM-EM decrease. At this stage the articular cartilage still appears macroscopically intact. The EM decrease is accompanied by structural alterations of the PCM in its collagen type VI and perlecan content, suggesting that the degeneration of these components and functional disruption of the PCM are closely intertwined events in OA pathophysiology.

The second study demonstrated that hPL media supplementation of JPCs enhances the formation of an organic material of superior quality in terms of its biochemical composition and also of its biomechanical characteristic, as indicated by its elasticity. The combination of biochemical characterization by means of RAMAN spectroscopy coupled with AFM based-biomechanical elasticity assessment provided structural and functional information that might help classify and differentiate the formation of poor quality of bone tissue.

## 4. Summary

Mechanical features influence nearly every aspect of cell biology and function. However, the underlying mechanisms of the role and how mechanical properties and biochemical signals are interconnected is not clearly understood. The advent of atomic force microscopy (AFM) provides a powerful tool for quantifying mechanical properties of living cell, typically the elastic modulus (EM). In the present study, a customized AFM approach was applied on load connective tissues to address and investigate two aspects of the musculoskeletal system. The first study investigated the EM changes that occur in the pericellular matrix (PCM) as a function of the cellular pattern reorganization throughout the course of osteoarthritis (OA). The second study investigated the effect of human platelet lysate (hPL) supplementation on EM and biochemical composition of jaw periosteum derived progenitor cells (JPCs).

During osteoarthritis (OA) triggered cartilage degeneration, the chondrocytes in the tissue spatially rearrange from single to double strings, and then to small and finally big clusters. The spatial patterns act as an image-based biomarker for tissue degeneration during OA. In a physiological state, chondrocytes are surrounded by a specialized form of extracellular matrix (ECM) termed the PCM. The PCM, which also dictates the biomechanical properties of the tissue, is also being progressively degraded throughout the course of OA. The hypothesis of this study was that OA related changes in the cellular organizational patterns (strings, double strings, and clusters) are associated with structural changes of the PCM and with a loss of elastic properties. The biomechanical properties were measured by AFM on specific pattern selected tissue. Biochemical changes of the main components of the PCM (collagen type VI and perlecan) were investigated by protein analysis techniques. The results indicated that there is a significant and stepwise EM decrease alongside each of the cellular pattern rearrangements. At the same time, the initially compact PCM was degraded progressively, losing its structural integrity. The earliest point with a significant reduction in protein content was at the transition from single strings to small clusters for collagen type VI, and from double strings to small clusters for perlecan. Interestingly, the first significant EM decrease was observed at the transition from single strings to double strings. It must be noted that at this stage, articular cartilage appears macroscopically intact. Both biomechanical properties (EM) as well as biochemical composition (protein content) were the lowest in



big clusters. This study is the first to describe the EM as well as structural changes of the PCM in relation to the OA related chondrocyte rearrangement, confirming the role of these patterns as an image-based biomarker for early OA events.

The hypothesis of the second study was that human plasma lysate (hPL) media enrichment leads to a higher quality of the ECM in JPCs when compared with the standard fetal calf serum (FCS) condition. For this purpose, JPCs cultured with the aforementioned media supplementations were analyzed in two study arms. RAMAN spectroscopy was used for biochemical characterization, and AFM was employed for biomechanical analysis. Raman spectroscopic measurements showed significantly higher phosphate to protein ratios and lower carbonate to phosphate ratios under hPL in comparison to FCS culturing. With respect to the ECM collagen maturity, higher ratios of proline to hydroxyproline as well as higher levels of collagen cross-linking were detected in hPL-cultured JPCs. This indicates that hPL induces a higher degree of collagen maturation in JPCs. AFM data showed a significant increase in EM of the ECM under hPL conditions. This study hence demonstrates that hPL media supplementation of JPCs leads to the formation of a higher ECM quality as when compared to the FCS standard settings.

In summary, both studies employed AFM-based elasticity measurements to investigate biomechanical features of load-bearing tissues. In both studies, the results obtained were significant and provide further insights which may now be fused into existing axioms of biochemical processes. Integration of both biomechanical and biochemical features will play a vital role in future scientific endeavors and will serve to establish an in-depth understanding of cellular biology.

## 5. Zusammenfassung

Mechanische Eigenschaften beeinflussen nahezu jeden Aspekt der Zelle in Bezug auf ihre Biologie und Funktion. An welchen Schaltstellen mechanische Eigenschaften und biochemische Signale jedoch miteinander verknüpft sind ist bisher nur wenig verstanden. Die Rasterkraftmikroskopie bietet hier die interessante Möglichkeit mechanische Eigenschaften von lebenden Zellen zu untersuchen. Am gebräuchlichsten ist hierbei die Untersuchung des Elastizitätsmoduls (EM), welches Aussagen über die Steifheit des Gewebes zulässt. In der hier präsentierten Arbeit wurden mittels Rasterkraftmikroskopie zwei Fragestellungen zum muskuloskelettalen System untersucht: Die erste Studie untersuchte die auftretenden EM-Veränderungen der Perizellulären Matrix (PZM) im Rahmen der räumlichen Umorganisation der Chondrozyten im Zuge der Knorpeldegeneration. In der zweiten Studie wurde der Einfluss von humanem Plättchenlysat (hPL) auf das EM sowie auf den biochemischen Aufbau von aus Kieferperiost gewonnenen Progenitorzellen gemessen.

Im Zuge der Knorpeldegeneration bei Arthrose verändert sich die räumliche Organisation der Knorpelzellen hin von einfachen Zellsäulen (Engl. "single strings") zu Doppelsäulen (Engl. "double strings") und schließlich zu kleinen (Engl. "small clusters") und großen Zellhaufen (Engl. "big clusters"). Diese Zellmuster dienen als bildbasierter Biomarker der degenerativen Veränderungen im Knorpel im Rahmen von Arthrose. Knorpelzellen sind im physiologischen Zustand unmittelbar von einer Sonderform der Extrazellulärmatrix (EZM) umgeben, der sogenannten perizellulären Matrix (PZM). Die PZM, die die Biomechanik der Zellen maßgeblich mitdiktiert, degradiert zunehmend während der Arthrose. Die Hypothese der hier durchgeführten Studie war, dass es im Rahmen der zellulären Musterveränderungen von einfachen Zellsäulen zu großen Zellhaufen auch zu strukturellen Veränderungen der PZM kommt, was ebenso einen Verlust der elastischen Eigenschaften mit sich zieht. Die Elastizität der PZM wurde dabei für jedes der zellulären Muster separat mittels Rasterkraftmikroskopie gemessen. Gleichzeitig wurden biochemische Veränderungen von zwei wesentlichen Bausteinen der PZM (Kollagen Typ VI und Perlekan) mittels Proteinanalysetechniken untersucht. Es konnte dabei gezeigt werden, dass es im Rahmen der Musteränderungen zu einer schrittweisen und signifikanten Reduktion des EM kommt. Der früheste Zeitpunkt einer signifikanten Reduktion an Proteingehalt wurde am Übergang von einfachen Zellsäulen

zu kleinen Zellhaufen für Kollagen Typ VI und von Doppelsäulen zu kleinen Zellhaufen für Perlekan beobachtet. Interessanterweise konnte der erste signifikante Rückgang des EM bereits am Übergang von einfachen zu doppelten Zellsäulen gemessen werden. Dies ist ein Zustand, in welchem der Knorpel makroskopisch noch intakt erscheint. Erwartungsgemäß zeigte sich bei großen Zellhaufen die größte Beeinträchtigung, sowohl proteinbiochemisch wie auch biomechanisch. Zusammenfassend ist dies die erste Studie, welche das EM der PZM, wie auch einige ihre Komponenten in einen direkten Zusammenhang mit der räumlichen Knorpelzellanordnung setzt, was somit die Bedeutung dieser als bildbasierten Biomarker für frühe Arthrose unterstreicht.

Die Hypothese der zweiten Studie war, dass die Anreicherung von Zellkulturmedium mit hPL eine bessere Qualität der EZM bei aus Kieferperiost gewonnenen Progenitorzellen erzielt, als wenn das Medium mit fetalem Kälberserum versehen wird. Hierzu wurde in zwei Studienarmen eine jeweilige Zellkultur mit den unterschiedlichen Nährlösungen durchgeführt. Sodann wurde die EZM biochemisch mittels RAMAN-Spektroskopie charakterisiert und das EM mittels Rasterkraftmikroskopie gemessen. In der Spektroskopie konnte ein signifikant höheres Phosphat-zu-Protein Verhältnis und ein niedrigeres Carbonat-zu-Phosphat Verhältnis unter hPL im Vergleich zur Kultur mit fetalem Kälberserum festgestellt werden. Auch in Bezug auf Reife des EZM-Kollagens konnten unter hPL höhere Verhältnisse von Prolin-zu-Hydroxyprolin und höhere Spiegel an Kollagen-Quervernetzung beobachtet werden. In der Rasterkraftmikroskopie zeigte sich weiterhin eine signifikante Zunahme des EM unter hPL-Bedingungen. Insofern zeigt die hier präsentierte Studie, dass Anreicherung von Zellkulturmedium mit hPL zur Ausbildung einer höherqualitativen EZM führt als die bisherige Standardbeimischung von fetalem Kälberserum.

Zusammenfassend konnten so in beiden Studien anhand von Elastizitätsmessungen lasttragenden Gewebes biomechanische Untersuchungen durchgeführt werden. In beiden Fällen ergab sich aus den Messergebnissen ein Informationsgewinn mit eindeutigen Ergebnissen, welche nun in ihrer biomechanischen Dimension in das übliche biochemische Verständnis integriert werden können. Die Schnittstelle von biomechanischen zu biochemischen Vorgängen in Geweben und Zellen wird auch in künftigen Untersuchungen von hoher Bedeutung für ein fundiertes funktionelles Verständnis der Biologie auf zellulärer Ebene sein.

## 6. Bibliography

- AICHER, W. K. & ROLAUFFS, B. 2014. The spatial organisation of joint surface chondrocytes: review of its potential roles in tissue functioning, disease and early, preclinical diagnosis of osteoarthritis. *Ann Rheum Dis*, 73, 645-53.
- ALEXOPOULOS, L. G., HAIDER, M. A., VAIL, T. P. & GUILAK, F. 2003. Alterations in the mechanical properties of the human chondrocyte pericellular matrix with osteoarthritis. *J Biomech Eng*, 125, 323-33.
- ALEXOPOULOS, L. G., WILLIAMS, G. M., UPTON, M. L., SETTON, L. A. & GUILAK, F. 2005. Osteoarthritic changes in the biphasic mechanical properties of the chondrocyte pericellular matrix in articular cartilage. *J Biomech*, 38, 509-17.
- ANTONINUS, A. A., WIDOWATI, W., WIJAYA, L., AGUSTINA, D., PURADISASTRA, S., SUMITRO, S. B., WIDODO, M. A. & BACHTIAR, I. 2015. Human platelet lysate enhances the proliferation of Wharton's jelly-derived mesenchymal stem cells. *Biomarkers and Genomic Medicine*, 7, 87-97.
- ATT, W., KUBO, K., YAMADA, M., MAEDA, H. & OGAWA, T. 2009. Biomechanical properties of jaw periosteum-derived mineralized culture on different titanium topography. *Int J Oral Maxillofac Implants*, 24, 831-41.
- BIDAN, C. M., VELDSINK, A. C., MEURS, H. & GOSENS, R. 2015. Airway and Extracellular Matrix Mechanics in COPD. 6.
- BONEWALD, L. F., HARRIS, S. E., ROSSER, J., DALLAS, M. R., DALLAS, S. L., CAMACHO, N. P., BOYAN, B. & BOSKEY, A. 2003a. von Kossa staining alone is not sufficient to confirm that mineralization in vitro represents bone formation. *Calcif Tissue Int*, 72, 537-47.
- BONEWALD, L. F., HARRIS, S. E., ROSSER, J., DALLAS, M. R., DALLAS, S. L., CAMACHO, N. P., BOYAN, B. & BOSKEY, A. 2003b. Von Kossa Staining Alone Is Not Sufficient to Confirm that Mineralization In Vitro Represents Bone Formation. *Calcified Tissue International*, 72, 537-547.
- BRAMA, P. A., TEKOPPELE, J. M., BANK, R. A., BARNEVELD, A. & VAN WEEREN, P. R. 2000. Functional adaptation of equine articular cartilage: the formation of regional biochemical characteristics up to age one year. *Equine Vet J*, 32, 217-21.





- BRAUCHLE, E., CARVAJAL BERRIO, D., RIEGER, M., SCHENKE-LAYLAND, K., REINERT, S. & ALEXANDER, D. 2017. Raman Spectroscopic Analyses of Jaw Periosteal Cell Mineralization. *Stem cells international*, 2017, 1651376-1651376.
- BRODERS-BONDON, F., NGUYEN HO-BOULDOIRES, T. H., FERNANDEZ-SANCHEZ, M.-E. & FARGE, E. 2018. Mechanotransduction in tumor progression: The dark side of the force. 217, 1571-1587.
- BRUDER, S. P., JAISWAL, N. & HAYNESWORTH, S. E. 1997. Growth kinetics, self-renewal, and the osteogenic potential of purified human mesenchymal stem cells during extensive subcultivation and following cryopreservation. *J Cell Biochem*, 64, 278-94.
- BUTLER, D. L., GOLDSTEIN, S. A., GULDBERG, R. E., GUO, X. E., KAMM, R., LAURENCIN, C. T., MCINTIRE, L. V., MOW, V. C., NEREM, R. M., SAH, R. L., SOSLOWSKY, L. J., SPILKER, R. L. & TRANQUILLO, R. T. 2009. The impact of biomechanics in tissue engineering and regenerative medicine. *Tissue engineering. Part B, Reviews*, 15, 477-484.
- CHANG, H. & KNOTHE TATE, M. L. 2012. Concise Review: The Periosteum: Tapping into a Reservoir of Clinically Useful Progenitor Cells. *STEM CELLS Translational Medicine*, 1, 480-491.
- CHEN, C., TAMBE, D. T., DENG, L. & YANG, L. 2013. Biomechanical properties and mechanobiology of the articular chondrocyte. 305, C1202-C1208.
- CHO, S., IRIANTO, J. & DISCHER, D. E. 2017. Mechanosensing by the nucleus: From pathways to scaling relationships. *J Cell Biol*, 216, 305-315.
- COSTA, K. D. & YIN, F. C. 1999. Analysis of indentation: implications for measuring mechanical properties with atomic force microscopy. *J Biomech Eng*, 121, 462-71.
- COX, T. R. & ERLER, J. T. 2011. Remodeling and homeostasis of the extracellular matrix: implications for fibrotic diseases and cancer. *Dis Model Mech*, 4, 165-78.
- DANALACHE, M., JACOBI, L. F., SCHWITALLE, M. & HOFMANN, U. K. 2019. Assessment of biomechanical properties of the extracellular and pericellular matrix and their interconnection throughout the course of osteoarthritis. *Journal of Biomechanics*, 109409.

- DARLING, E. M., WILUSZ, R. E., BOLOGNESI, M. P., ZAUSCHER, S. & GUILAK, F. 2010. Spatial mapping of the biomechanical properties of the pericellular matrix of articular cartilage measured in situ via atomic force microscopy. *Biophysical journal*, 98, 2848-2856.
- DE BARI, C., DELL'ACCIO, F., VANLAUWE, J., EYCKMANS, J., KHAN, I. M., ARCHER, C. W., JONES, E. A., MCGONAGLE, D., MITSIADIS, T. A., PITZALIS, C. & LUYTEN, F. P. 2006. Mesenchymal multipotency of adult human periosteal cells demonstrated by single-cell lineage analysis. *Arthritis Rheum*, 54, 1209-21.
- DENG, X., XIONG, F., LI, X., XIANG, B., LI, Z., WU, X., GUO, C., LI, X., LI, Y., LI, G., XIONG, W. & ZENG, Z. J. J. O. N. 2018. Application of atomic force microscopy in cancer research. 16, 102.
- DESROCHERS, J., AMREIN, M. A. & MATYAS, J. R. 2010. Structural and functional changes of the articular surface in a post-traumatic model of early osteoarthritis measured by atomic force microscopy. *J Biomech*, 43, 3091-8.
- DISCHER, D. E., JANMEY, P. & WANG, Y. L. 2005. Tissue cells feel and respond to the stiffness of their substrate. *Science*, 310, 1139-43.
- DJOUAD, F., BOUFFI, C., GHANNAM, S., NOEL, D. & JORGENSEN, C. 2009. Mesenchymal stem cells: innovative therapeutic tools for rheumatic diseases. *Nat Rev Rheumatol*, 5, 392-9.
- DOUCET, C., ERNOU, I., ZHANG, Y., LLENSE, J. R., BEGOT, L., HOLY, X. & LATAILLADE, J. J. 2005. Platelet lysates promote mesenchymal stem cell expansion: a safety substitute for animal serum in cell-based therapy applications. *J Cell Physiol*, 205, 228-36.
- DUFRÊNE, Y. F., ANDO, T., GARCIA, R., ALSTEENS, D., MARTINEZ-MARTIN, D., ENGEL, A., GERBER, C. & MÜLLER, D. J. 2017. Imaging modes of atomic force microscopy for application in molecular and cell biology. *Nature Nanotechnology*, 12, 295.
- DUFRENE, Y. F. & PELLING, A. E. 2013. Force nanoscopy of cell mechanics and cell adhesion. *Nanoscale*, 5, 4094-104.
- EGGLI, P. S., HERRMANN, W., HUNZIKER, E. B. & SCHENK, R. K. 1985. Matrix compartments in the growth plate of the proximal tibia of rats. *Anat Rec*, 211, 246-57.



- EL-KIRAT-CHATEL, S. & DUFRENE, Y. F. 2012. Nanoscale imaging of the Candida-macrophage interaction using correlated fluorescence-atomic force microscopy. *ACS Nano*, 6, 10792-9.
- ELLIS, R., GREEN, E. & WINLOVE, C. P. 2009. Structural analysis of glycosaminoglycans and proteoglycans by means of Raman microspectrometry. *Connect Tissue Res*, 50, 29-36.
- FARLAY, D., PANCZER, G., REY, C., DELMAS, P. D. & BOIVIN, G. 2010. Mineral maturity and crystallinity index are distinct characteristics of bone mineral. *Journal of bone and mineral metabolism*, 28, 433-445.
- FEKETE, N., ROJEWSKI, M. T., FURST, D., KREJA, L., IGNATIUS, A., DAUSEND, J. & SCHREZENMEIER, H. 2012. GMP-compliant isolation and large-scale expansion of bone marrow-derived MSC. *PLoS One*, 7, e43255.
- FELKA, T., ROTHDIENER, M., BAST, S., UYNUK-OOL, T., ZOUHAIR, S., OCHS, B. G., DE ZWART, P., STOECKLE, U., AICHER, W. K., HART, M. L., SHIOZAWA, T., GRODZINSKY, A. J., SCHENKE-LAYLAND, K., VENKATESAN, J. K., CUCCHIARINI, M., MADRY, H., KURZ, B. & ROLAUFFS, B. 2016a. Loss of spatial organization and destruction of the pericellular matrix in early osteoarthritis in vivo and in a novel in vitro methodology. *Osteoarthritis Cartilage*, 24, 1200-9.
- FELKA, T., ROTHDIENER, M., BAST, S., UYNUK-OOL, T., ZOUHAIR, S., OCHS, B. G., DE ZWART, P., STOECKLE, U., AICHER, W. K., HART, M. L., SHIOZAWA, T., GRODZINSKY, A. J., SCHENKE-LAYLAND, K., VENKATESAN, J. K., CUCCHIARINI, M., MADRY, H., KURZ, B. & ROLAUFFS, B. 2016b. Loss of spatial organization and destruction of the pericellular matrix in early osteoarthritis in vivo and in a novel in vitro methodology. *Osteoarthritis and Cartilage*, 24, 1200-1209.
- FELSON, D. T. 2009. Developments in the clinical understanding of osteoarthritis. *Arthritis Res Ther*, 11, 203.
- FELSON, D. T., ZHANG, Y., HANNAN, M. T., NAIMARK, A., WEISSMAN, B. N., ALIABADI, P. & LEVY, D. 1995. The incidence and natural history of knee osteoarthritis in the elderly. The Framingham Osteoarthritis Study. *Arthritis Rheum*, 38, 1500-5.

- FITZSIMMONS, R. E. B., MAZUREK, M. S., SOOS, A. & SIMMONS, C. A. 2018. Mesenchymal Stromal/Stem Cells in Regenerative Medicine and Tissue Engineering. *Stem Cells International*, 2018, 16.
- FRANTZ, C., STEWART, K. M. & WEAVER, V. M. 2010. The extracellular matrix at a glance. 123, 4195-4200.
- FREEMAN, J. J., WOPENKA, B., SILVA, M. J. & PASTERIS, J. D. 2001. Raman Spectroscopic Detection of Changes in Bioapatite in Mouse Femora as a Function of Age and In Vitro Fluoride Treatment. *Calcified Tissue International*, 68, 156-162.
- FRUSHOUR, B. G. & KOENIG, J. L. 1975. Raman scattering of collagen, gelatin, and elastin. *Biopolymers*, 14, 379-391.
- GAO, Y., LIU, S., HUANG, J., GUO, W., CHEN, J., ZHANG, L., ZHAO, B., PENG, J., WANG, A., WANG, Y., XU, W., LU, S., YUAN, M. & GUO, Q. 2014. The ECM-cell interaction of cartilage extracellular matrix on chondrocytes. *BioMed research international*, 2014, 648459-648459.
- GAVARA, N. 2017. A beginner's guide to atomic force microscopy probing for cell mechanics. *Microscopy research and technique*, 80, 75-84.
- GKRETSI, V. & STYLIANOPOULOS, T. 2018. Cell Adhesion and Matrix Stiffness: Coordinating Cancer Cell Invasion and Metastasis. *Frontiers in oncology*, 8, 145-145.
- GREGORY, C. A., GRADY GUNN, W., PEISTER, A. & PROCKOP, D. J. 2004. An Alizarin red-based assay of mineralization by adherent cells in culture: comparison with cetylpyridinium chloride extraction. *Analytical Biochemistry*, 329, 77-84.
- GUILAK, F., ALEXOPOULOS, L. G., UPTON, M. L., YOUN, I., CHOI, J. B., CAO, L., SETTON, L. A. & HAIDER, M. A. 2006. The pericellular matrix as a transducer of biomechanical and biochemical signals in articular cartilage. *Ann N Y Acad Sci*, 1068, 498-512.
- GUILAK, F., BUTLER, D. L., GOLDSTEIN, S. A. & BAAIJENS, F. P. 2014a. Biomechanics and mechanobiology in functional tissue engineering. *J Biomech*, 47, 1933-40.



- GUILAK, F., BUTLER, D. L., GOLDSTEIN, S. A. & BAAIJENS, F. P. T. 2014b. Biomechanics and mechanobiology in functional tissue engineering. *Journal of biomechanics*, 47, 1933-1940.
- GUILAK, F. & MOW, V. C. 2000. The mechanical environment of the chondrocyte: a biphasic finite element model of cell-matrix interactions in articular cartilage. *J Biomech*, 33, 1663-73.
- GUILAK, F., NIMS, R. J., DICKS, A., WU, C. L. & MEULENBELT, I. 2018. Osteoarthritis as a disease of the cartilage pericellular matrix. *Matrix Biol*, 71-72, 40-50.
- HAASE, K. & PELLING, A. E. 2015. Investigating cell mechanics with atomic force microscopy. *Journal of the Royal Society, Interface*, 12, 20140970-20140970.
- HADJIPANAYI, E., MUDERA, V. & BROWN, R. A. 2009. Close dependence of fibroblast proliferation on collagen scaffold matrix stiffness. *J Tissue Eng Regen Med*, 3, 77-84.
- HAMERMAN, D. 1989. The biology of osteoarthritis. *N Engl J Med*, 320, 1322-30.
- HEMEDA, H., GIEBEL, B. & WAGNER, W. 2014. Evaluation of human platelet lysate versus fetal bovine serum for culture of mesenchymal stromal cells. *Cytotherapy*, 16, 170-180.
- HOLLANDER, A. P., PIDOUX, I., REINER, A., RORABECK, C., BOURNE, R. & POOLE, A. R. 1995. Damage to type II collagen in aging and osteoarthritis starts at the articular surface, originates around chondrocytes, and extends into the cartilage with progressive degeneration. *J Clin Invest*, 96, 2859-69.
- HORIMIZU, M., KAWASE, T., TANAKA, T., OKUDA, K., NAGATA, M., BURNS, D. M. & YOSHIE, H. 2013. Biomechanical evaluation by AFM of cultured human cell-multilayered periosteal sheets. *Micron*, 48, 1-10.
- HOWELL, D. S. 1986. Pathogenesis of osteoarthritis. *Am J Med*, 80, 24-8.
- HUEY, D. J., HU, J. C. & ATHANASIOU, K. A. 2012. Unlike bone, cartilage regeneration remains elusive. *Science*, 338, 917-21.
- JANMEY, P. A. & MILLER, R. T. 2011. Mechanisms of mechanical signaling in development and disease. 124, 9-18.
- JANSHOFF, A., NEITZERT, M., OBERDORFER, Y. & FUCHS, H. 2000. Force Spectroscopy of Molecular Systems-Single Molecule Spectroscopy of Polymers and Biomolecules. *Angew Chem Int Ed Engl*, 39, 3212-3237.

- JORDAN, J. M., HELMICK, C. G., RENNER, J. B., LUTA, G., DRAGOMIR, A. D., WOODARD, J., FANG, F., SCHWARTZ, T. A., ABBATE, L. M., CALLAHAN, L. F., KALSBECK, W. D. & HOCHBERG, M. C. 2007. Prevalence of knee symptoms and radiographic and symptomatic knee osteoarthritis in African Americans and Caucasians: the Johnston County Osteoarthritis Project. *J Rheumatol*, 34, 172-80.
- KIM, Y., KO, H., KWON, I. K. & SHIN, K. 2016. Extracellular Matrix Revisited: Roles in Tissue Engineering. *International neurourology journal*, 20, S23-S29.
- KIVIRANTA, P., LAMMENTAUSTA, E., TOYRAS, J., KIVIRANTA, I. & JURVELIN, J. S. 2008. Indentation diagnostics of cartilage degeneration. *Osteoarthritis Cartilage*, 16, 796-804.
- KLEEMANN, R. U., KROCKER, D., CEDRARO, A., TUISCHER, J. & DUDA, G. N. 2005. Altered cartilage mechanics and histology in knee osteoarthritis: relation to clinical assessment (ICRS Grade). *Osteoarthritis Cartilage*, 13, 958-63.
- KORHONEN, R. K., WONG, M., AROKOSKI, J., LINDGREN, R., HELMINEN, H. J., HUNZIKER, E. B. & JURVELIN, J. S. 2002. Importance of the superficial tissue layer for the indentation stiffness of articular cartilage. *Med Eng Phys*, 24, 99-108.
- KUETTNER, K. E., AYDELOTTE, M. B. & THONAR, E. J. 1991. Articular cartilage matrix and structure: a minireview. *J Rheumatol Suppl*, 27, 46-8.
- KUNSTAR, A., LEFERINK, A. M., OKAGBARE, P. I., MORRIS, M. D., ROESSLER, B. J., OTTO, C., KAPERIEN, M., VAN BLITTERSWIJK, C. A., MORONI, L. & VAN APELDOORN, A. A. 2013. Label-free Raman monitoring of extracellular matrix formation in three-dimensional polymeric scaffolds. *J R Soc Interface*, 10, 20130464.
- KWON, T., GUNASEKARAN, S. & EOM, K. 2019. Atomic force microscopy-based cancer diagnosis by detecting cancer-specific biomolecules and cells. *Biochim Biophys Acta Rev Cancer*, 1871, 367-378.
- LANGE, J. R. & FABRY, B. 2013. Cell and tissue mechanics in cell migration. *Exp Cell Res*, 319, 2418-23.
- LARSON, C. M., KELLEY, S. S., BLACKWOOD, A. D., BANES, A. J. & LEE, G. M. 2002. Retention of the native chondrocyte pericellular matrix results in significantly improved matrix production. *Matrix Biol*, 21, 349-59.



- LIN, C., TAO, B., DENG, Y., HE, Y., SHEN, X., WANG, R., LU, L., PENG, Z., XIA, Z. & CAI, K. 2019. Matrix promote mesenchymal stromal cell migration with improved deformation via nuclear stiffness decrease. *Biomaterials*, 217, 119300.
- LIU, F., MIH, J. D., SHEA, B. S., KHO, A. T., SHARIF, A. S., TAGER, A. M. & TSCHUMPERLIN, D. J. 2010. Feedback amplification of fibrosis through matrix stiffening and COX-2 suppression. 190, 693-706.
- LOESER, R. F., GOLDRING, S. R., SCANZELLO, C. R. & GOLDRING, M. B. 2012. Osteoarthritis: a disease of the joint as an organ. *Arthritis and rheumatism*, 64, 1697-1707.
- LOTZ, M. K., OTSUKI, S., GROGAN, S. P., SAH, R., TERKELTAUB, R. & D'LIMA, D. 2010. Cartilage cell clusters. *Arthritis and rheumatism*, 62, 2206-2218.
- LV, H., WANG, H., ZHANG, Z., YANG, W., LIU, W., LI, Y. & LI, L. 2017. Biomaterial stiffness determines stem cell fate. *Life Sci*, 178, 42-48.
- MANKIN, H. J., DORFMAN, H., LIPPIELLO, L. & ZARINS, A. 1971. Biochemical and metabolic abnormalities in articular cartilage from osteo-arthritic human hips. II. Correlation of morphology with biochemical and metabolic data. *J Bone Joint Surg Am*, 53, 523-37.
- MAROUDAS, A. & VENN, M. 1977. Chemical composition and swelling of normal and osteoarthrotic femoral head cartilage. II. Swelling. *Ann Rheum Dis*, 36, 399-406.
- MARRESE, M., GUARINO, V. & AMBROSIO, L. 2017. Atomic Force Microscopy: A Powerful Tool to Address Scaffold Design in Tissue Engineering. *J Funct Biomater*, 8.
- MARTEL-PELLETIER, J., MCCOLLUM, R., FUJIMOTO, N., OBATA, K., CLOUTIER, J. M. & PELLETIER, J. P. 1994. Excess of metalloproteases over tissue inhibitor of metalloprotease may contribute to cartilage degradation in osteoarthritis and rheumatoid arthritis. *Lab Invest*, 70, 807-15.
- MCLEOD, M. A., WILUSZ, R. E. & GUILAK, F. 2013. Depth-dependent anisotropy of the micromechanical properties of the extracellular and pericellular matrices of articular cartilage evaluated via atomic force microscopy. *Journal of Biomechanics*, 46, 586-592.
- MELROSE, J., SMITH, S., CAKE, M., READ, R. & WHITELOCK, J. 2005. Perlecan displays variable spatial and temporal immunolocalisation patterns in the

- articular and growth plate cartilages of the ovine stifle joint. *Histochem Cell Biol*, 123, 561-71.
- MOEENDARBARY, E. & HARRIS, A. R. 2014. Cell mechanics: principles, practices, and prospects. 6, 371-388.
- MOW, V. C. & GUO, X. E. 2002. Mechano-electrochemical properties of articular cartilage: their inhomogeneities and anisotropies. *Annu Rev Biomed Eng*, 4, 175-209.
- MUIR, H. 1995. The chondrocyte, architect of cartilage. Biomechanics, structure, function and molecular biology of cartilage matrix macromolecules. *BioEssays*, 17, 1039-1048.
- NIEMINEN, M. T., RIEPPO, J., TOYRAS, J., HAKUMAKI, J. M., SILVENNOINEN, J., HYTTINEN, M. M., HELMINEN, H. J. & JURVELIN, J. S. 2001. T2 relaxation reveals spatial collagen architecture in articular cartilage: a comparative quantitative MRI and polarized light microscopic study. *Magn Reson Med*, 46, 487-93.
- OLIVERIA, S. A., FELSON, D. T., REED, J. I., CIRILLO, P. A. & WALKER, A. M. 1995. Incidence of symptomatic hand, hip, and knee osteoarthritis among patients in a health maintenance organization. *Arthritis Rheum*, 38, 1134-41.
- PARK, S., COSTA, K. D., ATESHIAN, G. A. & HONG, K. S. 2009. Mechanical properties of bovine articular cartilage under microscale indentation loading from atomic force microscopy. *Proc Inst Mech Eng H*, 223, 339-47.
- PETERS, H. C., OTTO, T. J., ENDERS, J. T., JIN, W., MOED, B. R. & ZHANG, Z. 2011. The protective role of the pericellular matrix in chondrocyte apoptosis. *Tissue Eng Part A*, 17, 2017-24.
- PETRERA, M., DE CROOS, J. N. A., IU, J., HURTIG, M., KANDEL, R. A. & THEODOROPOULOS, J. S. 2013. Supplementation With Platelet-Rich Plasma Improves the In-vitro Formation of Tissue-Engineered Cartilage With Enhanced Mechanical Properties. *Arthroscopy*, 29, 1685-1692.
- PIZZO, A. M., KOKINI, K., VAUGHN, L. C., WAISNER, B. Z. & VOYTIKHARBIN, S. L. 2005. Extracellular matrix (ECM) microstructural composition regulates local cell-ECM biomechanics and fundamental fibroblast behavior: a multidimensional perspective. 98, 1909-1921.





- PLAAS, A., OSBORN, B., YOSHIHARA, Y., BAI, Y., BLOOM, T., NELSON, F., MIKECZ, K. & SANDY, J. D. 2007. Aggrecanolytic in human osteoarthritis: confocal localization and biochemical characterization of ADAMTS5-hyaluronan complexes in articular cartilages. *Osteoarthritis Cartilage*, 15, 719-34.
- PLOTNIKOV, S. V., PASAPERA, A. M., SABASS, B. & WATERMAN, C. M. 2012. Force fluctuations within focal adhesions mediate ECM-rigidity sensing to guide directed cell migration. *Cell*, 151, 1513-27.
- POLINI, A. & YANG, F. 2017. 5 - Physicochemical characterization of nanofiber composites. In: RAMALINGAM, M. & RAMAKRISHNA, S. (eds.) *Nanofiber Composites for Biomedical Applications*. Woodhead Publishing.
- POOLE, A. R., ROSENBERG, L. C., REINER, A., IONESCU, M., BOGOCH, E. & ROUGHLEY, P. J. 1996. Contents and distributions of the proteoglycans decorin and biglycan in normal and osteoarthritic human articular cartilage. 14, 681-689.
- POOLE, C. A. 1997. Articular cartilage chondrons: form, function and failure. *J Anat*, 191 ( Pt 1), 1-13.
- POOLE, C. A., AYAD, S. & GILBERT, R. T. 1992. Chondrons from articular cartilage. V. Immunohistochemical evaluation of type VI collagen organisation in isolated chondrons by light, confocal and electron microscopy. *J Cell Sci*, 103 ( Pt 4), 1101-10.
- POOLE, C. A., GILBERT, R. T., HERBAGE, D. & HARTMANN, D. J. 1997. Immunolocalization of type IX collagen in normal and spontaneously osteoarthritic canine tibial cartilage and isolated chondrons. *Osteoarthritis Cartilage*, 5, 191-204.
- PRITZKER, K. P. H., GAY, S., JIMENEZ, S. A., OSTERGAARD, K., PELLETIER, J. P., REVELL, P. A., SALTER, D. & VAN DEN BERG, W. B. 2006. Osteoarthritis cartilage histopathology: grading and staging. *Osteoarthritis and Cartilage*, 14, 13-29.
- PUPPELS, G. J., DE MUL, F. F., OTTO, C., GREVE, J., ROBERT-NICOUD, M., ARNDT-JOVIN, D. J. & JOVIN, T. M. 1990. Studying single living cells and chromosomes by confocal Raman microspectroscopy. *Nature*, 347, 301-3.

- RAMOS, I., #XEA, MARTINS, S. R., MALKIN, A. & LYNG, F. M. 2015. Current Advances in the Application of Raman Spectroscopy for Molecular Diagnosis of Cervical Cancer. *BioMed Research International*, 2015, 9.
- RIANNA, C. & RADMACHER, M. 2016. Cell mechanics as a marker for diseases: Biomedical applications of AFM. 1760, 020057.
- ROBERTS, S. J., CHEN, Y., MOESEN, M., SCHROOTEN, J. & LUYTEN, F. P. 2011. Enhancement of osteogenic gene expression for the differentiation of human periosteal derived cells. *Stem Cell Research*, 7, 137-144.
- ROLAUFFS, B., WILLIAMS, J., GRODZINSKY, A., E KUETTNER, K. & A COLE, A. 2008. *Distinct horizontal patterns in the spatial organization of superficial zone chondrocytes of human joints*.
- ROLAUFFS, B., WILLIAMS, J. M., AURICH, M., GRODZINSKY, A. J., KUETTNER, K. E. & COLE, A. A. 2010. Proliferative remodeling of the spatial organization of human superficial chondrocytes distant from focal early osteoarthritis. *Arthritis and rheumatism*, 62, 489-498.
- ROSCHGER, P., PASCHALIS, E. P., FRATZL, P. & KLAUSHOFER, K. 2008. Bone mineralization density distribution in health and disease. *Bone*, 42, 456-66.
- SANDELL, L. J. & AIGNER, T. 2001. Articular cartilage and changes in arthritis. An introduction: cell biology of osteoarthritis. *Arthritis Res*, 3, 107-13.
- SCHALLMOSER, K. & STRUNK, D. 2013. Generation of a Pool of Human Platelet Lysate and Efficient Use in Cell Culture. *In: HELGASON, C. D. & MILLER, C. L. (eds.) Basic Cell Culture Protocols*. Totowa, NJ: Humana Press.
- SCHUMACHER, B. L., SU, J. L., LINDLEY, K. M., KUETTNER, K. E. & COLE, A. A. 2002. Horizontally oriented clusters of multiple chondrons in the superficial zone of ankle, but not knee articular cartilage. *Anat Rec*, 266, 241-8.
- SILVA, M. J., BRODT, M. D., WOPENKA, B., THOMOPOULOS, S., WILLIAMS, D., WASSEN, M. H., KO, M., KUSANO, N. & BANK, R. A. 2006. Decreased collagen organization and content are associated with reduced strength of demineralized and intact bone in the SAMP6 mouse. *J Bone Miner Res*, 21, 78-88.
- SMITH, B. T., SHUM, J., WONG, M., MIKOS, A. G. & YOUNG, S. 2015. Bone Tissue



- Engineering Challenges in Oral & Maxillofacial Surgery. *In: BERTASSONI, L. E. & COELHO, P. G. (eds.) Engineering Mineralized and Load Bearing Tissues.* Cham: Springer International Publishing.
- SMITH, L. R., CHO, S. & DISCHER, D. E. 2018. Stem Cell Differentiation is Regulated by Extracellular Matrix Mechanics. *Physiology (Bethesda)*, 33, 16-25.
- SODER, S., HAMBACH, L., LISSNER, R., KIRCHNER, T. & AIGNER, T. 2002. Ultrastructural localization of type VI collagen in normal adult and osteoarthritic human articular cartilage. *Osteoarthritis Cartilage*, 10, 464-70.
- SOPHIA FOX, A. J., BEDI, A. & RODEO, S. A. 2009. The basic science of articular cartilage: structure, composition, and function. *Sports Health*, 1, 461-8.
- STOCKWELL, R. A. 1971. The interrelationship of cell density and cartilage thickness in mammalian articular cartilage. *Journal of anatomy*, 109, 411-421.
- STOLZ, M., RAITERI, R., DANIELS, A. U., VANLANDINGHAM, M. R., BASCHONG, W. & AEBI, U. 2004. Dynamic Elastic Modulus of Porcine Articular Cartilage Determined at Two Different Levels of Tissue Organization by Indentation-Type Atomic Force Microscopy. *Biophysical Journal*, 86, 3269-3283.
- SUKI, B., STAMENOVIC, D. & HUBMAYR, R. 2011. Lung parenchymal mechanics. *Compr Physiol*, 1, 1317-51.
- SUN, M., CHI, G., XU, J., TAN, Y., XU, J., LV, S., XU, Z., XIA, Y., LI, L. & LI, Y. 2018. Extracellular matrix stiffness controls osteogenic differentiation of mesenchymal stem cells mediated by integrin  $\alpha 5$ . *Stem cell research & therapy*, 9, 52-52.
- TAY, C. Y., KOH, C. G., TAN, N. S., LEONG, D. T. & TAN, L. P. 2013. Mechanoregulation of stem cell fate via micro-/nano-scale manipulation for regenerative medicine. 8, 623-638.
- TESCHE, F. & MIOSGE, N. 2004. Perlecan in late stages of osteoarthritis of the human knee joint. *Osteoarthritis and Cartilage*, 12, 852-862.
- TYLEK, T., SCHILLING, T., SCHLEGELMILCH, K., RIES, M., RUDERT, M., JAKOB, F. & GROLL, J. 2019. Platelet lysate outperforms FCS and human serum for co-culture of primary human macrophages and hMSCs. *Scientific Reports*, 9, 3533.

- USUKURA, E., NARITA, A., YAGI, A., ITO, S. & USUKURA, J. 2016. An Unroofing Method to Observe the Cytoskeleton Directly at Molecular Resolution Using Atomic Force Microscopy. *Scientific Reports*, 6, 27472.
- VAN GEEMEN, D., RIEM VIS, P. W., SOEKHRADJ-SOECHIT, S., SLUIJTER, J. P., DE LIEFDE-VAN BEEST, M., KLUIN, J. & BOUTEN, C. V. 2011. Decreased mechanical properties of heart valve tissue constructs cultured in platelet lysate as compared to fetal bovine serum. *Tissue Eng Part C Methods*, 17, 607-17.
- VENN, M. & MAROUDAS, A. 1977. Chemical composition and swelling of normal and osteoarthrotic femoral head cartilage. I. Chemical composition. *Annals of the rheumatic diseases*, 36, 121-129.
- VIJI BABU, P. K. & RADMACHER, M. 2019. Mechanics of Brain Tissues Studied by Atomic Force Microscopy: A Perspective. *Frontiers in Neuroscience*, 13.
- VINCENT, T. L., MCLEAN, C. J., FULL, L. E., PESTON, D. & SAKLATVALA, J. 2007. FGF-2 is bound to perlecan in the pericellular matrix of articular cartilage, where it acts as a chondrocyte mechanotransducer. *Osteoarthritis and Cartilage*, 15, 752-763.
- VINCKIER, A. & SEMENZA, G. 1998. Measuring elasticity of biological materials by atomic force microscopy. *FEBS Lett*, 430, 12-6.
- WALKER, C., MOJARES, E. & DEL RIO HERNANDEZ, A. 2018. Role of Extracellular Matrix in Development and Cancer Progression. *Int J Mol Sci*, 19.
- WANNER, Y., UMRATH, F., WAIDMANN, M., REINERT, S. & ALEXANDER, D. 2017. Platelet Lysate: The Better Choice for Jaw Periosteal Cell Mineralization %J Stem Cells International. 2017, 10.
- WEIBRICH, G., KLEIS, W. K., HAFNER, G. & HITZLER, W. E. 2002. Growth factor levels in platelet-rich plasma and correlations with donor age, sex, and platelet count. *J Craniomaxillofac Surg*, 30, 97-102.
- WILUSZ, R. E., DEFRATE, L. E. & GUILAK, F. 2012a. A biomechanical role for perlecan in the pericellular matrix of articular cartilage. *Matrix biology : journal of the International Society for Matrix Biology*, 31, 320-327.
- WILUSZ, R. E., DEFRATE, L. E. & GUILAK, F. 2012b. Immunofluorescence-guided atomic force microscopy to measure the micromechanical properties of the pericellular matrix of porcine articular cartilage. *J R Soc Interface*, 9, 2997-3007.



- WILUSZ, R. E., SANCHEZ-ADAMS, J. & GUILAK, F. 2014. The structure and function of the pericellular matrix of articular cartilage. *Matrix Biology*, 39, 25-32.
- WILUSZ, R. E., ZAUSCHER, S. & GUILAK, F. 2013. Micromechanical mapping of early osteoarthritic changes in the pericellular matrix of human articular cartilage. *Osteoarthritis and cartilage*, 21, 1895-1903.
- YANG, P. J. & TEMENOFF, J. S. 2009. Engineering orthopedic tissue interfaces. *Tissue engineering. Part B, Reviews*, 15, 127-141.
- YERRAMSHETTY, J. S. & AKKUS, O. 2008. The associations between mineral crystallinity and the mechanical properties of human cortical bone. *Bone*, 42, 476-82.
- YOUN, I., CHOI, J. B., CAO, L., SETTON, L. A. & GUILAK, F. 2006. Zonal variations in the three-dimensional morphology of the chondron measured in situ using confocal microscopy. *Osteoarthritis and Cartilage*, 14, 889-897.
- YOUNG, J. D., MARTEL, J., YOUNG, D., YOUNG, A., HUNG, C.-M., YOUNG, L., CHAO, Y.-J., YOUNG, J. & WU, C.-Y. 2009. Characterization of Granulations of Calcium and Apatite in Serum as Pleomorphic Mineralo-Protein Complexes and as Precursors of Putative Nanobacteria. *PLOS ONE*, 4, e5421.
- YUKSEL, E., CHOO, J., WETTERGREEN, M. & LIEBSCHNER, M. 2005. Challenges in Soft Tissue Engineering. *Seminars in Plastic Surgery*, 19, 261-270.
- YUSKO, E. C. & ASBURY, C. L. 2014. Force is a signal that cells cannot ignore. *Molecular biology of the cell*, 25, 3717-3725.

## 7. Declaration of contribution

The dissertation work was carried out at the Department of Orthopaedic Surgery, University Hospital of Tübingen, Germany under the supervision of PD Dr. Ulf Krister Hofmann.

The study was designed by the following:

1. PD Dr. Ulf Krister Hofmann and myself, Department of Orthopaedic Surgery, Tübingen, for the 1<sup>st</sup> paper: Danalache et al: Changes in stiffness and biochemical composition of the pericellular matrix as a function of chondrocyte organization in osteoarthritic cartilage. *Osteoarthritis and Cartilage*, 2019.
2. Prof. Dr. Dorothea Alexander-Friedrich, Department of Oral and Maxillofacial Surgery, Tübingen for the 2<sup>nd</sup> paper: Danalache et al: Quality Analysis of Minerals Formed by Jaw Periosteal Cells under Different Culture Conditions. *International Journal of Molecular Sciences*, 2019.

I had the major contribution for both of the research papers published, with the collaboration and assistance of the co-authors as indicated in the “Authors contribution section” specified in each of the papers.

I carried out the majority of the experiments and received assistance from Janine Schneider for the AFM measurements on articular cartilage. Marita Munz did the cell characterization and handling and the RAMAN spectroscopy experiments were carried out by Sophie-Maria Kliesch at the company Quality Analysis GmbH (Nürtingen, Germany).

The statistical analysis was carried out independently by myself after consultation with PD Dr. Ulf Krister Hofmann and Prof. Dr. Dorothea Alexander-Friedrich.

I confirm that I wrote the thesis by myself and any additional sources of information have been duly cited.

20.01.2020, Tübingen



## Acknowledgments

*“Give credit to whom credit due.”*

*Samuel Adams*

Foremost I would like to express my extreme gratitude and respect to my advisor and mentor PD. Dr. Ulf Krister Hofmann for his continuous support throughout this Ph.D. journey, his patience, motivation and dedication. It is his overwhelming attitude and commitment that sorely and mainly were responsible for me completing this project that we have embarked on together 3 years ago. **Thank you for not giving up on me!**

I owe a deep sense of gratitude to Prof. Dr. Dorothea Alexander-Friedrich from the department of Oral and Maxillofacial surgery, for her keen interest in me at every step of my research. Her prompt support, timely suggestions with kindness, enthusiasm and dynamism has enabled me to complete this thesis. **You are a true inspiration for me!**

I am particularly grateful for the assistance given by Rosa Riester for her advice and technical assistance. **Thanks for your support and encouragement!**

A special and heartfelt appreciation goes to my favorite girls and more importantly friends: Anna-Lisa Erler and Janine Schneider. You both are my stone and without you guys and your support, I wouldn't have managed it. **Forever and ever friends!**

I would like to take this opportunity and thank Graham Lloyd-Smith for English language editing. I am deeply grateful for the speed of your response and support. **Thanks-much appreciated your help with this: “Neat stuff”!**

Finally but not least I want to thank my husband-Petrica Danalache, for being there throughout the entire time, for listening to me and my nagging, for being the shoulder that I cried on when things were rough, for waiting for me at home in the long never-ending weekends and pushing me to always move forward and never give up. **This one goes to you!**